

**Iron-Chromate Precipitates in Cr(VI)-Contaminated Soils:
Identification, Solubility, and
Solid Solution/Aqueous Solution Reactions**

Dirk Baron
M.S., Portland State University, 1990

A dissertation submitted to the faculty of the
Oregon Graduate Institute of Science & Technology
in partial fulfillment of the
requirements for the degree
Doctor of Philosophy
in
Environmental Science and Engineering


April 1996


The dissertation "Iron-Chromate Precipitates in Cr(VI)-Contaminated Soils: Identification, Solubility, and Solid Solution/Aqueous Solution Reactions" by Dirk Baron has been examined and approved by the following Examination Committee:


Carl D. Palmer, Dissertation Advisor
Associate Professor

David W. Blowes
Associate Professor, University of Waterloo, Canada

William Fish
Associate Professor

  James F. Pankow
Professor

 James T. Stanley
Adjunct Professor



ACKNOWLEDGEMENTS

Many people have contributed to this research and I am grateful to them all. Most importantly, I would like to thank Carl Palmer for his support and guidance throughout this project. His enthusiasm about this work and his willingness to sit down and work out the details helped a lot to make it all happen, especially during times when I could not really see the light at the end of the tunnel. Jim Stanley did all the detective work on the TEM and identified the elusive $\text{KFe}(\text{CrO}_4)_2 \cdot 2\text{H}_2\text{O}$. His help on some of the finer points of crystallography is also much appreciated. I also thank the other members of my committee, Jim Pankow, Bill Fish, and David Blowes, for their comments and suggestions on improving this manuscript.

Paul Wittbrodt, Chris Ward, and Cheryl Martin helped me find my way around the laboratory. They also contributed lots of good suggestions to my research. Thanks also go to my fellow students, including Alok Kumar, Jim Tesoriero, Diane Grady, Jane Allen, Tim Mayer, Claude Errera, Wentai Luo, Andrea Pavlick, Michelle Scherer, Tim Johnson, and everybody else, for many stimulating discussions and occasional extracurricular activities.

Judi Irvine's help and advice in many matters including the details of dealing with the administrative processes made my time at OGI much easier. Her cheerful presence in the department makes it a much more pleasant place.

Finally, I thank my parents Felizitas and Horst Baron for their unconditional love and support through all those years and the various twists and turns of my life.

Funding for this research project from the U.S. Environmental Protection Agency, R.S. Kerr Environmental Research Laboratory, Ada, Oklahoma, and from the EPA's Office of Exploratory Research is gratefully acknowledged. Additional funding was provided by a scholarship from the Association of Groundwater Scientists and Engineers.

TABLE OF CONTENTS

ACKNOWLEDGEMENTS	iii
TABLE OF CONTENTS	iv
LIST OF FIGURES	viii
LIST OF TABLES	xi
ABSTRACT	xiii
CHAPTER 1 Introduction	1
1.1 Background	1
1.2 Overview of the Dissertation	3
1.3 References	3
CHAPTER 2 Identification of two Iron-Chromate Precipitates in a Cr(VI)-Contaminated Soil	6
2.1 Introduction	7
2.2 Experimental Section	7
2.2.1 Site Description	7
2.2.2 Methods	8
2.3 Results	9
2.4 Discussion	16
2.4 Summary and Conclusions	19
2.6 References	19
CHAPTER 3 Solubility of $\text{KFe}_3(\text{CrO}_4)_2(\text{OH})_6$ at 4 - 35°C	21
3.1 Introduction	22
3.2 Experimental Methods	23

3.2.1	Synthesis of $\text{KFe}_3(\text{CrO}_4)_2(\text{OH})_6$	23
3.2.2	Characterization of Synthetic $\text{KFe}_3(\text{CrO}_4)_2(\text{OH})_6$	24
3.2.3	Dissolution Experiments	24
3.3	Results	25
3.3.1	Solid Characterization	25
3.3.2	Dissolution Experiments	30
3.4	Discussion	32
3.5	Summary	45
3.6	References	46
CHAPTER 4	Solubility of Jarosite at 4 - 35°C	50
4.1	Introduction	51
4.2	Previous Studies	52
4.3	Experimental Methods	56
4.3.1	Synthesis of Jarosite	56
4.3.2	Characterization of Synthetic Jarosite	56
4.3.3	Dissolution Experiments	56
4.4	Experimental Results	58
4.4.1	Solid Characterization	58
4.4.2	Dissolution Experiments	62
4.5	Discussion	66
4.6	Summary	75
4.7	References	77
CHAPTER 5	Solid Solution/Aqueous Solution Reactions between Jarosite and its Chromate Analog	80
5.1	Introduction	81
5.2	Experimental Section	82
5.2.1	Synthesis of $\text{KFe}_3(\text{Cr}_x\text{S}_{(1-x)}\text{O}_4)_2(\text{OH})_6$ Solid Solutions	82

5.2.2	Characterization of $\text{KFe}_3(\text{Cr}_x\text{S}_{(1-x)}\text{O}_4)_2(\text{OH})_6$	
	Solid Solutions	82
5.2.3	Dissolution Experiments	83
5.3.	Results	84
5.3.1	Solid Characterization	84
5.3.2	Dissolution Experiments	87
5.4	Discussion	90
5.5	Summary and Conclusions	95
5.6	References	96
CHAPTER 6	Solubility of $\text{KFe}(\text{CrO}_4)_2 \cdot 2\text{H}_2\text{O}$ at 4 - 75°C	99
6.1	Introduction	100
6.2	Experimental Section	101
6.2.1	Synthesis of $\text{KFe}(\text{CrO}_4)_2 \cdot 2\text{H}_2\text{O}$ for the Dissolution Experiments	101
6.2.2	Characterization of Synthetic $\text{KFe}(\text{CrO}_4)_2 \cdot 2\text{H}_2\text{O}$	101
6.2.3	Dissolution Experiments	102
6.2.4	Precipitation Experiments	103
6.3	Results	105
6.3.1	Characterization	105
6.3.2	Dissolution and Precipitation Experiments	107
6.4	Discussion	111
6.5	References	116
CHAPTER 7	Summary and Conclusions	118
7.1	Summary of Results	118
7.2	Overall Conclusions	120
7.3	Suggestions for Future Work	120
7.4	References	122

APPENDIX A	Supplemental Analytical Results	123
APPENDIX B	Activity Correction Models	126
VITA		128

LIST OF FIGURES

Figure 2-1. Powder X-ray diffraction spectra of (a) uncontaminated background soil and (b) chromium contaminated soil.	10
Figure 2-2. Scanning electron micrograph (a) with energy dispersive X-ray spectrum (b) of chromium-containing crystals from crust precipitated in soil fractures.	12
Figure 2-3. Scanning electron micrograph (a) with energy dispersive X-ray spectrum (b) of chromium-containing crystals in the bulk soil.	13
Figure 2-4. TEM electron diffraction patterns and EDS spectrum of $\text{KFe}_3(\text{CrO}_4)_2(\text{OH})_6$ crystals found in the contaminated soil.	14
Figure 2-5. TEM electron diffraction pattern and EDS spectrum of $\text{KFe}(\text{CrO}_4)_2 \cdot 2\text{H}_2\text{O}$ crystals precipitated in soil fractures.	15
Figure 2-6. Powder X-ray diffraction spectrum of crystals precipitated in soil fractures.	16
Figure 3.1 Powder x-ray diffraction pattern of synthetic $\text{KFe}_3(\text{CrO}_4)_2(\text{OH})_6$ used in this study.	27
Figure 3-2. FTIR spectrum of the synthetic $\text{KFe}_3(\text{CrO}_4)_2(\text{OH})_6$	28
Figure 3-3. Thermogravimetric analysis of synthetic $\text{KFe}_3(\text{CrO}_4)_2(\text{OH})_6$, (A) percent weight loss versus temperature, and (B) derivative.	30
Figure 3-4. Concentration of $[\text{K}]_{\text{tot}}$ (\blacktriangle), $[\text{Fe}]_{\text{tot}}$ (\blacksquare), and $[\text{CrO}_4]_{\text{tot}}$ (\bullet) in the dissolution experiment with initial pH 2 at 25°C.	33
Figure 3-5. Log of the ion activity product from five dissolution experiments at different pH values calculated without including FeCrO_4^+ in the speciation.	36
Figure 3-6. Log of the ion activity product from five dissolution experiments at different pH values calculated including the FeCrO_4^+ ion pair with $\log K = 8.0$ in the speciation.	37

Figure 3-7. Reported values for $\log K_{\text{FeCrO}_4}$ versus inverse temperature after activity corrections.	40
Figure 3-8. Calculated log ion activity product versus inverse temperature from four dissolution experiments at 4, 15, 25, and 35°C, initial pH 2.	41
Figure 3-9. pe-pH predominance diagram for the K-Fe-Cr-C-H ₂ O system.	42
Figure 3-10. Diagram of the predominance regions of ferrihydrite and $\text{KFe}_3(\text{CrO}_4)_2(\text{OH})_6$ in the K-Fe(III)-Cr(VI)-H ₂ O system.	43
Figure 3-11. Plot of $\log(C_0 - C)$ versus time for K_{tot} (■), Fe_{tot} (▲) and Cr_{tot} (▪) in the dissolution experiment KCRJAR-2.0.	44
Figure 4-1. Powder X-ray diffraction spectrum of the synthetic jarosite. Some of the strongest peaks and the corresponding d-spacings are indicated.	60
Figure 4-2. Thermogravimetric analysis of the synthetic jarosite. Curve A shows the weight loss versus temperature, curve B is its derivative.	61
Figure 4-3. FTIR spectrum of the synthetic jarosite	63
Figure 4-4. Concentrations of K_{tot} (▲), Fe_{tot} (■), and SO_4^{2-} (●) in the dissolution experiment with initial pH 2.0, equilibrium pH 2.10.	65
Figure 4-5. Calculated log ion activity products from five dissolution experiments at 25°C.	68
Figure 4-6. Free energy of formation for (K-Na-H ₃ O)-jarosite solid solutions from ALPERS et al. (1989) (□) and ZOTOV et al. (1973) (○).	70
Figure 4-7. Calculated log ion activity product versus temperature from four dissolution experiments at 4, 15, 25 and 35°C, initial pH 2 (■).	75
Figure 4-8. Plot of the log of the equilibrium concentration of potassium (C_0) minus the concentration of potassium at time t (C) for dissolution experiment KJAR-2.0, to test for first order behavior.	76
Figure 5-1. Main powder x-ray diffraction peaks of $\text{KFe}_3(\text{Cr}_x\text{S}_{(1-x)}\text{O}_4)_2(\text{OH})_6$ solid solutions.	86
Figure 5-2. Unit cell dimension of $\text{KFe}_3(\text{Cr}_x\text{S}_{(1-x)}\text{O}_4)_2(\text{OH})_6$ solid solutions as a function of composition.	87

Figure 5-3. Dissolution of synthetic solid Jar-25 as an example for the dissolution of $\text{KFe}_3(\text{Cr}_x\text{S}_{(1-x)}\text{O}_4)_2(\text{OH})_6$ solid solutions.	90
Figure 5-4. Steady state $\log \text{IAP}_{\text{ss}}$ values as a function of steady state aqueous mole fraction of Cr. Data is from the samples taken after 138 days.	93
Figure 5-5. Evolution of $\log \text{IAP}_{\text{ss}}$ values as a function of aqueous mole fraction of Cr during the dissolution of $\text{KFe}_3(\text{Cr}_x\text{S}_{(1-x)}\text{O}_4)_2(\text{OH})_6$ solid solutions.	94
Figure 5-6. Solid phase activity coefficients of the endmembers in the solid solutions as a function of composition	95
Figure 6-1. Powder x-ray diffraction pattern of the synthetic $\text{KFe}(\text{CrO}_4)_2 \cdot 2\text{H}_2\text{O}$ used in the dissolution experiments.	105
Figure 6-2. FTIR spectrum of the synthetic $\text{KFe}(\text{CrO}_4)_2 \cdot 2\text{H}_2\text{O}$ used in the dissolution experiments.	106
Figure 6-3. Concentration of $[\text{K}]_{\text{tot}}$ (\blacktriangle), $[\text{Fe}]_{\text{tot}}$ (\blacksquare), and $[\text{CrO}_4]_{\text{tot}}$ (\bullet) in the dissolution experiment with initial pH 1 at 25°C.	108
Figure 6-4. Log of the ion activity product from dissolution (\blacksquare) and precipitation (\square) experiments at different pH values and 25°C.	109
Figure 6-5. Calculated log ion activity product versus temperature from four dissolution experiments at 4, 15, 25, 35, 50, and 75°C, initial pH 1.0. . . .	114
Figure 6-8. Diagram of the predominance regions of $\text{KFe}(\text{CrO}_4)_2 \cdot 2\text{H}_2\text{O}$, $\text{KFe}_3(\text{CrO}_4)_2(\text{OH})_6$, and $\text{Fe}(\text{OH})_3$ in the K-Fe(III)-Cr(VI)- H_2O system. . . .	115

LIST OF TABLES

Table 2-1.	Comparison of additional d-spacings found in Cr(VI) contaminated soils with d-spacings reported by Bonnin and Lecerf (1966) for synthetic $\text{KFe}_3(\text{CrO}_4)_2(\text{OH})_6$.	11
Table 2-2.	Comparison of d-spacings from crusts in soil fractures with d-spacings reported by Bonnin (1970) for synthetic $\text{KFe}(\text{CrO}_4)_2 \cdot 2\text{H}_2\text{O}$.	17
Table 3-1.	Initial experimental conditions.	25
Table 3-2.	Powder X-ray diffraction peaks from synthetic $\text{KFe}_3(\text{CrO}_4)_2(\text{OH})_6$ used in dissolution experiments.	26
Table 3-3.	Final concentrations in the dissolution experiments.	32
Table 3-4.	Thermodynamic data used for calculations.	34
Table 3-5.	Calculated equilibrium activities; FeCrO_4^+ not included in the speciation.	35
Table 3-6.	Equilibrium activities calculated using FeCrO_4^+ with $\log K = 8.0$.	38
Table 3-7.	Summary of studies of the formation constant of FeCrO_4^+ .	49
Table 4-1.	Summary of solubilities and $\Delta G_{f,298}^0$ values reported for jarosite.	53
Table 4-2.	Thermodynamic data used in calculations.	55
Table 4-3.	Initial experimental conditions.	57
Table 4-4.	Powder x-ray diffraction peaks from synthetic jarosite used in dissolution experiments.	59
Table 4-5.	Final concentrations in the dissolution experiments.	64
Table 4-6.	Calculated equilibrium activities.	67

Table 5-1.	Summary of synthesis of $\text{KFe}_3(\text{Cr}_x\text{S}_{(1-x)}\text{O}_4)_2(\text{OH})_6$ solid solutions. . .	83
Table 5-2.	Powder X-ray diffraction analysis of $\text{KFe}_3(\text{Cr}_x\text{S}_{(1-x)}\text{O}_4)_2(\text{OH})_6$ solid solutions.	85
Table 5-3.	Final concentrations in the dissolution experiments.	88
Table 5-4.	Thermodynamic data used in calculations.	89
Table 5-5.	Calculated ion activities for the dissolution	91
Table 6-1.	Initial experimental conditions.	102
Table 6-2.	Powder x-ray diffraction peaks from synthetic $\text{KFe}(\text{CrO}_4)_2 \cdot 2\text{H}_2\text{O}$ used in the dissolution experiments.	104
Table 6-3.	Final concentrations in the precipitation and dissolution experiments.	107
Table 6-4.	Thermodynamic data used for calculations.	110
Table 6-5.	Results of MINTEQA2 speciation calculations.	111
Table A-1.	Complete analytical results from the final sample taken in the $\text{KFe}_3(\text{CrO}_4)_2(\text{OH})_6$ dissolution experiments (Chapter 3)	123
Table A-2.	Complete analytical results from the final sample in jarosite dissolution experiments (Chapter 4)	124
Table A-3.	Complete analytical results from the final sample in $\text{KFe}(\text{CrO}_4)_2 \cdot 2\text{H}_2\text{O}$ dissolution experiments (Chapter 6)	125
Table A-4.	Debye-Hückel parameters included in the MINTEQA2 database for ions considered in this study	127

ABSTRACT

Iron-Chromate Precipitates in Cr(VI)-Contaminated Soils:
Identification, Solubility, and Solid Solution/Aqueous Solution Reactions

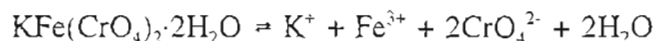
Dirk Baron

Oregon Graduate Institute of Science & Technology, 1996

Supervising Professor: Carl D. Palmer

Chromate-containing precipitates can affect the mobility of toxic Cr(VI) in the subsurface, control its concentration in groundwater, limit its bioavailability, and impede remediation of chromium contaminated sites. This dissertation focusses on two iron-chromate precipitates, $\text{KFe}_3(\text{CrO}_4)_2(\text{OH})_6$ (the chromate analog of the sulfate mineral jarosite) and $\text{KFe}(\text{CrO}_4)_2 \cdot 2\text{H}_2\text{O}$, that we identified in a soil contaminated by chrome plating solutions. The precipitates were identified using scanning and transmission electron microscopy, as well as powder x-ray diffraction. $\text{KFe}_3(\text{CrO}_4)_2(\text{OH})_6$ occurs as small (2-5 μm) crystals interspersed within the bulk soil. $\text{KFe}(\text{CrO}_4)_2 \cdot 2\text{H}_2\text{O}$ forms crusts of larger crystals (10-50 μm) in cracks and fractures of the soil.

$\text{KFe}(\text{CrO}_4)_2 \cdot 2\text{H}_2\text{O}$, $\text{KFe}_3(\text{CrO}_4)_2(\text{OH})_6$, and jarosite were synthesized and characterized. Thermodynamic properties of these phases were calculated from solubility experiments. For the reaction



the $\log K_{\text{sp}}$ at 25°C is -19.34 ± 0.13 , the enthalpy of reaction, $\Delta H_{r,298}^0$, is $18.8 \pm 1.7 \text{ kJ mol}^{-1}$, and the entropy of reaction, $\Delta S_{r,298}^0$, is $-310 \pm 45 \text{ J mol}^{-1} \text{ K}^{-1}$. Over the temperature range

of 4 to 75°C, the heat capacity of reaction, $\Delta C_{p,r}$, is $-460 \pm 130 \text{ J mol}^{-1} \text{ K}^{-1}$. For the reaction

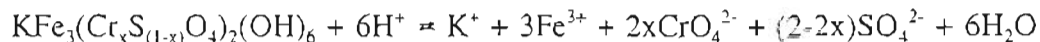


the $\log K_{sp}$ at 25°C is -18.7 ± 0.5 . The solubility does not vary significantly over the range of 4 to 35°C. For the reaction



the $\log K_{sp}$ at 25°C is -11.0 ± 0.3 , $\Delta H_{r,298}^0$ is $-45 \pm 5 \text{ kJ mol}^{-1}$, and $\Delta S_{r,298}^0$ is $-350 \pm 40 \text{ J mol}^{-1} \text{ K}^{-1}$. Over the range of 4 to 35°C, $\Delta C_{p,r}$ is $-2.1 \pm 0.2 \text{ kJ mol}^{-1} \text{ K}^{-1}$.

In addition, seven $\text{KFe}_3(\text{Cr}_x\text{S}_{(1-x)}\text{O}_4)_2(\text{OH})_6$ solid solutions with a wide range of Cr/S ratios were synthesized and characterized. These solid solutions dissolve congruently according to



and reach a stoichiometric saturation state after 40-60 days. Calculated stoichiometric saturation constants suggest that the solid solutions are close to ideal with a slightly negative excess free energy of mixing.

The calculated thermodynamic data indicate that $\text{KFe}_3(\text{CrO}_4)_2(\text{OH})_6$ is stable over a wide range of conditions and could form in large parts of a Cr(VI)-contaminated aquifer, limiting the mobility of Cr(VI) and interfering with remediation efforts. It is also likely that $\text{KFe}_3(\text{Cr}_x\text{S}_{(1-x)}\text{O}_4)_2(\text{OH})_6$ solid solutions could form in many chromium contaminated environments. $\text{KFe}(\text{CrO}_4)_2 \cdot 2\text{H}_2\text{O}$, however, is stable only at low pH and very high Cr(VI) concentrations, typical for the immediate vicinity of a release of acidic, chromate-rich solutions.

CHAPTER 1

Introduction

1.1 Background

Chromium is an important industrial metal that is widely used in many diverse products and processes including metal alloys, dyes, refractories, chemicals, fungicides, metal finishing, electroplating, wood preservation, and leather tanning (Nriagu, 1988a,b). Due to spills, leakage, and improper storage or disposal, chromium has been released into the environment at many sites and is one of the most common inorganic soil and groundwater contaminants (Palmer and Wittbrodt, 1991; Calder, 1988). In the environment chromium is primarily found the Cr(III) and Cr(VI) oxidation states which differ markedly in their mobility and toxicity. Cr(III) has a relatively low toxicity (van Weerelt et al., 1984) and is immobile under slightly acidic to moderately alkaline conditions. In contrast, Cr(VI), which occurs in the environment primarily in anionic form as CrO_4^{2-} (chromate), HCrO_4^- (bichromate), and $\text{Cr}_2\text{O}_7^{2-}$ (dichromate), is quite mobile and is acutely toxic, mutagenic (Bianchi et al., 1983; Beyersmann et al., 1984; Bonatti et al., 1976; Paschin et al., 1983), carcinogenic (Mancuso and Heuper, 1951; Mancuso, 1951; Waterhouse, 1975; Yassi and Nieboer, 1988; Ono, 1988), and teratogenic (Abassi and Soni, 1984). Due to the potential health hazards associated with chromate and because it is such a common soil and groundwater contaminant, there is a need to understand the processes that control the mobility of chromium released into the environment in order to assess the risk to human health and the environment associated with such releases and to aid in the clean-up of chromium contaminated sites.

One of the key processes affecting chromium mobility in the environment is the precipitation and dissolution of chromate containing solid phases. Chromate-laden

solutions released into soils can alter the chemical environment of the soil, resulting in the dissolution of native soil minerals and the precipitation of new phases that incorporate Cr(VI). These precipitates can be pure phases or form solid solutions with common soil minerals. The formation of such precipitates can affect Cr(VI) mobility, control its concentration in subsurface waters, and may limit its bioavailability.

The overall objectives of this research project are to document the occurrence of iron-chromate precipitates in chromium contaminated soil and to determine the conditions under which they can form and to what extent they may control Cr(VI) mobility and interfere with the clean-up of chromium contaminated aquifers. Two iron-chromate precipitates, $\text{KFe}_3(\text{CrO}_4)_2(\text{OH})_6$ (the chromate analog of the common sulfate mineral jarosite) and $\text{KFe}(\text{CrO}_4)_2 \cdot 2\text{H}_2\text{O}$, were identified in soil from the United Chrome Products Site, a former hard chrome plating facility where chrome plating solutions have contaminated soil and groundwater. Although both these iron chromate phases have been synthesized and described (Bonnin, 1970; Bonnin and Lecerf, 1966; Powers et al., 1975; Graverneau and Hardy, 1972) they have not previously been reported to occur in the environment and nothing was known about the solubility of these phases. Since $\text{KFe}_3(\text{CrO}_4)_2(\text{OH})_6$ is the structural analog of the sulfate mineral jarosite ($\text{KFe}_3(\text{SO}_4)_2(\text{OH})_6$), solid solutions between these two phases ($\text{KFe}_3(\text{Cr}_x\text{S}_{(1-x)}\text{O}_4)_2(\text{OH})_6$) were also investigated. Sulfate is a common groundwater constituent and is present in plating solutions. The equivalent charge, similar structure, and comparable thermochemical radii of chromate and sulfate make it likely that such solid solutions can also form in chromium contaminated soils. The aqueous Cr(VI) concentrations in solutions equilibrated with such solid solutions could be dramatically different from concentrations in solutions equilibrated with pure $\text{KFe}_3(\text{CrO}_4)_2(\text{OH})_6$. In order to investigate the solid solution/aqueous solution reactions between jarosite and its chromate analog, it was also necessary to determine the solubility of pure jarosite which was not well known. Based on the measured solubilities and the observed solid solution/aqueous solution reactions between jarosite and its chromate analog, the conditions under which these phases are likely to form are determined and their impact on Cr(VI)-mobility and the remediation of Cr(VI)-contaminated soil is discussed.

1.2 Overview of the Dissertation

In addition to the introduction, this dissertation consists of five experimental chapters and a final chapter that summarizes the research results, presents overall conclusions, and discusses directions for future research. The experimental chapters describe the identification of the two iron-chromate precipitates in chromium contaminated soil from the United Chrome Products site in Corvallis, Oregon (Chapter 2), experiments to determine the solubility of $\text{KFe}_3(\text{CrO}_4)_2(\text{OH})_6$ (Chapter 3) and jarosite (Chapter 4), experiments to elucidate solid solution/aqueous solution reactions between jarosite and its chromate analog (Chapter 5), and experiments to determine the solubility of $\text{KFe}(\text{CrO}_4)_2 \cdot 2\text{H}_2\text{O}$ (Chapter 6).

The experimental chapters (Chapters 2-6) have been prepared as stand-alone contributions for publication in scientific journals. Their formatting reflects the requirements of the different journals. Although each paper can stand alone, they are arranged in a logical order leading up to the overall conclusions of this research project. Chapter 2 and Chapter 4 have been published in *Environmental Science & Technology* (Baron et al., 1996), and *Geochimica et Cosmochimica Acta* (Baron and Palmer, 1996), respectively. Chapter 3 has been accepted for publication in *Geochimica et Cosmochimica Acta*. Chapter 5 was prepared for submission to *Geochimica et Cosmochimica Acta*, and Chapter 6 was prepared for submission to *Environmental Science & Technology*.

1.3 References

- Abbasi S.A., Soni R. (1984) Teratogenic effects of chromium(VI) in the environment as evidenced by the impact of larvae of amphibian *Rana tigrina*: Implications in the environmental management of chromium. *Int. J. Environ. Stud.* **23**, 131-137.
- Baron D. and Palmer C.D. (1996) Solubility of jarosite at 4 - 35°C. *Geochim. Cosmochim. Acta* **60**, 185-195.
- Baron D., Stanley J.T., and Palmer C.D. (1996) Identification of two Fe-chromate precipitates in a Cr(VI)-contaminated soil. *Environ. Sci. Technol.* **30**, 964-968.
- Beyersmann D., Koester A., Buttner B. and Flessel P. (1984). Model reactions of

chromium compounds with mammalian and bacterial cells. *Toxicol. Environ. Chem.* **8**, 279-286.

Bianchi V.A., Zantedeschi A., Montaldi A., and Majone F. (1984) Trivalent chromium is neither cytotoxic nor mutagenic in permeabilized hamster fibroblasts. *Toxicological Letters* **23**, 51-59

Bonatti S., Meini M., and Abbondolo A. (1976) Genetic effects of potassium chromate in *Schizosaccharomyces pombe*. *Mutat. Res.* **38**, 147-149.

Bonnin A. (1970) Préparations et étude de chromates de fer. Ph.D. Dissertation, Univ. Rennes, France.

Bonnin A. and Lecerf A. (1966) Deux nouveaux chromates de fer: FeCrO_4OH et $\text{KFe}_3(\text{CrO}_4)_2(\text{OH})_6$. *C. R. Seances Acad. Sci. Paris Sér. C* **262**, 1782-1784.

Calder L.M. (1988) Chromium contamination of groundwater. In: *Chromium in the natural and human environments* (eds. J.O. Nriagu and E. Nieboer), 215-230. John Wiley and Sons, New York.

Gravereau P. and Hardy A. (1972) La série $\text{M}^{\text{I}}\text{M}^{\text{III}}(\text{XO}_4)_2 \cdot n\text{H}_2\text{O}$: structure cristalline de $\text{KFe}(\text{CrO}_4)_2 \cdot 2\text{H}_2\text{O}$, nouveau type dans la série des chromates des fer dihydratés. *Acta Crystallogr. Sec.B* **28**, 2333-2337.

Manusco T.F. (1951) Occupational cancer and other health hazards in a chrome plant. A medical appraisal. II. Clinical and toxicological aspects. *Ind. Med. Sur.* **20**, 393-407.

Manusco T.F. and Heuper W.C. (1951) Occupational cancer and other health hazards in a chrome plant. A medical appraisal. I. Lung cancer in chromate workers. *Ind. Med. Sur.* **20**, 358-363.

Nriagu J.O. (1988a) Historical Perspectives. In: *Chromium in the natural and human environments* (eds. J.O. Nriagu and E. Nieboer), 1-20. John Wiley and Sons, New York.

Nriagu J.O. (1988b) Production and uses of chromium. In: *Chromium in the natural and human environments* (eds. J.O. Nriagu and E. Nieboer) 81-104. John Wiley and Sons, New York.

Ono B.I. (1988) Genetic approaches in the study of chromium toxicity and resistance in yeast and bacteria. In: *Chromium in the Natural and Human Environments* (eds. J.O. Nriagu and E. Nieboer), 351-368. John Wiley and Sons, New York.

Palmer C.D. and Wittbrodt P.R. (1991) Processes affecting the remediation of chromium contaminated sites. *Environ. Health Perspect.* **92**, 25-40.

Paschin Y.V., Kozachenko V.I., and Salnikova L.E. (1983) Differential Mutagenic response at the HGPRT locus in V-79 and CHO cells after treatment with chromate. *Mutat. Res.* **122**, 361-365.

Powers D.A., Rossman G.R., Schugar H.J., and Gray H.B. (1975) Magnetic behavior and infrared spectra of jarosite, basic iron sulfate, and their chromate analogs. *J. Solid State Chem.* **13**, 1-13.

van Weerelt M., Pfeiffer W.C., and Fiszman M. (1984) Uptake and release of $^{51}\text{Cr(VI)}$ and $^{51}\text{Cr(III)}$ by barnacles (*Balanus sp.*). *Mar. Environ. Res.* **11**, 201-211.

Yassi A. and Nieboer E. (1988) Carcinogenicity of chromium compounds. In: *Chromium in the Natural and Human Environments* (eds. J.O. Nriagu and E. Nieboer), 443-496. John Wiley and Sons, New York.

CHAPTER 2

Identification of two Iron-Chromate Precipitates in a Cr(VI)-Contaminated Soil

Two Fe-chromate precipitates, $\text{KFe}_3(\text{CrO}_4)_2(\text{OH})_6$ (the chromate analog of the sulfate mineral jarosite) and $\text{KFe}(\text{CrO}_4)_2 \cdot 2\text{H}_2\text{O}$, were discovered in a soil contaminated by chrome plating solutions. The precipitates were identified by electron microscopy and powder x-ray diffraction. $\text{KFe}_3(\text{CrO}_4)_2(\text{OH})_6$ was found as small crystals interspersed within the bulk soil. $\text{KFe}(\text{CrO}_4)_2 \cdot 2\text{H}_2\text{O}$ forms crusts in cracks and fractures of the soil. Powder x-ray diffraction of the whole soil indicates that most of the Cr(VI) in the soil is present as $\text{KFe}_3(\text{CrO}_4)_2(\text{OH})_6$ and that the overall amount of $\text{KFe}(\text{CrO}_4)_2 \cdot 2\text{H}_2\text{O}$ in the soil is relatively small. The reaction for the transformation between these two phases indicates that $\text{KFe}(\text{CrO}_4)_2 \cdot 2\text{H}_2\text{O}$ is likely to form in more acidic, K^+ - and HCrO_4^- -rich environments than $\text{KFe}_3(\text{CrO}_4)_2(\text{OH})_6$. Although both of these chromate phases have been synthesized and described, to our knowledge, this study is the first report of their occurrence in the environment.

2.1 Introduction

Chromium is a widely used, toxic industrial metal that has been released into the environment at many sites (Calder, 1988; Palmer and Wittbrodt, 1991). Chromate-laden solutions released into soils by leakage from industrial facilities or by improper waste disposal can alter the chemical environment of soils resulting in the dissolution of native soil minerals and the precipitation of new phases that incorporate Cr(VI). These precipitates can limit the mobility of Cr(VI) in the subsurface and regulate the bioavailability of Cr(VI). The identification of such precipitates can improve our estimates of the potential risks to human health and the environment at contaminated sites and can greatly contribute to the rational design of remediation systems. In this paper, we report the discovery of two iron-chromate precipitates in the soil at a former hard-chrome plating facility.

2.2 Experimental Section

2.2.1 Site Description

The United Chrome Products site in Corvallis, Oregon, USA, is a hard-chrome plating facility that operated between 1956 and 1985. The site is located in the Willamette Valley. Local soils are silt loams of the Amity and Dayton Series (fine-silty, mixed, mesic Argiaquic Xeric Argialbolls and fine, montmorillonitic, mesic Typic Albaqualfs, respectively). Leakage from the plating tanks resulted in the contamination of soil and groundwater. The exact composition of the plating solutions used at this facility is not known. However, in general, hard chrome plating solutions consist of 1.5-4.5 molar solutions CrO_3 with a small amount of H_2SO_4 (Cr:S = 80-130:1) (Fernald, 1984). These solutions are highly acidic with a pH of less than zero. However, the pH in the groundwater under the plating tanks was generally around 4, and the lowest measured pH value was 2.3 (CH2M Hill, 1990). Reported concentrations of hexavalent chromium in the groundwater were as great as 19,000 mg/L (19 g/L). Soils contained as much as 60,000 mg/kg (6%) chromium (McKinley et al., 1992). In 1988, the plating tanks were removed and underlying soils which had a purple appearance (Munsell color 5RP 2/2) were exposed. Closer examination also revealed crusts of small crystals

precipitated in fractures in the discolored soil. When these crystals were ground, they appeared red (Munsell color 2.5 YR 4/6). A background soil sample was taken about 100 m upgradient of the contaminated area for comparison. The background soil sample was chemically analyzed and found to be uncontaminated.

2.2.2 Methods

Whole soil samples for powder x-ray diffraction (XRD) analysis were air-dried and ground in a mortar for 30 minutes and then analyzed without additional preparation with a Nicolet I2 diffractometer. For the uncontaminated soil the stepsize was $0.05^\circ 2\theta$ and the sampling time 2 sec, for the chromium contaminated soil the stepsize was $0.02^\circ 2\theta$ and the sampling time was 5 sec. The crystalline crusts precipitated in soil fractures were separated from the rest of the soil and crushed to obtain a fine powder and analyzed using a Siemens D5000 diffractometer. To allow analysis of the very small amount of sample that was available, a 'zero background plate', consisting of a single crystal quartz plate mounted in a supporting frame, was used as a sample holder. Stepsize was $0.025^\circ 2\theta$ and the sampling time was 1 sec.

The contaminated soil and the crusts were examined under a Zeiss 960 Digital scanning electron microscope (SEM) with a Link energy dispersive x-ray spectrometer (EDS). Samples for scanning electron microscopy were air-dried and mounted with carbon. The samples were initially coated with carbon ($\sim 400 \text{ \AA}$). Samples of the bulk soil were later coated with Au-Pd ($\sim 200 \text{ \AA}$) to reduce charging. EDS spectra were obtained at a 31 mm working distance with an accelerating voltage of 20 kV with no window.

Samples for transmission electron microscopy (TEM) were prepared by sprinkling small amounts of sample on copper grids. The samples were examined under a Hitachi 800 TEM/STEM (scanning transmission electron microscope) with a 200 kV accelerator voltage, fitted with a Noran EDS detector and a 5500 Noran analyzer. Selected Area Diffraction (SAD) and Convergent Beam Electron Diffraction (CBED) patterns of individual crystals were obtained.

2.3 Results

To identify possible chromium precipitates in the Cr(VI)-contaminated soil, a sample of the purple soil was analyzed by powder X-ray diffraction (XRD) and compared to uncontaminated background soil (Figure 2-1). The major minerals in the uncontaminated soil are quartz, feldspar (labradorite), and clay. In general, powder-X ray diffraction allows identification of crystalline phases that make up more than about 5-10% of the soil. Minor soil constituents and amorphous phases cannot be detected by XRD of a whole soil sample. Therefore, this XRD scan does not rule out the presence of other minor soil constituents such as iron oxides and hydroxides. The chromium contaminated soil shows additional peaks with the greatest intensities occurring at 3.13, 3.16, and 5.17 Å. These d-spacings are consistent with $\text{KFe}_3(\text{CrO}_4)_2(\text{OH})_6$, the chromate analog of the sulfate mineral jarosite (Bonnin, 1970; Bonnin and Lecerf, 1966; Powers et al., 1975; Cudennec et al., 1980; Townsend et al., 1986). Comparison of the additional peaks found in the contaminated soil with the d-spacings and corresponding intensities reported for $\text{KFe}_3(\text{CrO}_4)_2(\text{OH})_6$ (Bonnin and Lecerf, 1966) (Table 2-1) clearly demonstrate an excellent match.

The soil was then examined using scanning electron microscopy with energy dispersive X-ray spectroscopy (EDS) to determine if the composition of the crystals is consistent with $\text{KFe}_3(\text{CrO}_4)_2(\text{OH})_6$ and to ascertain if other chromium containing phases were present. The crusts in fractures in the soil consist of 10-50 µm, well formed platy crystals containing K, Fe, and Cr (Figure 2-2). Small (~2-5 µm) K-Fe-Cr containing crystals were also found interspersed within the bulk soil (Figure 2-3). The Fe:Cr ratios from the EDS spectra for the small crystals are 2.8 times greater than the ratios for the larger crystals, indicating that these crystals contain a larger amount of Fe, relative to Cr and K.

To determine if the K-Fe-Cr-containing crystals in the crust are structurally different from those in the bulk soil, electron diffraction patterns from single crystals were obtained under the transmission electron microscope. Patterns from crystals found within the bulk soil identify these as hexagonal, space group $R\bar{3}m$, and confirmed the identification as the chromate analog of jarosite (Figure 2-4). The crystals found in the

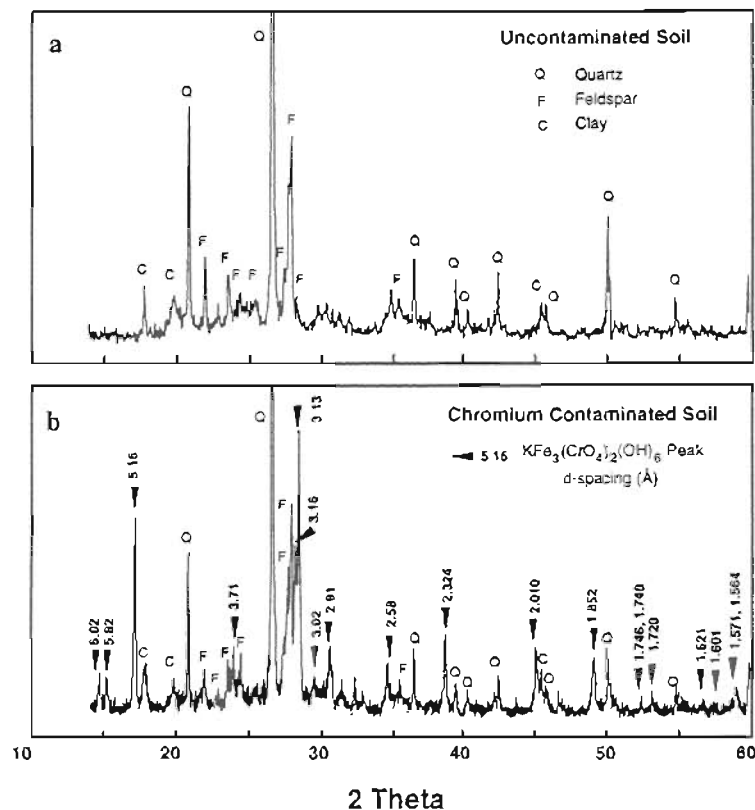


Figure 2-1. Powder x-ray diffraction spectra of (a) uncontaminated background soil and of (b) chromium contaminated soil. The additional peaks in the contaminated soil indicate the presence of a large amount of $\text{KFe}_3(\text{CrO}_4)_2(\text{OH})_6$.

soil fractures are monoclinic, space group C2/m , consistent with $\text{KFe}(\text{CrO}_4)_2 \cdot 2\text{H}_2\text{O}$ (Bonnin, 1970; Gravereau and Hardy, 1972; Mellier and Gravereau, 1972) (Figure 2-5). To assure that the individual crystals of $\text{KFe}(\text{CrO}_4)_2 \cdot 2\text{H}_2\text{O}$ identified under the TEM were representative of the crusts and not rare occurrences in the soil, we obtained an XRD spectrum of the surface crusts. The crusts were carefully scraped from the soil onto a zero-background plate to try to minimize the amount of underlying soil in the subsample. The XRD scan (Figure 2-6) yielded $\text{KFe}_3(\text{CrO}_4)_2(\text{OH})_6$ peaks as well as weaker peaks corresponding to quartz and feldspar. In addition, there are 10 peaks (Table 2-2) matching very well with the d-spacings and corresponding intensities reported by Bonnin

Table 2-1. Comparison of additional d-spacings found in Cr(VI) contaminated soils with d-spacings reported by Bonnin and Lecerf (1966) for synthetic $\text{KFe}_3(\text{CrO}_4)_2(\text{OH})_6$.

synthetic $\text{KFe}_3(\text{CrO}_4)_2(\text{OH})_6$ (Bonnin and Lecerf, 1966)			Whole Soil	
h,k,l	d-spacing (Å)	rel. Int.	d-spacing (Å)	rel. Int.
1 0 1	6.04	12	6.02	14
0 0 3	5.82	8	5.82	12
0 1 2	5.18	33	5.16	69
1 1 0	3.715	11	3.71	24
1 0 4	3.617	2		
0 2 1	3.166 }	100	3.16 }	100
1 1 3	3.127 }		3.13 }	
0 1 5	3.071	1		
2 0 2	3.02	7	3.02	13
0 0 6	2.908	15	2.91	24
0 2 4	2.588	8	2.58	18
1 2 2	2.325	20	2.324	28
0 1 8	2.067	<1		
0 3 3	2.013	25	2.010	23
0 2 7	1.971	3		
0 0 9	1.938	4		
2 2 0	1.858	24	1.852	20
2 0 8	1.805	<1		
2 2 3	1.770	<1		
3 1 2	1.750 }	5	1.746	4
2 1 7	1.741 }		1.740	6
1 1 9	1.720	4	1.720	7
1 3 4	1.652	2		
1 2 8	1.624	4	1.621	5
4 0 1	1.6013	5	1.601	4
3 1 5	1.5871 }	6	1.571	4
0 4 2	1.5788 }		1.564	9

(1970) for $\text{KFe}(\text{CrO}_4)_2 \cdot 2\text{H}_2\text{O}$. Four of the $\text{KFe}(\text{CrO}_4)_2 \cdot 2\text{H}_2\text{O}$ peaks (d-spacings 5.17, 3.13, 3.02, and 2.58 Å) are overlain by $\text{KFe}_3(\text{CrO}_4)_2(\text{OH})_6$ peaks. The 2.75 Å peak from the crusts has a greater intensity than expected from the data for the synthetic

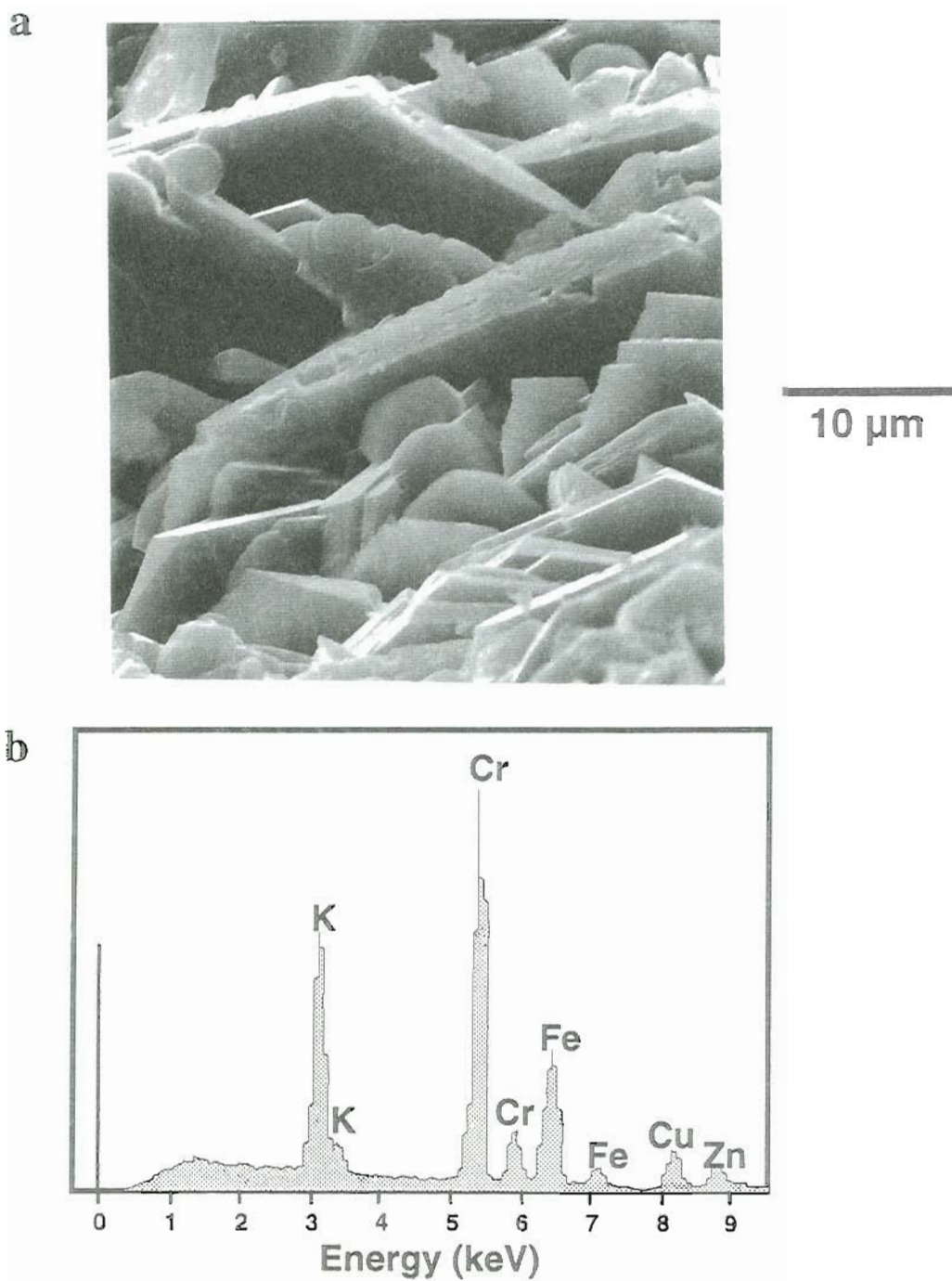
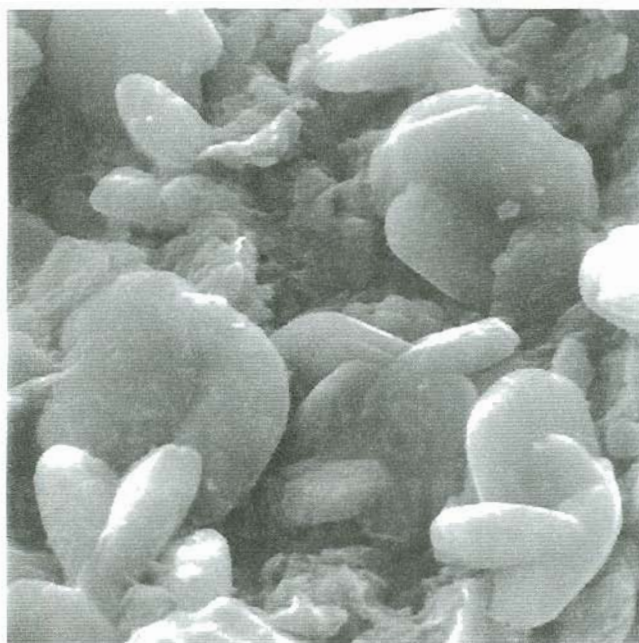


Figure 2-2. Scanning electron micrograph with energy dispersive X-ray spectrum of chromium containing crystals from crusts precipitated in soil fractures. The crystals were identified as $\text{KFe}(\text{CrO}_4)_2 \cdot 2\text{H}_2\text{O}$; Cu and Zn peaks contributed by the sample holder.

a



2 μm

b

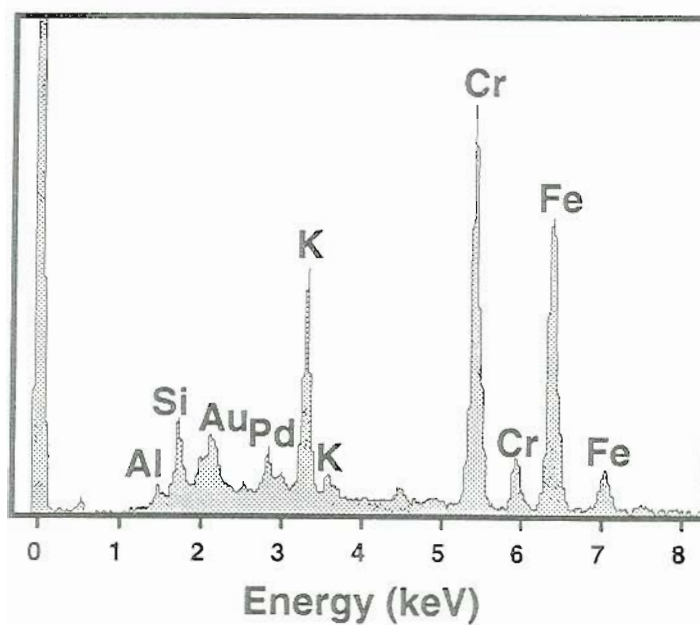


Figure 2-3. Scanning electron micrograph with energy dispersive X-ray spectrum of chromium containing crystals in the bulk soil. The crystals were identified as $\text{KFe}_3(\text{CrO}_4)_2(\text{OH})_6$. Si and Al peaks attributed to surrounding aluminosilicates; Au and Pd peaks are from the sample coating.

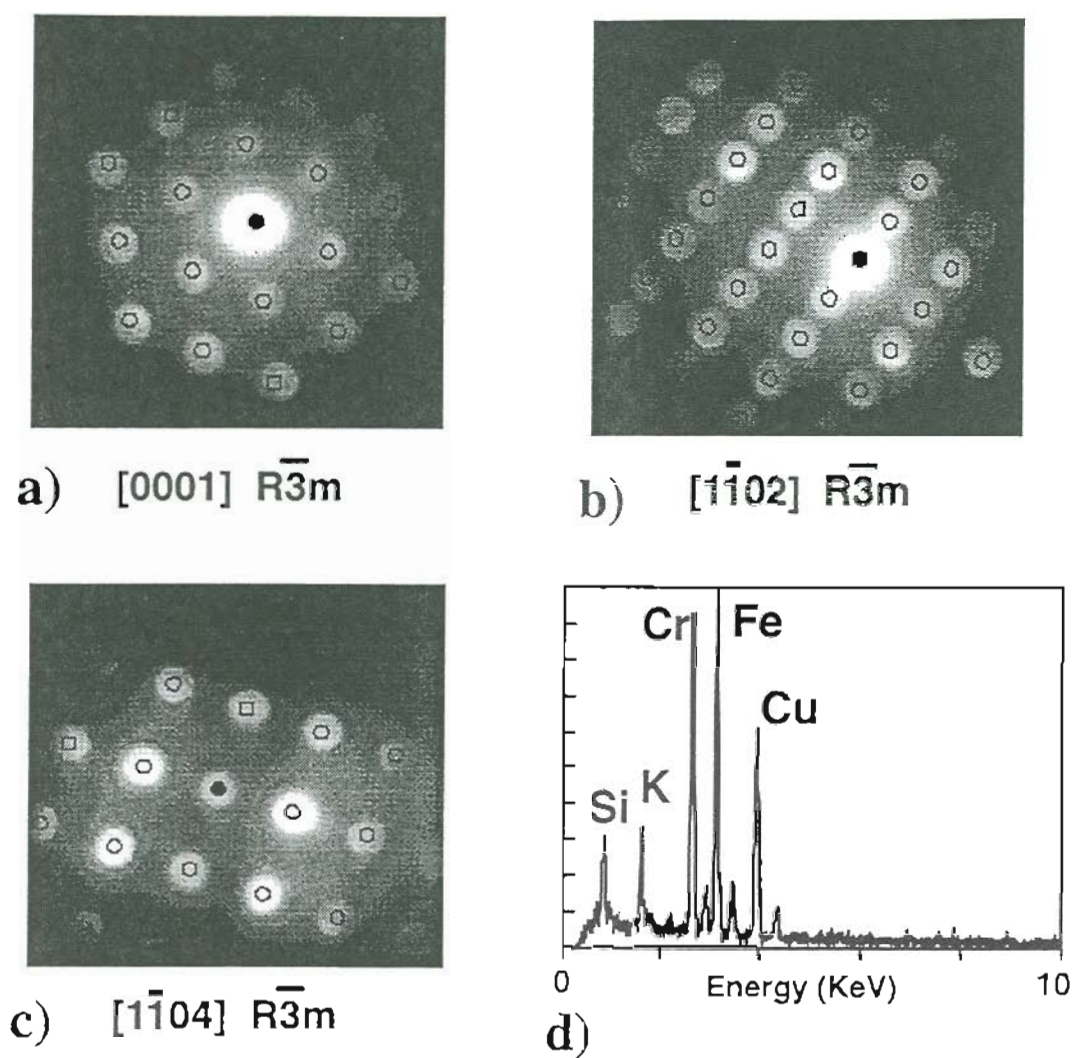


Figure 2-4. TEM electron diffraction patterns and EDS spectrum of $\text{KFe}_3(\text{CrO}_4)_2(\text{OH})_6$ crystals found in the contaminated soil. a) - c) electron diffraction patterns, circles superimposed over the electron diffraction patterns are the theoretical patterns for $\text{KFe}_3(\text{CrO}_4)_2(\text{OH})_6$; d) EDS spectrum, Si peak attributed to surrounding silicates, Cu peaks are from the brass specimen holder.

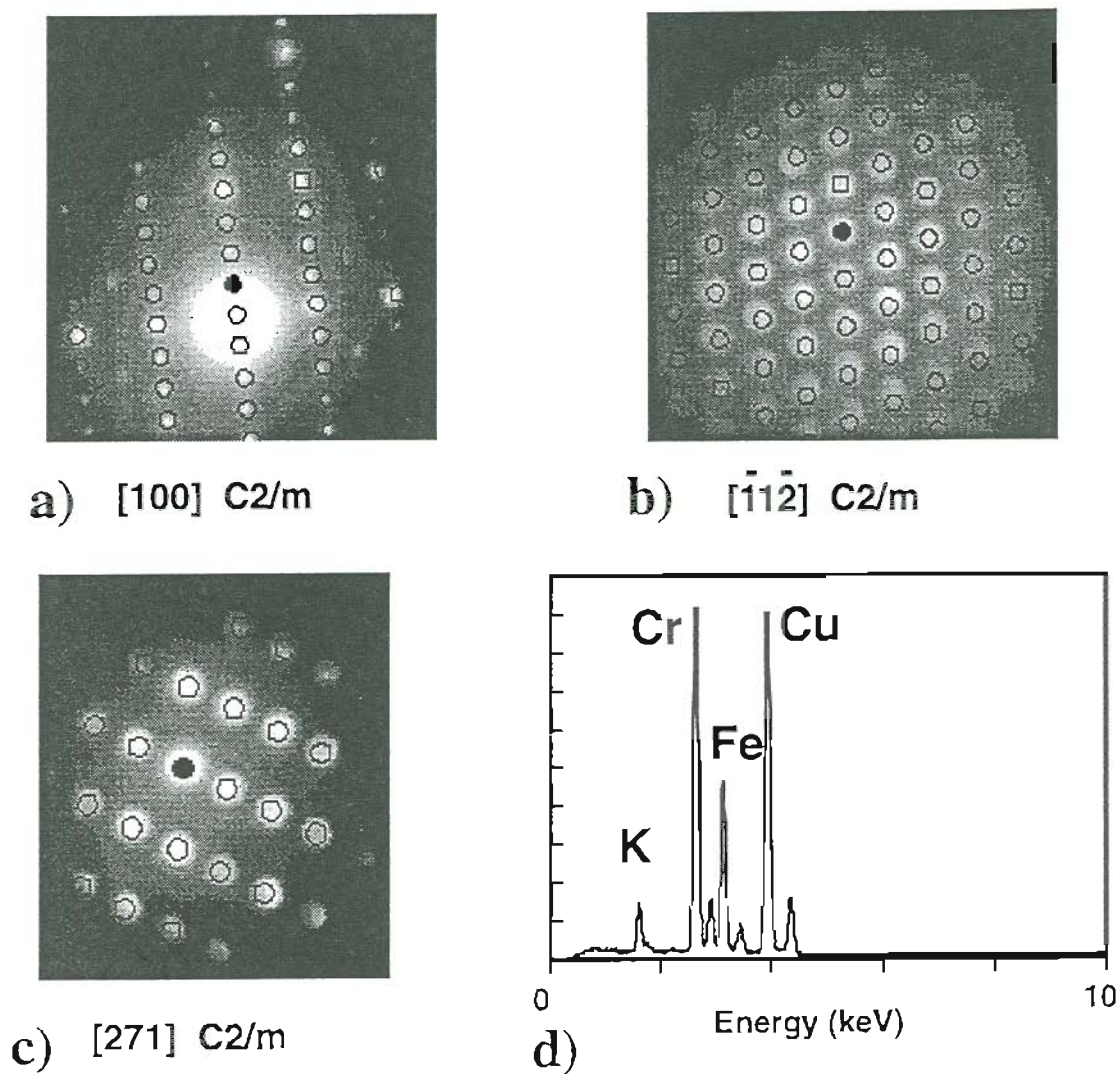


Figure 2-5. TEM electron diffraction patterns and EDS spectrum of $\text{KFe}(\text{CrO}_4)_2 \cdot 2\text{H}_2\text{O}$ crystals precipitated in soil fractures. a) - c) electron diffraction patterns, circles superimposed over the electron diffraction patterns are the theoretical patterns for $\text{KFe}(\text{CrO}_4)_2 \cdot 2\text{H}_2\text{O}$; d) EDS spectrum, the Cu peaks are from the brass specimen holder.

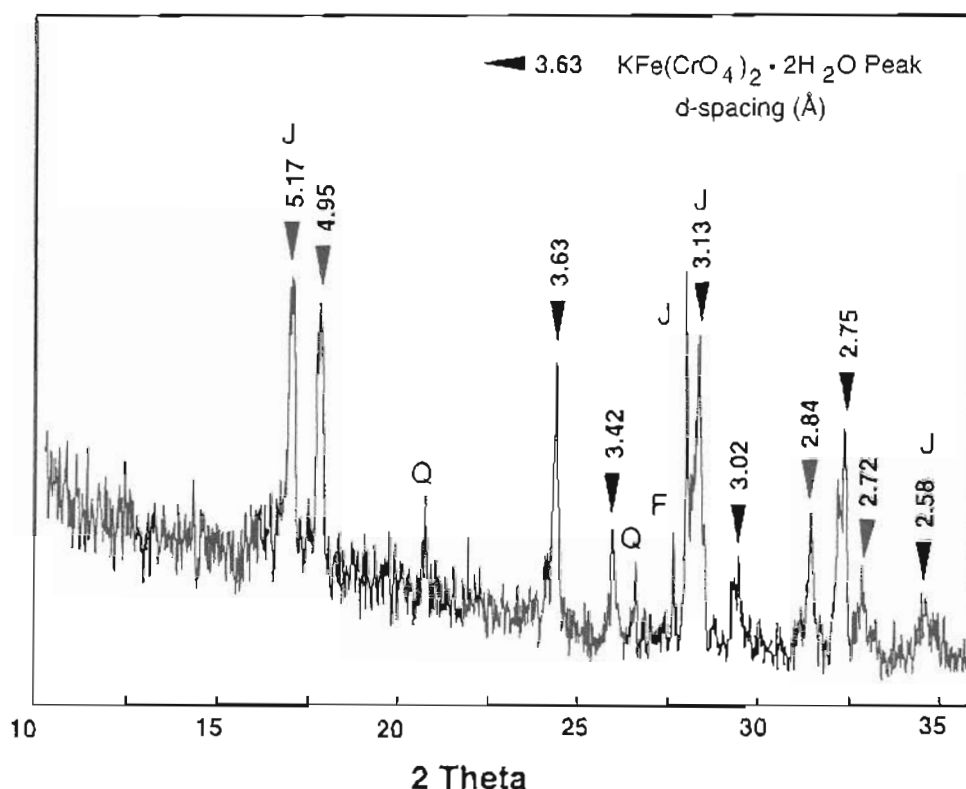


Figure 2-6. Powder x-ray diffraction spectrum of crystals precipitated in soil fractures. Peaks associated with $\text{KFe}(\text{CrO}_4)_2 \cdot 2\text{H}_2\text{O}$ are marked with corresponding d-spacings. Peaks corresponding to $\text{KFe}_3(\text{CrO}_4)_2(\text{OH})_6$ (J), quartz (Q) and feldspar (F) are also marked. The $\text{KFe}(\text{CrO}_4)_2 \cdot 2\text{H}_2\text{O}$ peaks for the d-spacings of 3.13 and 5.16 Å coincide with the main $\text{KFe}_3(\text{CrO}_4)_2(\text{OH})_6$ peaks.

$\text{KFe}(\text{CrO}_4)_2 \cdot 2\text{H}_2\text{O}$. Although traces of the underlying bulk soil were present in the sample for XRD analysis, the XRD scan confirms that the crusts are composed primarily of $\text{KFe}(\text{CrO}_4)_2 \cdot 2\text{H}_2\text{O}$.

2.4 Discussion

$\text{KFe}_3(\text{CrO}_4)_2(\text{OH})_6$ is the structural analog of jarosite ($\text{KFe}_3(\text{SO}_4)_2(\text{OH})_6$), a mineral that commonly occurs in acid sulfate soils (Wagner et al., 1982; Carson and Dixon, 1983) and acid mine drainage (Chapman et al., 1983; Alpers et al., 1989). We are not aware

Table 2-2. Comparison of d-spacings from crusts in soil fractures with d-spacings reported by Bonnin (1970) for synthetic $\text{KFe}(\text{CrO}_4)_2 \cdot 2\text{H}_2\text{O}$.

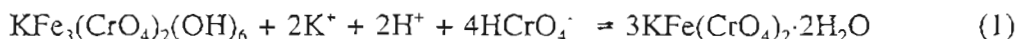
synthetic $\text{KFe}(\text{CrO}_4)_2 \cdot 2\text{H}_2\text{O}$ (Bonnin, 1970)			Crusts in Fractures	
h,k,l	d-spacing (Å)	rel. Int.	d-spacing (Å)	rel. Int.
2 0 $\bar{1}$	5.17	s	5.16	88
2 0 $\bar{2}$	4.95	s	4.95	78
1 1 $\bar{2}$	3.63	s	3.63	78
2 0 $\bar{3}$	3.42	w	3.42	34
1 1 1	3.13	vs	3.13	100
3 1 $\bar{2}$	3.02	m	3.02	31
3 1 $\bar{3}$	2.83	m	2.84	44
0 2 0	2.75	m	2.75	75
3 1 $\bar{1}$ }	2.71	m	2.72	31
4 0 $\bar{3}$ }				
1 1 $\bar{1}$	2.584	w	2.58	22

vs strongest peak
s strong peak
m medium peak
w weak peak

of any naturally occurring sulfate analog to $\text{KFe}(\text{CrO}_4)_2 \cdot 2\text{H}_2\text{O}$. Although both of these chromate phases have been synthesized and described, to our knowledge, this study is the first reported identification in the environment. Although two ferric-chromate phases are present in the contaminated soil, the absence of $\text{KFe}(\text{CrO}_4)_2 \cdot 2\text{H}_2\text{O}$ peaks in the XRD of the whole soil indicates that most of the Cr(VI) has precipitated as the chromate analog of jarosite. $\text{KFe}(\text{CrO}_4)_2 \cdot 2\text{H}_2\text{O}$ is found only in fractures, the preferred flow paths within the saturated soil.

There are no published thermodynamic data for either the chromate analog of jarosite nor $\text{KFe}(\text{CrO}_4)_2 \cdot 2\text{H}_2\text{O}$ that we can use to constrain the conditions under which they are likely to form. However, the occurrence of the chromate analog of jarosite in

an acid-chromate environment is consistent with the common occurrence of jarosite in acid-sulfate environments. Assuming that all the available Fe(III) in the soil is bound by these chromate phases, the conversion of $\text{KFe}_3(\text{CrO}_4)_2(\text{OH})_6$ to $\text{KFe}(\text{CrO}_4)_2 \cdot 2\text{H}_2\text{O}$ by



indicates that $\text{KFe}(\text{CrO}_4)_2 \cdot 2\text{H}_2\text{O}$ forms in more acidic, more Cr(VI)-enriched waters than those in which $\text{KFe}_3(\text{CrO}_4)_2(\text{OH})_6$ is stable. As acidic plating solutions entered the subsurface along preferred pathways, $\text{KFe}(\text{CrO}_4)_2 \cdot 2\text{H}_2\text{O}$ was the phase initially precipitated from the contaminated groundwater. Cr(VI) and H^+ were primarily from the plating solutions. K^+ was derived from both the plating solution and as an exchangeable cation from the native soil. Fe(III) could have been derived from steel corrosion products in the plating solutions or obtained from naturally occurring iron oxides and hydroxides within the native soil. Although the XRD scan of the soil did not identify iron (oxy)-hydroxides as one of the major soil constituents, ammonium oxalate and dithionate, citrate, bicarbonate (DCB) extractions indicate that the soil contains about 0.004 mg/g of iron as amorphous hydroxides and about 3 mg/g of iron as crystalline oxides and hydroxides (Palmer and Wittbrodt, 1990). As the remaining solutes in the contaminated groundwater migrated farther into the sediments, the pH continued to increase due to dilution and the buffer intensity of the soil. Eventually, Cr(VI) and H^+ concentrations decreased to a level where the chromate analog of jarosite became the stable phase. This hypothesis is consistent with the observed spatial distribution of the phases in the soil, the increasing pH with distance from the source, high Cr(VI) concentrations, and the low Fe concentration observed even in the most acidic waters.

The potential impact of these iron-chromate phases on Cr(VI)-mobility and the remediation of Cr(VI)-contaminated soil is difficult to assess at this time. Key parameters that are needed include solubility data, the quantity of each phase within the soil, and the time scales for the precipitation and dissolution of these phases. A further complicating factor is the potential formation of solid solutions, particularly with sulfate. Sulfate is a common groundwater constituent and is present in the plating solutions. The equivalent

charge, similar structure, and comparable thermochemical radii of chromate and sulfate suggest that solid solutions between these ferric-chromate phases and their sulfate analogues could also form. The aqueous Cr(VI) concentrations in solutions equilibrated with such solid solutions could be dramatically different from concentrations in solutions equilibrated with the pure chromate phases.

2.4 Summary and Conclusions

Two ferric-chromate precipitates were identified in the chromium contaminated soil. $\text{KFe}_3(\text{CrO}_4)_2(\text{OH})_6$ was found as small crystals interspersed within the bulk soil. $\text{KFe}(\text{CrO}_4)_2 \cdot 2\text{H}_2\text{O}$ forms crusts in cracks and fractures of the soil. The discovery of these ferric-chromate phases is a key step in identifying relevant geochemical processes that affect Cr(VI) mobility and impact proposed cleanup operations. Thermodynamic and kinetic studies are needed to determine the potential effect of these phases on the mobility of Cr(VI) in the subsurface. Ultimately, these results should aid in the rational design of cost-effective remediation of chromate-contaminated soils, sediments, and groundwater.

2.6 References

- Alpers C.N., Nordstrom D.K., and Ball J.W. (1989) Solubility of jarosite solid solutions precipitated from acid mine water, Iron Mountain, California, U.S.A.. *Sci. Géol., Bull.* **42**, 281-298.
- Bonnin A. (1970) Préparations et étude de chromates de fer. Ph.D. Dissertation, Univ. Rennes, France.
- Bonnin A. and Lecerf A. (1966) Deux nouveaux chromates de fer: FeCrO_4OH et $\text{KFe}_3(\text{CrO}_4)_2(\text{OH})_6$. *C. R. Seances Acad. Sci. Paris, Sér. C* **262**, 1782-1784.
- Calder L.M. (1988) Chromium contamination in groundwater. In: *Chromium in the Natural and Human Environments* (eds. J.O. Nriagu and E. Nieboer), 215-230. John Wiley and Sons, New York.
- Carson C.D and Dixon J.B. (1983) Mineralogy and acidity of an inland acid sulfate soil of Texas. *Soil Sci. Soc. Am. J.* **47**, 828-833.

Chapman B.M., Jones D.R., and Jung R.F. (1983) Processes controlling metal ion attenuation in acid mine drainage streams. *Geochim. Cosmochim. Acta* **47**, 1957-1973.

CH2M Hill (1990) *Deep Aquifer Data Report, United Chrome Products Site, Corvallis, Oregon* CH2M Hill, Corvallis, OR.

Cudennec Y., Riou A., Bonnin A., and Caillet P. (1980) Études cristallographiques et infrarouges d'hydroxychromates de fer et d'aluminium de structure alunite. *Rev. Chim. Minér.* **17**, 158-167.

Fernald E.H. (1984) Chromium plating. In *Metal Finishing, Guidebook Directory Issue '84* (eds. P.H. Langdon, P.A. Crispino, and S.L. Condgon), 200-210. Metal and Plastics Publications, Inc., Hackensack, NJ.

Gravereau P. and Hardy A. (1972) La série $M^I M^{III} (XO_4)_2 \cdot nH_2O$: structure cristalline de $KFe(CrO_4)_2 \cdot 2H_2O$, nouveau type dans la série des chromates des fer dihydratés. *Acta Crystallogr. Sec. B* **28**, 2333-2337.

McKinley W.S., Pratt R.C., and McPhillips L.C. (1992) Cleaning up chromium. *Civ. Eng.* **62**, 69-71.

Mellier A. and Gravereau P. (1972) Spectres de vibration infrarouge à bases températures de chromates doubles métalliques dihydratés de type $M_1 Fe(CrO_4)_2 \cdot 2H_2O$ avec $M_1 = Na, K, Tl$. *C. R. Seances Acad. Sci. Paris, Sér. B* **274**, 1024-1027.

Palmer C.D. and Wittbrodt P.R. (1991) Processes affecting the Remediation of chromium-contaminated sites. *Environ. Health. Perspect.* **92**, 25-40.

Palmer C.D. and Wittbrodt P.R. (1990) Geochemical Characterization of the United Chrome Products Site, Final Report. In *Stage 2 Deep Aquifer Drilling Technical Report, United Chrome Products Site, Corvallis, OR* CH2M-Hill, Corvallis, OR.

Powers D.A., Rossman G.R., Schugar H.J., and Gray H.B. (1975) Magnetic behavior and infrared spectra of jarosite, basic iron sulfate, and their chromate analogs. *J. Solid State Chem.* **13**, 1-13.

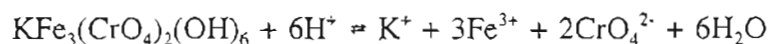
Townsend M.G., Longworth G., and Roudout E. (1986) Triangular-spin, kagome plane in jarosites. *Phys. Rev. B* **33**, 4919-4926.

Wagner D.P., Fanning D.S., Foss, J.E., Patterson, M.S., and Snow P.A. (1982) Morphological and mineralogical features related to sulfide oxidation under natural and disturbed land surfaces in Maryland. In *Acid Sulfate Weathering* (ed. Kittrick J.A.), 109-125. Soil Sci. Soc. Am.; Spec. Publ. 10: Madison, WI.

CHAPTER 3

Solubility of $\text{KFe}_3(\text{CrO}_4)_2(\text{OH})_6$ at 4 - 35°C

The solubility of $\text{KFe}_3(\text{CrO}_4)_2(\text{OH})_6$, the chromate analog of the sulfate mineral jarosite, was studied in a series of dissolution experiments. Experiments were conducted at 4-35°C and pH values between 1.5 and 3.0 using synthetic $\text{KFe}_3(\text{CrO}_4)_2(\text{OH})_6$. The solids were kept in the reaction vessel for up to 6 months. Equilibrium was established in the experiments after between 2 and 4 months. The log K_{sp} for the dissolution reaction of $\text{KFe}_3(\text{CrO}_4)_2(\text{OH})_6$



at 25°C is -18.7 ± 0.5 . Based on this measured solubility product, the free energy of formation, $\Delta G_{f,298}^0$, is $-3307.4 \pm 2.9 \text{ kJ mol}^{-1}$. The dissolution experiments at 25°C indicate the formation of a FeCrO_4^+ ion pair with a log $K_{\text{FeCrO}_4^+} = 8.0 \pm 0.1$. This result combined with previously published spectroscopic data between 0 and 25°C yields a formation constant of the form $2.303 \log K_{\text{FeCrO}_4^+} = -\Delta H^0/RT + \Delta S^0/R$, where $\Delta H^0 = 19.1 \pm 2.2 \text{ kJ mol}^{-1}$ and $\Delta S^0 = 214 \pm 8 \text{ J K}^{-1} \text{ mol}^{-1}$. The equilibrium ion activity products calculated from the experiments at 4, 15, 25 and 35°C do not show a statistically significant trend indicating a weak temperature dependence of the solubility product over the temperature range of the experiments. The rate of the dissolution reaction can be described by a first order model. The measured solubility indicates that the chromate analog of jarosite is stable over a wide range of conditions and could form in large parts of a Cr(VI)-contaminated aquifer.

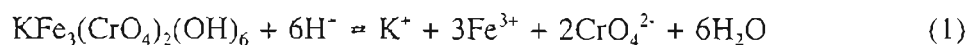
3.1 Introduction

Chromate-laden solutions released into soils by leakage from industrial facilities or by improper waste disposal practices can alter the chemical environment of native soils resulting in the dissolution of soil minerals and the precipitation of new phases that incorporate Cr(VI). The formation of these precipitates can affect Cr(VI) mobility, control its concentration in subsurface waters, and may limit its bioavailability. Identifying such precipitates and determining the conditions under which they form and remain stable can improve our estimates of the potential risks to human health and the environment at contaminated sites and can greatly contribute to the rational design of remediation systems. This study focusses on one such precipitate, $\text{KFe}_3(\text{CrO}_4)_2(\text{OH})_6$, which has recently been identified in chromium contaminated soils (Baron et al., 1995). We report here on a study of the solubility of $\text{KFe}_3(\text{CrO}_4)_2(\text{OH})_6$ under the acidic and low temperature conditions typical for the environment where this solid has been observed to form.

$\text{KFe}_3(\text{CrO}_4)_2(\text{OH})_6$ is the structural analog of jarosite ($\text{KFe}_3(\text{SO}_4)_2(\text{OH})_6$) (Bonnin and Lecerf, 1966; Powers et al., 1975; Cudennec et al., 1980), a common mineral in acid sulfate soils (Van Breemen, 1973; Carson and Dixon, 1983) and acid mine drainage (Chapman et al., 1983; Alpers et al., 1989). The chromate analog of jarosite is a member of the alunite-jarosite group of isostructural minerals described by the general formula $\text{AB}_3(\text{XO}_4)_2(\text{OH})_6$ where A sites are occupied by a large cation in 12-fold coordination, most commonly K^+ , Na^+ and H_3O^+ (hydronium) (Parker, 1962; Kubisz, 1964; Brophy and Sheridan, 1965), while B sites are occupied by a cation in octahedral coordination, most commonly Fe^{3+} (jarosites) and Al^{3+} (alunites). A small amount of Cr^{3+} substitution on the B position has been observed in a natrojarosite precipitated from a Cr^{3+} -containing solution (Saarinen, 1977) and jarosites with a complete Cr^{3+} substitution on the B position have been synthesized (Townsend et al., 1986; Ramirez et al., 1993). The anion position is usually occupied by SO_4^{2-} , but substitution by PO_4^{3-} , AsO_3^{3-} , CO_3^{2-} , SbO_4^{3-} , CrO_4^{2-} , SiO_4^{4-} (Scott, 1987) and SeO_4^{2-} (Dutrizac et al., 1981) has also been reported. Both natural and synthetic jarosites often have a significant amount of H_3O^+ -substitution on the alkali position (Brophy and Sheridan, 1965; Kubisz, 1970; Dutrizac and Kaiman, 1976).

A deficiency in Fe with values for the Fe:SO₄ molar ratio significantly lower than the ideal 3:2 stoichiometry is also common (Kubisz, 1970; Härtig et al., 1984; Ripmeester et al., 1986; Alpers et al., 1989; Baron and Palmer, 1995).

KFe₃(CrO₄)₂(OH)₆ has been synthesized and described (Bonnin and Lecerf, 1966; Powers et al., 1975; Cudennec et al., 1980; Townsend et al., 1986) and it has been suggested that a complete solid solution series exists between jarosite and its chromate analog (Dutrizac, 1984). Although there has been speculation about conditions under which the chromate analog of jarosite could form (Kulp and Adler, 1950) it had not been found in the environment until its recent discovery in Cr(VI)-contaminated soils (Baron et al., 1995). The purpose of this study is to measure the solubility of KFe₃(CrO₄)₂(OH)₆ and to determine the solubility product (K_{sp}) for the dissolution reaction of the chromate analog of jarosite



at the acidic conditions and low temperatures typical for the environment where this solid has been observed to form. This information is required to determine the range of conditions under which the chromate analog of jarosite is stable and the extent to which it may affect the mobility of Cr(VI) in subsurface environments and interfere with the remediation of Cr(VI)-contaminated soil and groundwater.

3.2 Experimental Methods

3.2.1 Synthesis of KFe₃(CrO₄)₂(OH)₆

Synthetic KFe₃(CrO₄)₂(OH)₆ used in the experiments was prepared by dissolving 4.85 g of Aldrich 98% reagent grade K₂CrO₄ and 10.1 g of Aldrich reagent grade Fe(NO₃)₃·9H₂O in 100 ml H₂O at 95°C, 1 atm. To achieve a controlled mixing, the chromate and the nitrate were each dissolved in 45 ml of H₂O. The solutions were then slowly (approximately 30 ml/hour) added to a covered beaker on a hot plate with an initial 10 ml of H₂O and continuously stirred. After four hours, the precipitate was allowed to settle and the residual solution was decanted. The precipitate was then washed

thoroughly with ultrapure water (18 megaohm cm) and dried at 110°C for 24 hrs.

3.2.2 Characterization of Synthetic $\text{KFe}_3(\text{CrO}_4)_2(\text{OH})_6$

The synthetic solid was characterized using powder x-ray diffraction (XRD), scanning electron microscopy with energy dispersive spectroscopy (SEM/EDX), Fourier Transform Infrared Spectroscopy (FTIR), and thermogravimetric analysis (TGA). A small amount of the precipitate was digested in HCl and analyzed for K and Fe using atomic absorption spectroscopy (AAS) and Cr(VI) using the diphenylcarbazide method.

3.2.3 Dissolution Experiments

Two sets of dissolution experiments were implemented. The first set was conducted at 25°C and the starting pH was varied between 1.5 and 3.0. In the second set of experiments, the temperature was varied between 4 and 35°C with an initial pH of 2.0 for all experiments. For the dissolution experiments, 5 to 30 mg of the synthetic $\text{KFe}_3(\text{CrO}_4)_2(\text{OH})_6$ were added to ultrapure water with the pH adjusted to the desired value using reagent grade perchloric acid. To avoid the potential formation of Fe(III)-hydroxides at the higher pH values, 5.0×10^{-4} and 2.5×10^{-3} M of CaCrO_4 (Johnson Matthey, 99.5%) were added to the experiments with initial pH 2.6 and 3.0, respectively. Calcium chromate was chosen because Ca^{2+} , unlike many other cations, is not expected to be incorporated in the jarosite crystal structure. The solutions were placed in 20 ml glass vials and were stirred with a stirbar at a moderate rate (about 100 rpm) to provide good mixing. The temperatures were maintained to within 0.1°C of the desired value using circulating water baths. The experiment with initial pH 2 and at 25°C was conducted prior to the other experiments to establish the approximate time required to achieve equilibrium. To allow more frequent sampling and analysis for K_{tot} , Fe_{tot} , $\text{Cr(VI)}_{\text{tot}}$ and pH for every sample, this experiment was conducted with 100 mg of synthetic jarosite in 500 ml of ultrapure water in polyethylene bottles. The starting conditions for all dissolution experiments are listed in Table 3-1. All experiments were conducted in triplicate. The experiments were sampled in regular intervals to determine when equilibrium had been achieved. Ten samples were collected from the experiments

in which the pH was varied and 9 samples was collected from the experiments in which the temperature was varied. For each sample, 1 ml of the jarosite suspension was withdrawn. The samples were filtered using a 0.1µm filter to remove suspended solids. They were then analyzed for potassium using AAS. After the K concentration had not changed significantly (± 5 percent) for at least three consecutive samples, a 4 ml sample was taken and analyzed for pH, Fe_{tot} and K_{tot} using AAS, and $\text{Cr(VI)}_{\text{tot}}$ using the diphenylcarbazide method. Since the dissolution experiments were conducted in an oxidizing perchloric acid solution and reductants capable of reducing ferric iron were not present in the solution, it was assumed that all the iron was present as ferric iron.

Table 3-1. Initial experimental conditions.

	amount of solution (ml)	amount of solid (mg)	initial pH	Temperature (°C)	[CaCrO ₄] (mol/l)
KCRJAR-1.5	20	30	1.50	25	-
KCRJAR-2.0	500	200	2.00	25	-
KCRJAR-2.3	20	5	2.30	25	-
KCRJAR-2.6	20	5	2.60	25	5.0×10^{-4}
KCRJAR-3.0	20	5	3.00	25	2.5×10^{-3}
KCRJAR-4C	20	5	2.00	4	-
KCRJAR-15C	20	5	2.00	15	-
KCRJAR-35C	20	5	2.00	35	-

All experiments were conducted in triplicate.

3.3 Results

3.3.1 Solid Characterization

The red (2.5YR 4/8) precipitate produced in the synthesis was identified as the chromate analog of jarosite by comparing powder x-ray diffraction patterns with those for $\text{KFe}_3(\text{CrO}_4)_2(\text{OH})_6$ reported in JCPDS card 20-894 (JCPDS, 1994) (Table 3-2, Figure 3-1).

Table 3-2. Powder X-ray diffraction peaks from synthetic $\text{KFe}_3(\text{CrO}_4)_2(\text{OH})_6$ used in dissolution experiments.

h,k,l	$\text{KFe}_3(\text{CrO}_4)_2(\text{OH})_6$ Bonnin and Lecerf (1966) (JCPDS Card 20-894)		XRD-Synthetic $\text{KFe}_3(\text{CrO}_4)_2(\text{OH})_6$ used in this study	
	d-spacing (Å)	relative Intensity	d-spacing (Å)	relative Intensity
1 0 1	6.04	12	6.09	17
0 0 3	5.82	8	5.86	17
0 1 2	5.18	33	5.19	41
1 1 0	3.715	11	3.72	25
1 0 4	3.617	2		
0 2 1	3.166	100	3.17	96
1 1 3	3.127		3.136	100
0 1 5	3.071	1		
2 0 2	3.02	7	3.034	19
0 0 6	2.908	15	2.917	20
0 2 4	2.588	8	2.593	13
1 2 2	2.325	20	2.327	28
0 1 8	2.067	<1		
0 3 3	2.013	25	2.018	35
0 2 7	1.971	3		
0 0 9	1.938	4		
2 2 0	1.858	24	1.857	33
2 0 8	1.805	<1		
2 2 3	1.770	<1		
3 1 2	1.750	5	1.751	12
2 1 7	1.741		1.746	12
1 1 9	1.720	4	1.723	17
1 3 4	1.652	2		
1 2 8	1.624	4	1.625	8
4 0 1	1.6013	5	1.603	7
3 1 5	1.5871	6	1.587	11
0 4 2	1.5788		1.576	13

All the peaks produced by the precipitate could be identified as $\text{KFe}_3(\text{CrO}_4)_2(\text{OH})_6$ peaks. The absence of unidentified peaks indicates that no other crystalline phases are present

in the precipitate at detectable levels. $\text{KFe}_3(\text{CrO}_4)_2(\text{OH})_6$ has a hexagonal structure and crystallizes in space group $R\bar{3}m$ (Bonnin and Lecerf, 1966). Using the measured d-spacings and a least-squares procedure, the unit cell dimensions were calculated as $a_0 = 7.427 \pm 0.006 \text{ \AA}$ and $c_0 = 17.50 \pm 0.04 \text{ \AA}$, which is in excellent agreement with the $a_0 = 7.430 \text{ \AA}$ and $c_0 = 17.44 \text{ \AA}$ reported in JCPDS card 20-894. Examination with SEM/EDX showed that the precipitate consists of uniform, K, Fe and Cr containing multicrystalline particles, ranging in size from 20-250 μm . No secondary crystalline or amorphous phases were observed.

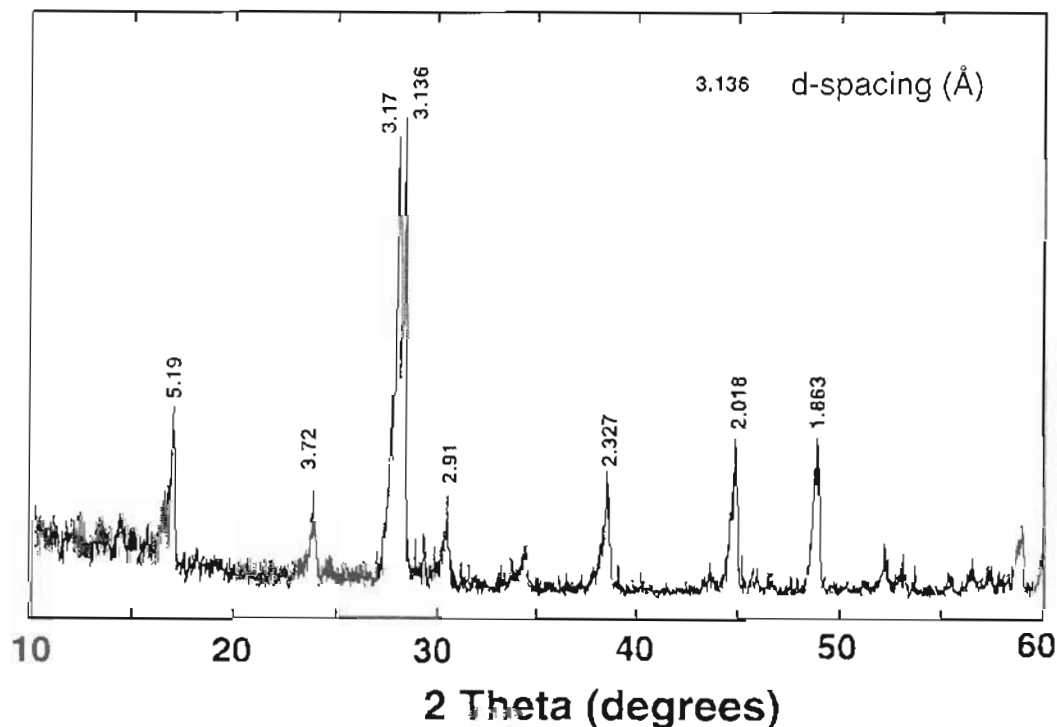


Figure 3-1. Powder x-ray diffraction pattern of synthetic $\text{KFe}_3(\text{CrO}_4)_2(\text{OH})_6$ used in this study. Some of the strongest peaks and the corresponding d-spacings are indicated.

Wet chemical analysis yielded a composition of the precipitate very close that of 'ideal' endmember $\text{KFe}_3(\text{CrO}_4)_2(\text{OH})_6$ with a K:Fe:CrO₄ ratio of 0.95:2.98:2 compared to the ideal 1:3:2 ratio. The deviations from the ideal formula are within the analytical error

of approximately 5 percent. The synthetic $\text{KFe}_3(\text{CrO}_4)_2(\text{OH})_6$ does not have a non-ideal stoichiometry as is commonly observed in both natural and synthetic jarosites which often show a significant amount of hydronium substitution of the alkali position (BROPHY and Sheridan, 1965; Kubisz, 1964; Dutrizac and Kaiman, 1976) and an Fe deficiency (Kubisz, 1970; Alpers et al., 1989; Baron and Palmer, 1995).

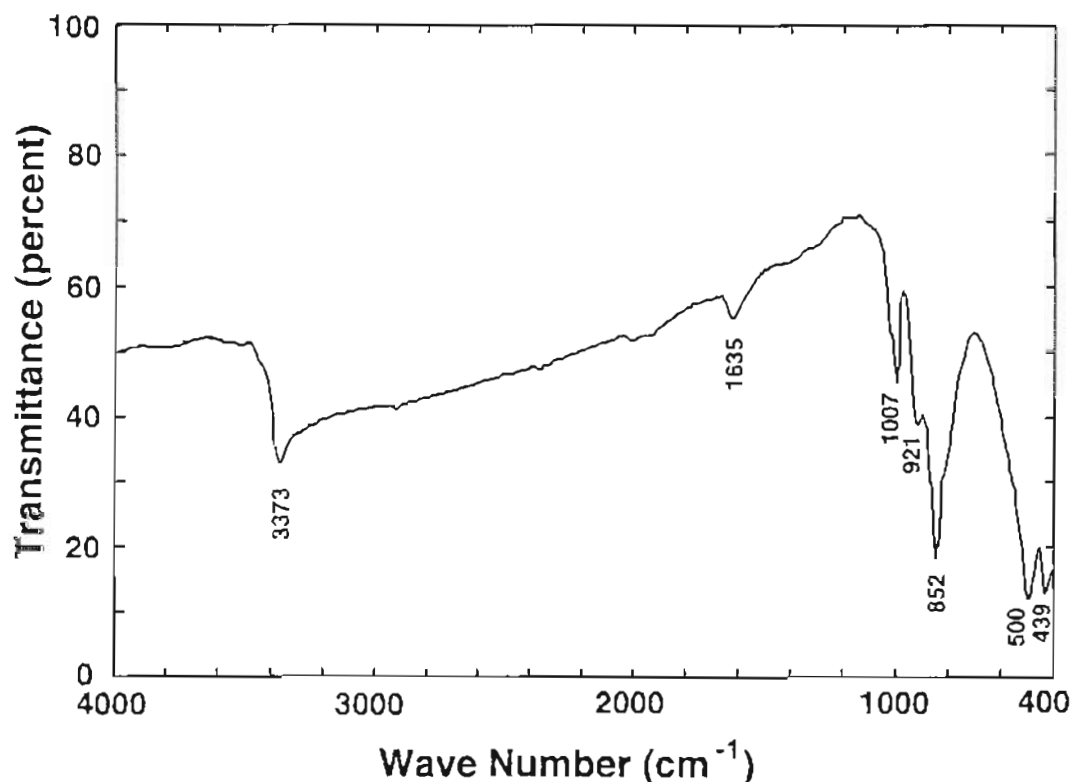


Figure 3-2. FTIR spectrum of the synthetic $\text{KFe}_3(\text{CrO}_4)_2(\text{OH})_6$. The main vibrational bands in the spectrum are marked. They correspond to (Powers et al., 1975) the O-H stretch (3373 cm^{-1}), HOH deformation (1635 cm^{-1}), OH deformation (1007 cm^{-1}), the ν_3 mode of CrO_4^{2-} (921 and 852 cm^{-1}), and to the vibrations of the FeO_6 coordination octahedron (500 and 439 cm^{-1}).

Comparison of the FTIR spectrum of the precipitate (Figure 3-2) with a reported scan of $\text{KFe}_3(\text{CrO}_4)_2(\text{OH})_6$ (Powers et al., 1975) confirmed the identification as the chromate analog of jarosite and the absence of other phases in the precipitate. The only easily identifiable peak associated with hydronium in jarosites lies in the $1535\text{-}1575 \text{ cm}^{-1}$

region as a weak peak on the shoulder of stronger peak at $1635\text{--}1640\text{ cm}^{-1}$ associated with water (Kubisz, 1972; Wilkins et al., 1974). The absence of this peak in the spectrum confirms that there is no significant hydronium in the crystal structure of the synthetic $\text{KFe}_3(\text{CrO}_4)_2(\text{OH})_6$.

Based on these analyses, the precipitate was identified as a $\text{KFe}_3(\text{CrO}_4)_2(\text{OH})_6$ with a composition very close to the ideal stoichiometry. There is no indication of any other phases in the precipitate.

The results of the thermogravimetric analysis of the synthetic $\text{KFe}_3(\text{CrO}_4)_2(\text{OH})_6$ heated from 30 to 900°C at a rate of $20^\circ\text{C}/\text{min}$ are shown in Figure 3-3. Curve A shows the weight loss with increasing temperature and curve B its derivative. The total weight loss over the interval is 19.0 weight percent. The derivative curve shows that weight loss occurs in three main intervals: (1) a small loss of about 1.5 weight percent between 200 and 280°C , represented by a peak at 250°C , (2) the major weight loss of 10.5 % between 280 and 380°C , represented by a peak at 345°C , and (3) a final 7.0 % weight loss between 400 and 620°C , represented by a peak at 450°C and a small peak at 600°C .

The weight loss in the interval between 200 and 280°C is analogous to a small weight loss commonly observed in jarosites (Kubisz, 1972; Härtig et al., 1984; Alpers et al., 1989; Baron and Palmer, 1995). It represents the loss of small amounts of absorbed water and "excess" water in the jarosite crystal structure. Excess water consists of small amounts of hydronium substituting for potassium and small amounts of water substituting for OH^- to balance the deficit of positive charges caused by Fe-deficiencies (Kubisz, 1972; Härtig et al., 1984; Baron and Palmer, 1995). Based on the thermal decomposition of jarosite (Baron and Palmer, 1995), we suspect that the weight loss in the interval between 280 and 380°C represents the breakdown of $\text{KFe}_3(\text{CrO}_4)_2(\text{OH})_6$ into potassium and iron chromate, iron oxide and water according to



The observed weight loss of 10.5 % is in good agreement with the loss of 10.0 % expected from equation (2). The final weight losses between 400 and 620°C represent

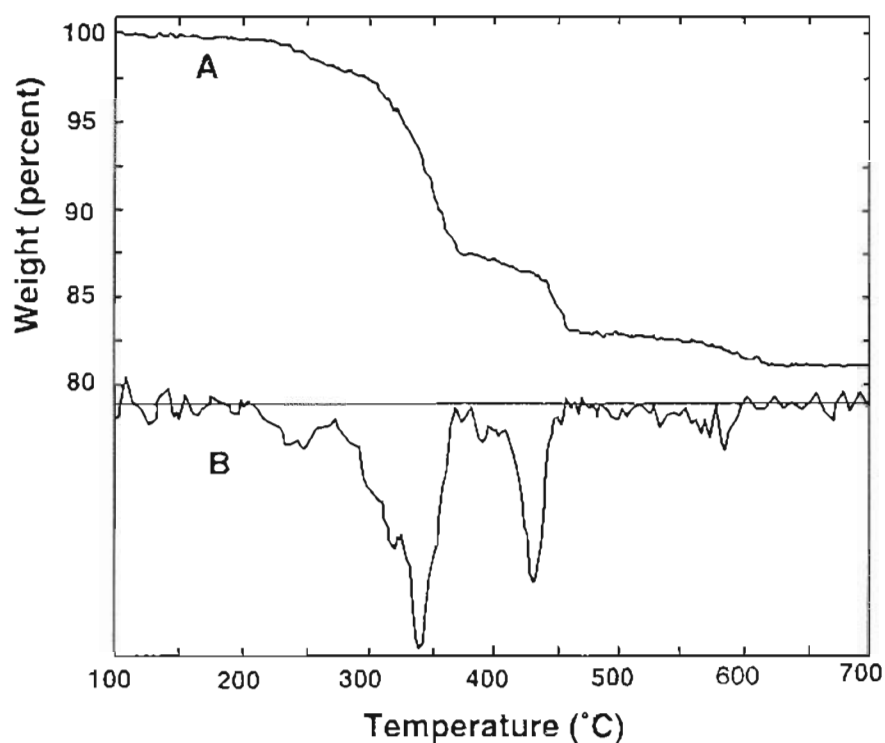
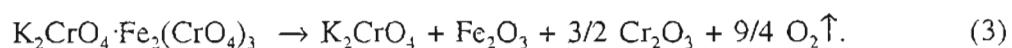


Figure 3-3. Thermogravimetric analysis of synthetic $\text{KFe}_3(\text{CrO}_4)_2(\text{OH})_6$, (A) percent weight loss versus temperature, and (B) derivative.

the further breakdown of $\text{K}_2\text{CrO}_4 \cdot \text{Fe}_2(\text{CrO}_4)_3$ into K_2CrO_4 , Fe_2O_3 and CrO_3 . The CrO_3 produced by this breakdown is subsequently transformed to Cr_2O_3 and O_2 (Cotton and Wilkinson, 1988), resulting in the overall reaction



The observed weight loss of 7.0 % is in good agreement to the 6.7 % weight loss expected from equation (3).

3.3.2 Dissolution Experiments

In the dissolution experiments, the bulk of the reaction occurred within the first week of the experiment with rates declining over time. For example, the evolution of the

solution composition over time in the dissolution experiment at 25°C, initial pH 2 (KCRJAR-2.0) shows a rapid increase over the first 100 hours reaching approximately 80 % of the equilibrium value while the remaining 20 % required an additional 600 to 800 hours (Figure 3-4). Equilibrium was reached in the dissolution experiments after between approximately 40 to 105 days (Table 3-3). The equilibrium compositions of the solutions in the dissolution experiments are summarized in Table 3-3. The complete analytical results for the final sample from the triplicate experiments are summarized in Table A-1 in Appendix A. Based on the measured equilibrium pH, K_{tot} , Fe_{tot} and $\text{Cr(VI)}_{\text{tot}}$, equilibrium aqueous activities of K^+ , Fe^{3+} , and CrO_4^{2-} were calculated using the geochemical speciation model MINTEQA2 (Allison et al., 1990) (Table 3-5). Activity corrections were made using the Davies Equation. Thermodynamic data used in the calculations are listed in Table 3-4. If the dissolution reaction of the chromate analog of jarosite is written as in equation (1), then the log ion activity product (IAP) is given by

$$\log \text{IAP} = \log\{\text{K}^+\} + 3 \log\{\text{Fe}^{3+}\} + 2 \log\{\text{CrO}_4^{2-}\} + 6 \log\{\text{H}_2\text{O}\} + 6 \text{pH} \quad (4)$$

where { } denotes activity. At equilibrium, the IAP is equal to the solubility product, K_{sp} . Based on the calculated activities of H^+ , K^+ , Fe^{3+} , and CrO_4^{2-} , the equilibrium IAP was calculated using equation (4). The results of these calculations are presented in Table 3-5. The average charge balance error in the MINTEQA2 simulations was 3 percent. The errors associated with the log IAP values represent the standard deviation from the triplicate experiments. The analytical error calculated from the precision of the analytical measurements ($\pm 10\%$) and the precision of the pH buffer solutions (± 0.02 pH units) is ± 0.25 log units (assuming that the covariance between these parameters equals zero). In general, the error from the triplicate experiments is in the same range as the analytical error, indicating that the error from the triplicate experiments represents the analytical error. The error reported with the log IAP values is the error from the triplicate experiments. However, in the cases where the error from the triplicate experiments is smaller than the analytical error, the analytical error is reported as the error associated with the log IAP values.

Table 3-3. Final concentrations in the dissolution experiments.

	pH final	[Cr(VI)] _{tot} (mmol L ⁻¹)	[K] _{tot} (mmol L ⁻¹)	[Fe] _{tot} (mmol L ⁻¹)	Equilibrium established after approx. (days)	Experiment Duration (days)
KCRJAR-1.5	1.67±0.06	1.57±0.3	0.832±0.034	2.75 ±0.1	50	166
KCRJAR-2.0	2.13±0.01	0.404±0.002	0.180±0.001	0.540±0.003	40	149
KCRJAR-2.3	2.40±0.01	0.282±0.017	0.117±0.008	0.260±0.014	65	166
KCRJAR-2.6	2.65±0.02	0.550±0.014	0.041±0.005	0.111±0.006	65	166
KCRJAR-3.0	3.05±0.01	2.36±0.23	0.019±0.003	0.021±0.004	85	166
KCRJAR-4C	2.03±0.01	0.389±0.03	0.192±0.008	0.555±0.026	85	176
KCRJAR-15C	2.05±0.01	0.419±0.004	0.200±0.002	0.586±0.005	65	176
KCRJAR-35C	2.09±0.09	0.53±0.13	0.35±0.03	0.93±0.09	105	176

* The reported concentrations represent the mean ± the standard deviation from triplicate experiments.

To evaluate the effect of different activity correction models, ion activity products were also calculated using the extended Debye-Hückel equation. At the low ionic strengths of the experiments, the difference between these two methods is small. For the experiment with the highest ionic strength (0.042 mol/l), the IAP calculated with the extended Debye-Hückel equation is about 0.3 log units higher than the one calculated using the Davies equation. For all other experiments the difference between the IAP calculated with the two methods is less than 0.05 log units. The activity correction models used in this study are described in detail in Appendix B.

3.4 Discussion

The log IAP values calculated from equilibrium activities in the experiments at 25°C and different pH values vary from -18.81 at pH 1.67 to -16.46 at pH 3.05 and show a clear trend of increasing values with increasing pH (Table 3-5, Figure 3-5). This result is unexpected because the equilibrium IAP equals the solubility product, K_{sp} , and should thus be constant. One explanation for the observed behavior and the trend is the

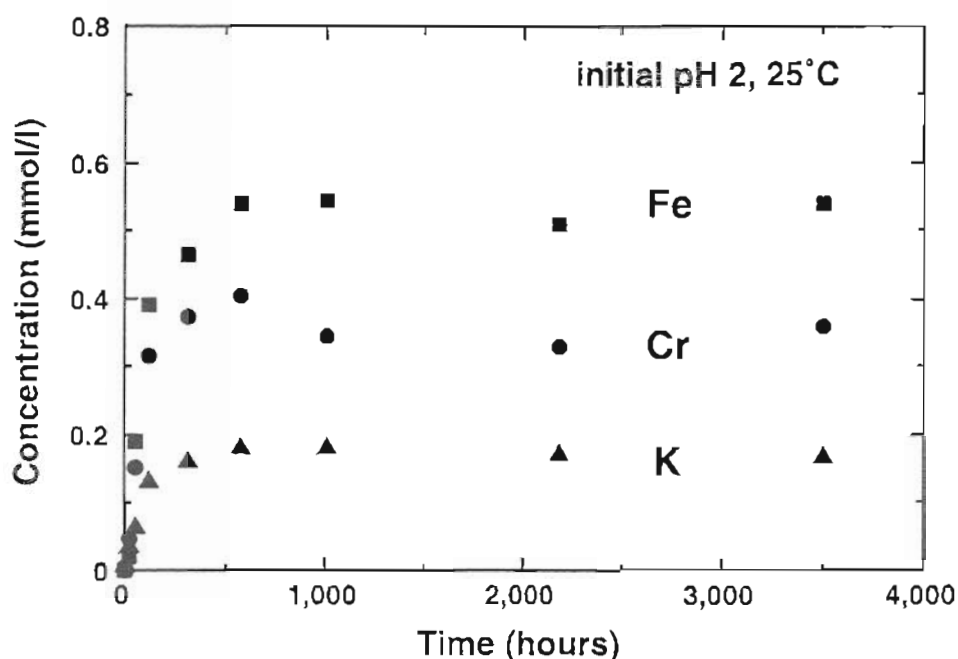


Figure 3-4. Concentration of $[K]_{\text{tot}}$ (▲), $[Fe]_{\text{tot}}$ (■), and $[CrO_4]_{\text{tot}}$ (●) in the dissolution experiment with initial pH 2 at 25°C. Data points represent the average of triplicate experiments.

formation of $Fe(III)-CrO_4^{2-}$ ion pairs that were not included in the speciation model. Little is known about the formation of these ion pairs and they are not included in the MINTEQA2 data base (Allison et al., 1990). As an analogy, the sulfate ion with a very similar thermochemical radius (2.30 Å for sulfate and 2.40 Å for chromate; Waddington, 1959) and equivalent charge is known to form several important ion pairs with $Fe(III)$, including $FeSO_4^+$, $FeHSO_4^{2+}$, and $Fe(SO_4)_2^-$. We therefore included in the MINTEQ database $FeCrO_4^+$, which, based on the analogy to the $Fe-SO_4$ system, appeared to be the most likely ion pair to form. We ran a series of simulations, varying the formation constant, $K_{FeCrO_4^+}$, where

$$\log K_{FeCrO_4^+} = \log\{Fe^{3+}\} + \log\{CrO_4^{2-}\} - \log\{FeCrO_4^+\} \quad (5)$$

Table 3-4. Thermodynamic data used for calculations.

Formula	State	$\Delta G^\circ_{f,298}$ (kJ/mol)	ΔH°_f (kJ/mol)	log K_f	Source
Fe^{3+}	aq	-17.87±1.0	-	-	2
FeCrO_4^+	aq	-	-	8.0	see text for discussion
FeOH^{2+}	aq	-	43.5	-2.19	1
$\text{Fe}(\text{OH})_2^+$	aq	-	71.6	-5.67	4
$\text{Fe}_2(\text{OH})_2^{4+}$	aq	-	56.5	-2.95	1
K^+	aq	-282.5±0.1	-	-	3
KCrO_4^+	aq	-	-	0.799	1
CrO_4^{2-}	aq	-720.86	-	-	2
HCrO_4^-	aq	-	3.8	6.5089	1
$\text{Cr}_2\text{O}_7^{2-}$	aq	-	-	14.5571	1
H_2CrO_4^0	aq	-	-	5.6513	1
OH^-	aq	-	-	-13.998	1
H_2O	l	-237.1±0.04	-	-	3

Sources:

- (1) Allison et al. (1990)
- (2) Naumov et al. (1971)
- (3) Cox et al. (1989)
- (4) Nordstrom and Munoz (1994)

and minimized the variation in the calculated IAP values for the chromate analog of jarosite. Including the FeCrO_4^+ ion pair eliminated the apparent trend in the IAP and reduced the range in the calculated log IAP values from almost 2.5 log units to less than one log unit. The best fit was achieved with a value of $\log K_{\text{FeCrO}_4^+} = 8.0 \pm 0.1$ which results in a calculated log K_{Sp} of -18.7 ± 0.5 (Table 3-6, Figure 3-6). The error in our estimate of $\log K_{\text{FeCrO}_4^+}$ is based on the standard deviation of the analytical measurements of the concentrations of Fe and Cr from the triplicate dissolution experiments. The error in the log K_{Sp} value represents the total standard deviation over all experiments. An

Table 3-5. Calculated equilibrium activities; FeCrO_4^+ not included in the speciation.

	pH	$\log \{\text{CrO}_4^{2-}\}$	$\log \{\text{K}^+\}$	$\log \{\text{Fe}^{3+}\}$	Ionic Strength (mol/l)	calculated $\log \text{IAP}$
KCRJAR-1.5	1.67	-7.78	-3.16	-3.37	4.47×10^{-2}	-18.81 ± 0.39
KCRJAR-2.0	2.13	-7.84	-3.80	-3.89	1.20×10^{-2}	-18.37 ± 0.25
KCRJAR-2.3	2.40	-7.70	-3.97	-4.24	5.88×10^{-3}	-17.69 ± 0.25
KCRJAR-2.6	2.65	-7.16	-4.42	-4.75	4.39×10^{-3}	-17.09 ± 0.25
KCRJAR-3.0	3.05	-6.18	-4.76	-5.88	8.79×10^{-3}	-16.46 ± 0.25
KCRJAR-4C	2.03	-7.92	-3.77	-3.75	1.35×10^{-2}	-18.68 ± 0.25
KCRJAR-15C	2.05	-7.88	-3.71	-3.78	1.32×10^{-2}	-18.51 ± 0.25
KCRJAR-35C	2.09	-7.78	-3.51	-3.76	1.38×10^{-2}	-17.81 ± 0.64

F-test indicates that the variance among the $\log \text{IAP}$ values at different pH values is significantly greater than the variances within the triplicate experiments at the 95% confidence level ($F=10.6$, $n_1=5$, $n_2=15$, $df_1=4$, $df_2=10$). One reason for the remaining variation in the calculated ion activity products may be other Fe(III)-Cr(VI) ion pairs that are forming in the solution but are not included in the calculations.

Subsequent to making these calculations we became aware of several spectroscopic studies of the interaction of Cr(VI) and Fe(III) by Esperson and King (1963), Espenson and Helzer (1969), Burkhart and Thompson (1972), and Olazabal et al. (1994). In all four studies, evidence for the formation of FeCrO_4^+ was found. Published data for the $\log K$ and the stoichiometric formation constant (K_{stoich}) for FeCrO_4^+ for the reaction



are summarized in Table 3-7. We applied activity corrections to reported K_{stoich} values measured at $I=0.084$ mol/l and $I=0.2$ mol/l using the Davies Equation as incorporated into MINTEQA2 (Table 3-7) and calculated $\log K_{\text{FeCrO}_4^+}$ values. There is a clear trend of

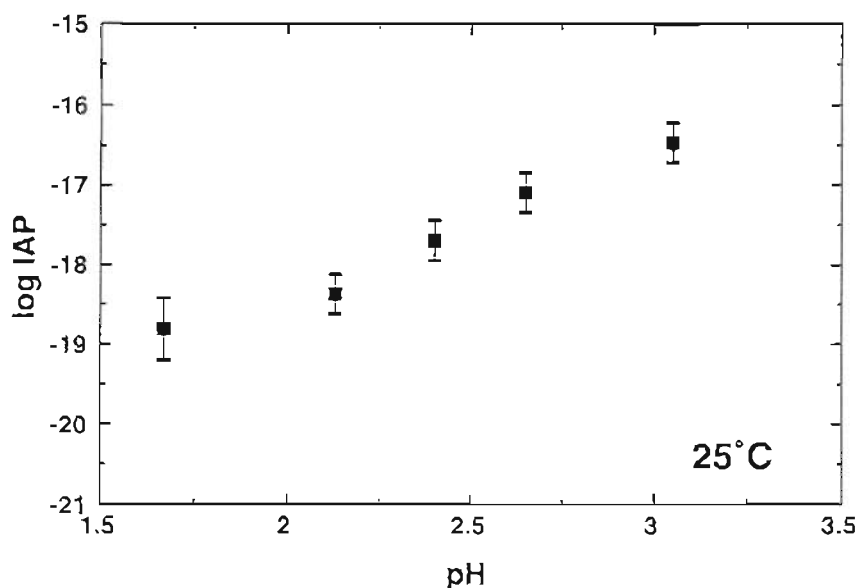


Figure 3-5. Log of the ion activity product from five dissolution experiments at different pH values calculated without including FeCrO_4^+ in the speciation.

increasing $\log K_{\text{FeCrO}_4^+}$ with increasing temperature (Figure 3-7). Using weighting factors of $1/\sigma_i^2$, where σ_i is the standard deviation of the $\log K_{\text{FeCrO}_4^+}$ at temperature T_i , we fitted the values of $\log K_{\text{FeCrO}_4^+}$ from the three spectroscopic studies and the value determined in the present study to a constant enthalpy and entropy model of the form

$$2.303 \log K_{\text{FeCrO}_4^+} = -\Delta H^0/RT + \Delta S^0/R \quad (7)$$

where ΔH^0 is the change in standard enthalpy, and ΔS^0 is the change in standard entropy for reaction (6), and R is the gas constant ($8.314 \times 10^{-3} \text{ kJ mol}^{-1} \text{ K}^{-1}$) and T the temperature in K. The regression (Figure 3-7) yields $\Delta H^0 = 19.1 \pm 2.2 \text{ kJ mol}^{-1}$ and $\Delta S^0 = 214 \pm 8 \text{ J K}^{-1} \text{ mol}^{-1}$ ($n=9$, $r^2 = 0.92$, $df=7$). Using equation (7), $\log K_{\text{FeCrO}_4^+, 298}$ is calculated to be 7.8 ± 0.5 . We recommend this value as the currently best estimate of $\log K_{\text{FeCrO}_4^+, 298}$. Recalculating the $\log K_{\text{Sp}}$ of $\text{KFe}_3(\text{CrO}_4)_2(\text{OH})_6$ using $\log K_{\text{FeCrO}_4^+, 298} = 7.8$ results in a slightly greater $\log K_{\text{Sp}}$ of -18.4 ± 0.8 .

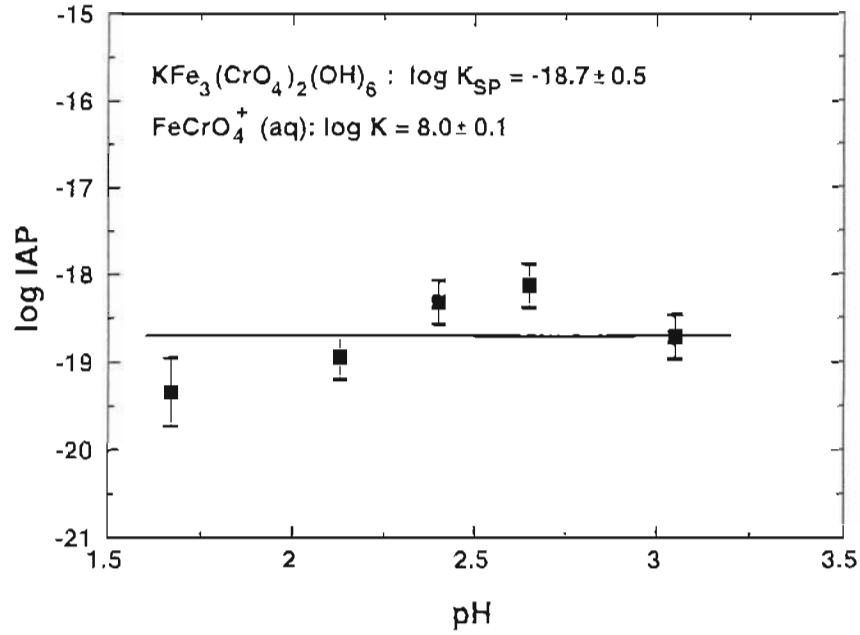


Figure 3-6. Log of the ion activity product from five dissolution experiments at different pH values calculated including the FeCrO_4^+ ion pair with $\log K = 8.0$ in the speciation. Solid line represents the average of the five log ion activity product values (-18.7 ± 0.5).

Based on the solubility product for the chromate analog of jarosite, the free energy of formation of this solid can be calculated. At equilibrium, the Gibbs free energy of reaction at 25°C, $\Delta G_{r,298}^0$ is given by

$$\begin{aligned} \Delta G_{r,298}^0 = & \Delta G_{f,298}^0(\text{K}^+) + 3\Delta G_{f,298}^0(\text{Fe}^{3+}) + 2\Delta G_{f,298}^0(\text{CrO}_4^{2-}) \\ & + 6\Delta G_{f,298}^0(\text{H}_2\text{O}) - \Delta G_{f,298}^0(\text{KFe}_3(\text{CrO}_4)_2(\text{OH})_6) \end{aligned} \quad (8)$$

with the free energy of reaction related to the K_{sp} by

$$\Delta G_{r,298}^0 = -2.303 RT \log K_{\text{sp}} \quad (9)$$

Solving for the free energy of formation of the chromate analog of jarosite

Table 3-6. Equilibrium activities calculated using FeCrO_4^+ with $\log K = 8.0$.

	pH	$\log \{\text{CrO}_4^{2-}\}$	$\log \{\text{K}^+\}$	$\log \{\text{Fe}^{3+}\}$	Ionic Strength (mol/l)	calculated $\log \text{IAP}^*$
KCRJAR-1.5	1.67	-7.94	-3.16	-3.44	4.24×10^{-2}	-19.34±0.39
KCRJAR-2.0	2.13	-7.98	-3.79	-3.99	1.16×10^{-2}	-18.94±0.25
KCRJAR-2.3	2.40	-7.82	-3.97	-4.37	5.65×10^{-3}	-18.32±0.25
KCRJAR-2.6	2.65	-7.21	-4.42	-5.06	4.24×10^{-3}	-18.12±0.25
KCRJAR-3.0	3.05	-6.18	-4.76	-6.63	8.75×10^{-3}	-18.71±0.25
KCRJAR-4C	2.03	-8.03	-3.77	-3.82	1.31×10^{-2}	-19.11±0.25
KCRJAR-15C	2.05	-8.02	-3.71	-3.87	1.27×10^{-2}	-19.06±0.25
KCRJAR-35C	2.09	-7.99	-3.51	-3.86	1.31×10^{-2}	-18.53±0.64

$$\begin{aligned} \Delta G_{f,298}^0(\text{KFe}_3(\text{CrO}_4)_2(\text{OH})_6) = & \Delta G_{f,298}^0(\text{K}^+) + 3\Delta G_{f,298}^0(\text{Fe}^{3+}) \\ & + 2\Delta G_{f,298}^0(\text{CrO}_4^{2-}) + 6\Delta G_{f,298}^0(\text{H}_2\text{O}) + RT \ln K_{\text{sp}} \end{aligned} \quad (10)$$

and using the free energies given in Table 3-4, we calculate $\Delta G_{f,298}^0(\text{KFe}_3(\text{CrO}_4)_2(\text{OH})_6) = -3307.4 \pm 2.9 \text{ kJ mol}^{-1}$ where the variation represents the error introduced by the uncertainty in the K_{sp} value only. Including the error in the free energies of the individual ions (Table 3-4) results in an additional uncertainty of $\pm 3.3 \text{ kJ mol}^{-1}$. Considering that the error in the free energies of some of the individual ions may be larger than reported in Table 3-4 would result in an even larger uncertainty in the estimate of $\Delta G_{f,298}^0(\text{KFe}_3(\text{CrO}_4)_2(\text{OH})_6)$. For example, for $\Delta G_{f,298}^0(\text{Fe}^{3+})$ values as high as -4.6 kJ mol^{-1} have been reported (Wagman et al. (1969)). Propagating an uncertainty of 13.3 kJ mol^{-1} for $\Delta G_{f,298}^0(\text{Fe}^{3+})$ through equation (10) results in an overall uncertainty of $\pm 46 \text{ kJ mol}^{-1}$ for $\Delta G_{f,298}^0(\text{KFe}_3(\text{CrO}_4)_2(\text{OH})_6)$.

The $\log \text{IAP}$ values calculated for the experiments at 4, 15, 25, and 35°C including FeCrO_4^+ with $\log K = 8.0$ vary between -19.11 at 4° and -18.53 at 35°C (Table 3-6, Figure 3-8). There is a slight apparent trend with the solubility increasing with

Table 3-7. Summary of studies of the formation constant of FeCrO_4^+ .

Temperature (°C)	I (mol/L)	$\log K_{\text{stoich}}$	number of determinations	$\log K_{\text{FeCrO}_4^+}$	Reference
0	0.084	6.54 ± 0.062	12	7.37 ± 0.06	1
1	0.084	6.67 ± 0.023	?	7.50 ± 0.02	2
1	0.2	6.49 ± 0.007	5	7.55 ± 0.01	2
1	1	6.37 ± 0.042	?	-	2
9.3	0.2	6.61 ± 0.012	5	7.67 ± 0.01	2
17.2	0.2	6.71 ± 0.005	6	7.77 ± 0.01	2
25	0.2	6.80 ± 0.029	6	7.86 ± 0.03	2
25	0.084	6.96 ± 0.031	2	7.80 ± 0.03	2
25	1	6.62 ± 0.037	2	-	2
25	1	6.14 ± 0.05	?	-	3
25	variable	-	?	7.77 ± 0.02	4
25	4.2×10^{-3} - 4.2×10^{-2}	-	1	8.0 ± 0.1	5

- 1 Espenson and King (1963)
- 2 Burkhart and Thompson (1972)
- 3 Espenson and Helzer (1969)
- 4 Olazabal et al. (1994)
- 5 this study

temperature which would indicate a positive enthalpy of reaction. However, when fitting the data to a linear constant enthalpy function and a nonlinear variable enthalpy of reaction and constant heat capacity function, the values obtained for the enthalpy of reaction are not significantly different from zero at the 95% confidence level ($t=2.3$, $df=2$ for the linear model; $t=3.5$, $df=1$ for the nonlinear model). Based on these experiments, therefore, it appears that in the range from 4 to 35°C, the solubility product depends only weakly on temperature and the enthalpy of reaction at 25°C is approximately zero.

The solubility product of the chromate analog of jarosite of $\log K = -18.7 \pm 0.5$ determined from our experiments is significantly lower than the value of -11.0 ± 0.2

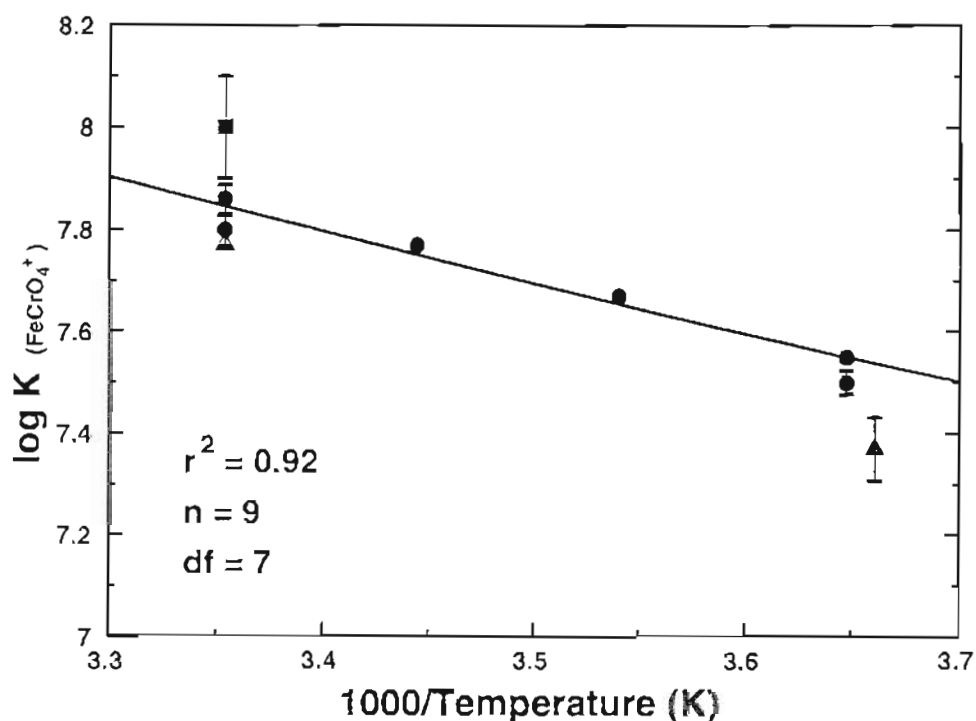


Figure 3-7. Reported values for $\log K_{\text{FeCrO}_4^+}$ versus inverse temperature after activity corrections. Data from Espenson and King (1963) (▲), Burkhart and Thompson (1972) (•), Olazabal et al. (1994) (Δ), and this study (■). The solid line represents the best fit to a constant enthalpy and constant entropy function, equation (7).

reported for jarosite (Baron and Palmer, 1995), indicating that the chromate analog of jarosite is stable under a wider range of pH conditions than jarosite which is stable only under very acidic conditions. A pe-pH predominance diagram for the Fe-Cr-K-C-H₂O-system is shown in Figure 3-9. The diagram is based on an activity of dissolved $\text{Fe}_{\text{tot}} = 10^{-4}$ M ($\text{Fe}^{3+} = 10^{-4}$ M and $\text{Fe}^{2+} = 10^{-4}$ M), an activity of dissolved $\text{K}_{\text{tot}} = 10^{-4}$ M, an activity of dissolved $\text{Cr}_{\text{tot}} = 10^{-2}$ M ($\text{Cr(VI)}_{\text{tot}} = \text{CrO}_4^{2-} + \text{HCrO}_4^- = 10^{-2}$ M and $\text{Cr}^{3+} = 10^{-2}$ M) and a pCO_2 of 10^{-2} atm. Solubility products and equilibrium constants for aqueous species were taken from Nordstrom and Munoz (1994) and Richard and Bourg (1991), additional constants are listed in Table 3-4. The pe-pH predominance diagram illustrates that under oxidizing conditions $\text{KFe}_3(\text{CrO}_4)_2(\text{OH})_6$ is the thermodynamically favored solid

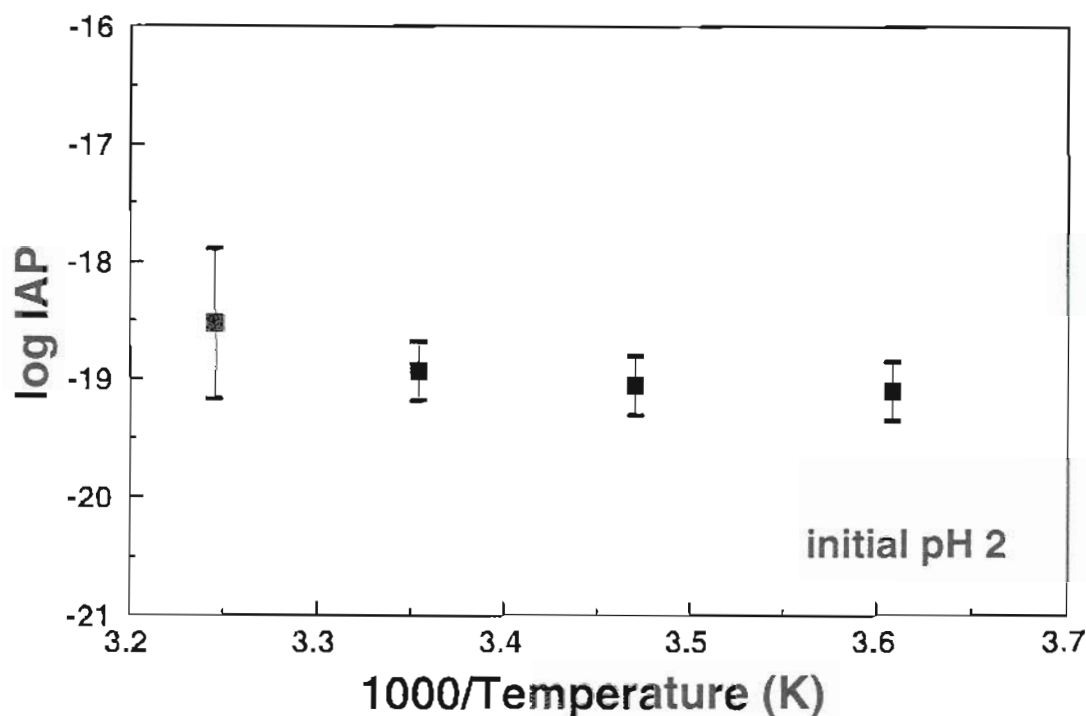
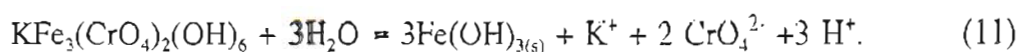


Figure 3-8. Calculated log ion activity product versus inverse temperature from four dissolution experiments at 4, 15, 25, and 35°C, initial pH 2.

under a wide range of acidic pH values and stable up to almost neutral conditions. In soils, Cr(VI) may persist well beyond its stability field because the reduction by soil organic matter is slow or kinetically inhibited (e.g. Bartlett (1991). Ferrous iron, however readily reduces Cr(VI) to Cr(III) (e.g. Palmer and Wittbrodt, 1991). We have therefore also included in Figure 3-9 the extended stability field of $\text{KFe}_3(\text{CrO}_4)_2(\text{OH})_6$ if the reduction of Cr(VI) is assumed to be kinetically inhibited until Fe(II) becomes available.

The transition between $\text{KFe}_3(\text{CrO}_4)_2(\text{OH})_6$ and hydrous ferric oxide (represented here in an idealized way as $\text{Fe}(\text{OH})_{3(s)}$) is of particular interest because hydrous ferric oxide limits the stability field of $\text{KFe}_3(\text{CrO}_4)_2(\text{OH})_6$ at higher pH values. The transition between these two solids is given by



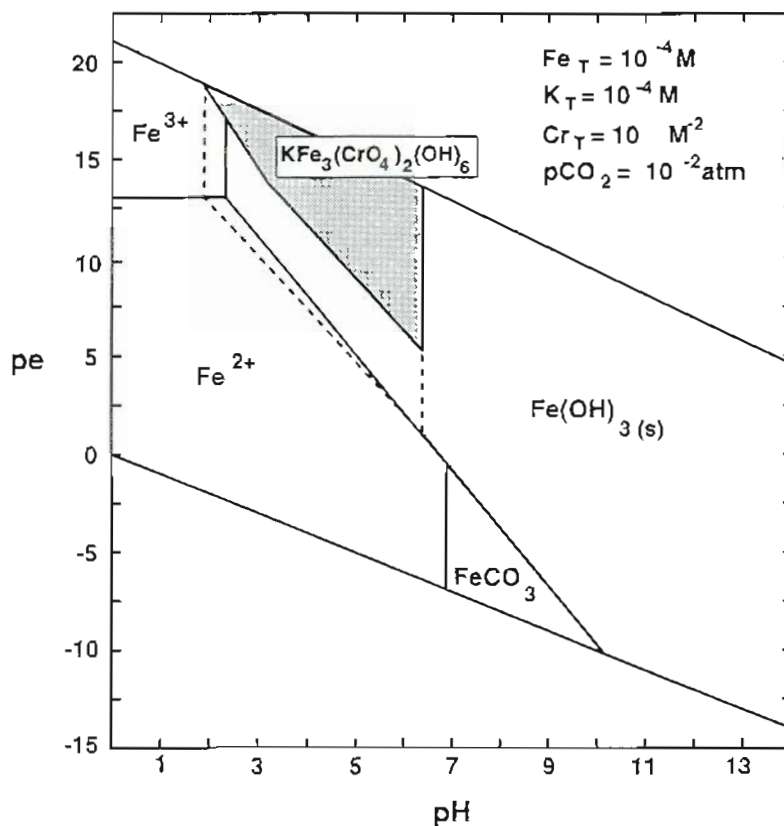


Figure 3-9. pe-pH predominance diagram for the K-Fe-Cr-C-H₂O system. The diagram is based on an activity of dissolved $\text{Fe}_{\text{tot}} = 10^{-4} \text{ mol/l}$, an activity of $\text{K}^+ = 10^{-4} \text{ mol/l}$, an activity of dissolved $\text{Cr}(\text{VI})_{\text{tot}} = 10^{-2} \text{ mol/l}$, and a pCO_2 of 10^{-2} atm . The dashed line represents the extended stability field of $\text{KFe}_3(\text{CrO}_4)_2(\text{OH})_6$ if $\text{Fe}(\text{II})$ is considered the only reductant for $\text{Cr}(\text{VI})$.

At equilibrium, this transformation can be expressed as

$$\begin{aligned} \log K_{\text{SP}}(\text{KFe}_3(\text{CrO}_4)_2(\text{OH})_6) - 3 \log K_{\text{SP}}(\text{Fe}(\text{OH})_3(\text{s})) \\ = \log\{\text{K}^+\} + 2 \log\{\text{CrO}_4^{2-}\} + 3 \log\{\text{H}^+\} + 3 \log\{\text{H}_2\text{O}\}. \quad (12) \end{aligned}$$

Therefore, the transition pH, pH_T , is

$$\begin{aligned} \text{pH}_T = & -\frac{1}{3} \log K_{\text{Sp}}(\text{KFe}_3(\text{CrO}_4)_2(\text{OH})_6) + \log K_{\text{Sp}}(\text{Fe}(\text{OH})_{3(\text{s})}) \\ & + \frac{1}{3} \log \{ \text{K}^+ \} + \frac{2}{3} \log \{ \text{CrO}_4^{2-} \} + \log \{ \text{H}_2\text{O} \}. \end{aligned} \quad (13)$$

From equation (13), it becomes apparent that pH_T is a function of the solubility products of $\text{KFe}_3(\text{CrO}_4)_2(\text{OH})_6$ and $\text{Fe}(\text{OH})_{3(\text{s})}$, and the activities of K^+ and CrO_4^{2-} . In general, higher combined activities of K^+ and CrO_4^{2-} result in a higher pH_T and a larger stability field for the chromate analog of jarosite. The predominance regions for $\text{KFe}_3(\text{CrO}_4)_2(\text{OH})_6$ and ferrihydrite as a function of pH and the activities of K^+ and $\text{Cr(VI)}_{\text{tot}}$ are shown in Figure 3-10. Based on the above discussion and on Figures 3-9 and 3-10, it appears possible that the chromate analog of jarosite forms in large parts of a Cr(VI)-contaminated aquifer.

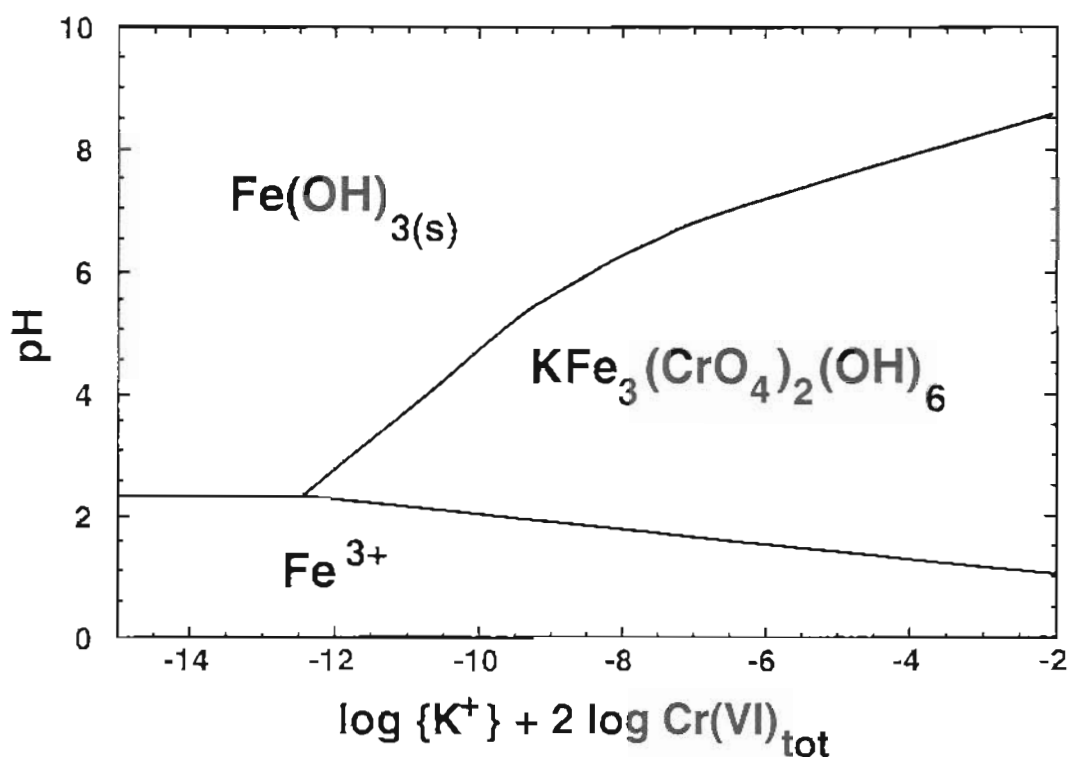


Figure 3-10. Diagram of the predominance regions of $\text{Fe}(\text{OH})_{3(\text{s})}$ and $\text{KFe}_3(\text{CrO}_4)_2(\text{OH})_6$ in the K-Fe(III)-Cr(VI)- H_2O system as a function of pH and $\log [\text{K}^+] + 2 \log [\text{Cr(VI)}]_{\text{tot}}$.

The dissolution experiment with initial pH 2.0 at 25°C (Figure 3-4) was used to

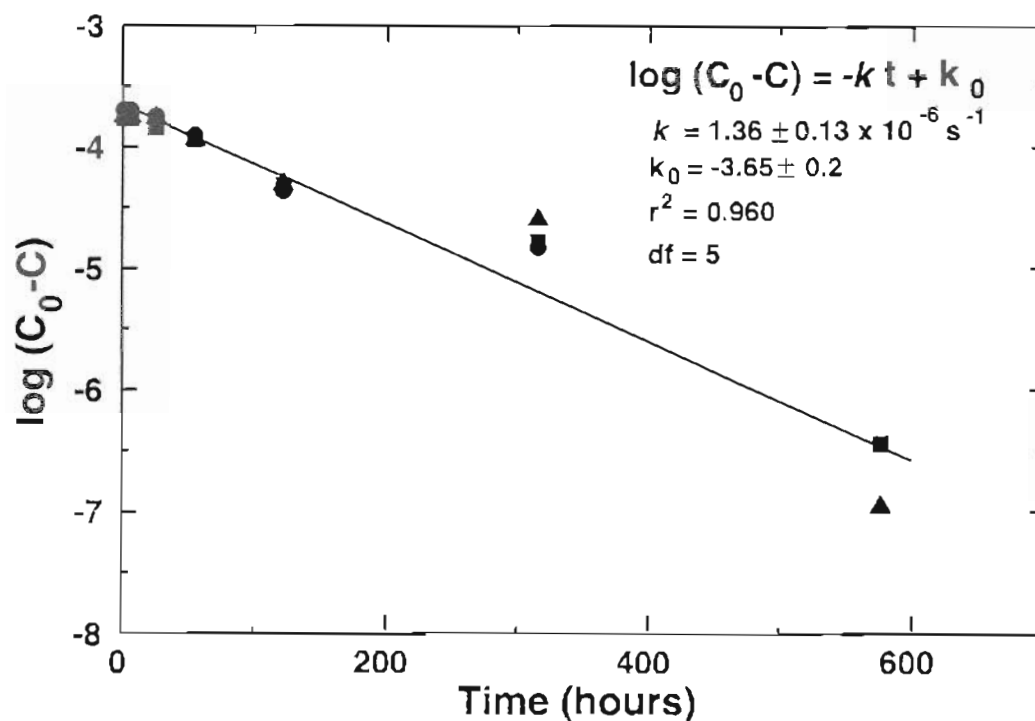


Figure 3-11. Plot of $\log(C_0 - C)$ versus time for K_{tot} (■), Fe_{tot} (▲) and Cr_{tot} (●) in the dissolution experiment KCRJAR-2.0. C is the normalized concentration in mol/l obtained by dividing the measured aqueous concentration of the ion by its stoichiometric coefficient in the chromate analog of jarosite. C_0 is the normalized equilibrium concentration. The solid line is the regression.

evaluate the general kinetics of the dissolution reaction of the chromate analog of jarosite. This experiment was sampled most frequently and it is the only one with sufficient data for a reaction rate analysis. The concentrations of K_{tot} , $\frac{1}{3}Fe_{tot}$ and $\frac{1}{2}Cr_{tot}$ were plotted as $\log(C_0 - C)$ versus time, where C_0 is the concentration at equilibrium and C is the concentration at time t , to test for first-order behavior (Figure 3-11). The concentrations of Fe and Cr are divided by 3 and 2, respectively, to normalize the concentrations to the number of Fe and Cr atoms in $KFe_3(CrO_4)_2(OH)_6$. The linearity of the plot indicates that the dissolution kinetics can be described by a first-order model of the form

$$\frac{dC}{dt} = -k(C_0 - C) \quad (14)$$

where k is the apparent rate coefficient. Integration of equation (14) yields a linear equation for $\log(C_0 - C)$ versus time. The slope of the line is the apparent rate coefficient, k , and the intercept, k_0 , is $\log C_0$. The data were also plotted as $(C_0 - C)^{-1}$ versus time and C/t versus C to test for second-order behavior but deviations from second-order behavior become obvious in both kinds of plots. The dissolution reaction at pH 2 and 25°C can be best described by a first-order model with an apparent rate coefficient, k , of approximately $4.9 \pm 0.5 \times 10^{-3} \text{ s}^{-1}$.

3.5 Summary

The solubility product and the free energy of formation of a synthetic $\text{KFe}_3(\text{CrO}_4)_2(\text{OH})_6$ at 25°C were determined as $\log K_{\text{sp}} = -18.7 \pm 0.5$ and $\Delta G_{f,298}^0 = -3307.4 \pm 2.9 \text{ kJ mol}^{-1}$ in a set of dissolution experiments conducted in the temperature range of 4 - 35°C and pH 1.5 to 3. The dissolution experiments at 25°C also suggest the formation of a FeCrO_4^+ ion pair with a $\log K = 8.0 \pm 0.1$. Combining this data with previously published $\log K$ values and stoichiometric formation constants for FeCrO_4^+ from spectroscopic studies to which we applied activity corrections, we determined that the enthalpy of formation of FeCrO_4^+ is $19.1 \pm 2.2 \text{ kJ mol}^{-1}$ and that the entropy of formation of FeCrO_4^+ is $214 \pm 8 \text{ J K}^{-1} \text{ mol}^{-1}$. Based on the experiments conducted at different temperatures there appears to be little temperature dependence of the solubility product and the enthalpy of reaction appears to be approximately zero under the conditions of the experiments. The rate of the dissolution reaction can be described by a first-order model. The solubility product of the chromate analog of jarosite is significantly lower than that of jarosite, indicating that this solid can be stable under a wider range of pH-conditions than jarosite. Based on the low solubility of the chromate analog of jarosite it appears that this solid could form in large parts of a Cr(VI) contaminated aquifer and may affect remediation of chromium contaminated soils and

groundwaters.

3.6 References

- Allison J.D., Brown D.S., and Novo-Gradac K.J. (1990) *MINTEQA2/PRODEFA2, a geochemical assessment model for environmental systems: version 3.0*. U.S. Environmental Protection Agency, Athens, GA.
- Alpers C.N., Nordstrom D.K., and Ball J.W. (1989) Solubility of jarosite solid solutions precipitated from acid mine water, Iron Mountain, California, U.S.A.. *Sci. Géol., Bull.* **42**, 281-298.
- Baron D., Stanley J.T., and Palmer C.D. (1995) Identification of two Fe-chromate minerals in Cr(VI)-contaminated soil *Environ. Sci. Technol.* **30**, 964-968.
- Baron D. and Palmer C.D. (1995) Solubility of jarosite at 4 - 35°C. *Geochim. Cosmochim. Acta* **60**, 185-195.
- Bartlett R.J. (1991) Chromium cycling in soils and water: links, gaps, and methods. *Environ. Health Perspect.* **92**, 17-24.
- Bonnin A. and Lecerf A. (1966) Deux nouveaux chromates de fer: FeCrO_4OH et $\text{KFe}_3(\text{CrO}_4)_2(\text{OH})_6$. *C. R. Seances Acad. Sci. Paris Sér. C* **262**, 1782-1784.
- Brophy G.P. and Sheridan M.F. (1965) Sulfate studies. IV. The jarosite-natrojarosite-hydronium jarosite solid solution series. *Am. Miner.* **50**, 112-126.
- Burkhart M.J. and Thompson R.C. (1972) Association of chromium(VI) with neptunium(IV) and thorium(IV) in perchlorate solution. *J. Am. Chem. Soc.* **94**, 2999-3002.
- Carson C.D. and Dixon J.B. (1983) Mineralogy and acidity of an inland acid sulfate soil of Texas. *Soil Sci. Soc. Am. J.* **47**, 828-833.
- Chapman B.M., Jones D.R., and Jung R.F. (1983) Processes controlling metal ion attenuation in acid mine drainage streams. *Geochim. Cosmochim. Acta* **47**, 1957-1973.
- Cotton F.A. and Wilkinson G. (1988) *Advanced inorganic chemistry*. John Wiley & Sons, Inc.
- Cox J.D., Wagman D.D., and Medvedev V.A. (1989) *CODATA Key Values for Thermodynamics*. Hemisphere Publishing Corporation.
- Cudennec Y., Riou A., Bonnin A., and Caillet P. (1980) Études cristallographiques et

infrarouges d'hydroxychromates de fer et d'aluminium de structure alunite. *Rev. Chim. Minér.* **17**, 158-167.

Dutrizac J.E. (1984) The behavior of impurities during jarosite precipitation. In *Hydrometallurgical Process Fundamentals* (ed. R.G. Bautista) NATO Conference Series. VI, Materials Science, Vol. 10, 125-169. Plenum Press, New York,

Dutrizac J.E. and Kaiman S. (1976) Synthesis and properties of jarosite-type compounds. *Can. Miner.* **14**, 151-158.

Dutrizac J.E., Dinardo O., and Kaiman S. (1981) Selenate Analogs of jarosite-type compounds. *Hydrometallurgy* **6**, 327-337.

Espenson J.H. and Helzer S.R. (1969) Kinetic studies on the 1:1 complex of iron(III) and chromate ions in perchloric acid solution. *Inorg. Chem.* **8**, 1051-1053.

Espenson J.H. and King E.L. (1963) Kinetics and mechanisms of reactions of chromium(VI) and iron(II) species in acidic solution. *J. Amer. Chem. Soc.* **85**, 3328-3333.

Härtig C., Brand P., and Bohmhammel K. (1984) Fe-Al-Isomorphie und Strukturwasser in Kristallen vom Jarosit-Alunit-Typ. *Z. anorg. allg. Chem.* **508**, 159-164.

JCPDS (Joint Committee on Powder Diffraction Standards) (1994) Powder diffraction file. Swarthmore, Pennsylvania, International Center for Diffraction Data.

Kubisz J. (1964) A study of minerals in the alunite-jarosite group. *Polska Akad. Nauk., Prace Geol.* **22**, 1-93.

Kubisz J. (1970) Studies on synthetic alkali-hydronium jarosite. I. Synthesis of jarosite and natrojarosite. *Mineral. Polonica* **1**, 47-57.

Kubisz J. (1972) Studies on synthetic alkali-hydronium jarosite. III. Infrared adsorption study. *Mineral. Polonica* **3**, 23-37.

Kulp J.L. and Adler H.H. (1950) Thermal study of jarosite. *Am. J. Sci.* **248**, 475-487

Nordstrom D.K. and Munoz J.L. (1994) *Geochemical Thermodynamics (2nd Edition)*. Blackwell Scientific Publications. Boston, Mass.

Naumov G.B., Ryzhenko I.L., and Khodakovskiy I.L. (1971) *Handbook of Thermodynamic Data* (translated from Russian by G.J. Soleimani, edited by I. Barnes and V. Speltz), Washington D.C. NTIS publication PB-226 722.

Olazabal M.A., Etxebarria N., Fernandez L.A., and Madariaga J.M. (1994) Study of the

complexation and precipitation equilibria in the system Cr(VI)-Fe(III)-H₂O. *J. Solution Chem.* **23**, 1111-1123.

Palmer C.D. and Wittbrodt P.R. (1991) Processes affecting the remediation of chromium contaminated sites. *Environ. Health Perspect.* **92**, 25-40.

Parker R.L. (1962) Isomorphous substitutions in natural and synthetic alunite. *Am. Miner.* **47**, 127-136.

Powers D.A., Rossman G.R., Schugar H.J., and Gray H.B. (1975) Magnetic behavior and infrared spectra of jarosite, basic iron sulfate, and their chromate analogs. *J. Solid State Chem.* **13**, 1-13.

Ramirez A.P., Broholm C., Lee S.H., Collins M.F., Heller L., Kloc C., and Bucher E. (1993) Magnetism in a chromium jarosite Kagomé lattice KCr₃(OH)₆(SO₄)₂ (abstr.) *J. Appl. Phys.* **73**, 5658.

Richard F.C. and Bourg A.C.M. (1991) Aqueous geochemistry of chromium: a review. *Wat. Res.* **25**, 807-816.

Ripmeester J.A., Ratcliffe C.I., Dutrizac J.E., and Jambor J.L. (1986) Hydronium ion in the alunite-jarosite group. *Can. Miner.* **24**, 435-447.

Saarinen H.U.A. (1977) Separating nickel, cobalt and chromium from iron in metallurgical products. *U.S. Patent* 4,042,474.

Scott M.S. (1987) Solid solution in, and classification of, gossan-derived members of the alunite-jarosite family, northwest Queensland, Australia. *Am. Miner.* **72**, 178-187.

Townsend M.G., Longworth G., and Roudaut E. (1986) Triangular-spin, kagome plane in jarosites. *Phys. Rev. B* **33**, 4919-4926.

Van Breemen N. (1973) Soil forming processes in acid sulfate soils. In *Acid Sulfate Soils, Proc. Int. Symp. on Acid Sulfate Soils* (ed. H. Dost), Vol I. Publ.18 ILRI, 66-130. Wageningen, The Netherlands.

Waddington T.C. (1959) Lattice energies. In *Advances in inorganic chemistry and radiochemistry, Vol. 1* (eds. H.J. Emeléus and A.G. Sharpe), 157-221. Academic Press Inc., New York.

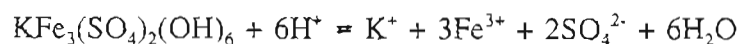
Wagman D.D., Evans W.H., Parker V.B., Halow I., Bailey S.M., and Schumm R.H. (1969) Selected values of chemical thermodynamic properties. *National Bureau of Standards Tech. Note* 270-4. U.S. Department of Commerce.

Wilkins R.W.T., Mateen A., and West G.W. (1974) The spectroscopic study of oxonium in minerals. *Am. Miner.* **59**, 811-819.

CHAPTER 4

Solubility of Jarosite at 4 - 35°C

The solubility of jarosite ($\text{KFe}_3(\text{SO}_4)_2(\text{OH})_6$) was studied in a series of dissolution experiments. The experiments were conducted at 4-35°C and pH values between 1.5 and 3.0 using a synthetic jarosite with a composition very close to ideal. The solids were left in the reaction vessel for up to 6 months. Equilibrium was established in the experiments after approximately 3 to 4 months. The $\log K_{\text{sp}}$ for the jarosite dissolution reaction



at 25°C is determined to be -11.0 ± 0.3 . From this measured solubility product, the free energy of formation, $\Delta G_{\text{f},298}^0$, is calculated to be $-3309.8 \pm 1.7 \text{ kJ mol}^{-1}$. Based on the temperature dependence of the solubility product, the enthalpy of reaction at 25°C, $\Delta H_{\text{r},298}^0$, is $-45 \pm 5 \text{ kJ mol}^{-1}$, the entropy of reaction, $\Delta S_{\text{r},298}^0$, is $-350 \pm 40 \text{ J mol}^{-1} \text{ K}^{-1}$ and the heat capacity of the reaction, $\Delta C_{\text{p,r}}$, over the temperature range of the experiments is determined to be $-2.1 \pm 0.2 \text{ kJ mol}^{-1} \text{ K}^{-1}$. The rate of the dissolution reaction can be described by a first-order model.

4.1 Introduction

Jarosite ($\text{KFe}_3(\text{SO}_4)_2(\text{OH})_6$) is a common mineral in acidic, sulfate-rich environments formed by the oxidation of sulfides, especially pyrite. Such environments include acid sulfate soils formed from pyrite-bearing sediments (Van Breemen, 1973; Carson and Dixon, 1983), weathering of sulfide ore deposits (Bladh, 1982), acid-hypersaline lake sediments (Long et al., 1992; Alpers et al., 1992), acid mine drainage (Nordstrom, 1977; Chapman et al., 1983; Alpers et al., 1989), and weathering of coal refuse from pyritic coal seams (Sullivan and Sobek, 1982). Jarosite has also been reported in hot springs (Tkachenko and Zotow, 1974) and hydrothermal environments (Keith et al., 1979; Stoffregen and Rye, 1992). Precipitation of jarosite is also of interest to metallurgists because of its ability to scavenge unwanted elements from hydrometallurgical ore processing solutions (Dutrizac, 1983).

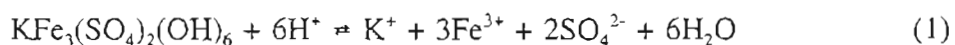
Jarosite is a member of the jarosite-alunite group of isostructural minerals described by the general formula $\text{AB}_3(\text{SO}_4)_2(\text{OH})_6$ where the B site is occupied by Fe^{3+} (jarosites) and Al^{3+} (alunites) and the A site is occupied most commonly by K^+ , Na^+ , and H_3O^+ (hydronium) (Parker, 1962; Kubisz, 1964; Brophy and Sheridan, 1965). Jarosite is the potassium-iron endmember of the jarosite-alunite group. Extensive substitution by other ions within the jarosite crystal structure has also been reported (Dutrizac and Kaiman, 1976). Both natural and synthetic jarosites often have a significant amount of H_3O^+ -substitution on the alkali position (Brophy and Sheridan, 1965; Kubisz, 1970; Dutrizac and Kaiman, 1976). Deficiency in Fe with values for the Fe: SO_4 molar ratio significantly lower than the ideal 3:2 stoichiometry is also common (Kubisz, 1970; Alpers et al., 1989). Values of the Fe: SO_4 molar ratio as low as 2.33:2 (Ripmeester et al., 1986), and 2.20:2 to 2.57:2 (Härtig et al., 1984) are reported.

Despite the common occurrence of jarosite and its interest to geochemists, geologists and metallurgists, uncertainty exists regarding the solubility of jarosite with the reported solubility product varying by more than seven orders of magnitude. To evaluate the conditions under which jarosite may form and remain stable, more accurate thermodynamic data are needed. Such information is also required to further establish the thermodynamic mixing terms in the K- H_2O -Na jarosite solid-solution system (Alpers

et al., 1989). The purpose of this study is to measure the solubility product of jarosite at temperatures typical of weathering or supergene conditions.

4.2 Previous Studies

Only a few experimental studies of the solubility of jarosite have been conducted and we are not aware of any calorimetric studies of its free energy of formation. There remains a large degree of uncertainty about the thermodynamic properties of jarosite. If the dissolution of jarosite is written as



then the log of the ion activity product (IAP) is

$$\log \text{IAP} = \log\{\text{K}^+\} + 3 \log\{\text{Fe}^{3+}\} + 2 \log\{\text{SO}_4^{2-}\} + 6 \log\{\text{H}_2\text{O}\} + 6 \text{pH} \quad (2)$$

where brackets denote aqueous activity. At equilibrium, the IAP is equal to the solubility product, K_{sp} . The log K_{sp} reported for reaction (1) at 25°C varies from -7.12 to -14.8 and the reported free energy of formation, $\Delta G_{\text{f},298}^0$, of jarosite varies from -3317.9 to -3192±25 kJ mol⁻¹ (Table 4-1). The reasons for the large variation include (1) inconsistent thermodynamic data for calculation of free energies and aqueous ion activities, (2) substitution of other ions, particularly hydronium, in the jarosite crystal structure, and to a smaller degree (3) variation introduced by different experimental approaches, and (4) analytical uncertainty.

Brown (1970) conducted a dissolution experiment in which synthetic jarosite was dissolved at 25°C for six months and a free-drift precipitation experiment from which jarosite was precipitated from a supersaturated solution. In neither of the experiments was equilibrium demonstrated. The free energy of formation $\Delta G_{\text{f},298}^0$ was calculated as -3192±25 kJ mol⁻¹ from the dissolution experiment and as -3276±84 from the precipitation experiment. Zotov et al. (1973) noted an arithmetical error in Brown's calculation

Table 4-1. Summary of solubilities and $\Delta G_{f,298}^0$ values reported for jarosite.

	Reported $\log K_{sp}$ at 25°C	Reported $\Delta G_{f,298}^0$ (kJ mol ⁻¹)	Comments	Recalculated $\Delta G_{f,298}^0$ (kJ mol ⁻¹) *
Allison et al. (1990)	-14.8	-	-	-3331.4
Alpers et al. (1989)	-11.14	-3300.2±2.6	for (K _{0.83} Na _{0.07} H ₃ O ⁺ _{0.10})-jarosite precipitated from acid mine drainage water in the laboratory at ambient temperature	-3300.1±2.6
Bladh (1982)	-7.12	-	-	-3287.6
Brown (1970)	-	-3276±84	from precipitation experiment	-
	-	-3192±25	from dissolution experiment	-
	-	-3302±84	recalculated by Zotov et al. (1973) who noted an arithmetic error in Brown's calculations and used thermodynamic data from Naumov et al. (1971)	-3302±84
	-	-3300±25		-3300±25
	-	-3299	recalculated from the dissolution experiment by van Breemen (1973) using thermodynamic data from Robie and Waldbaum (1968)	-
Chapman et al. (1983)	-9.21	-	based on Kashkay et al. (1975) and thermodynamic data from Naumov et al. (1971)	-
Hladky and Slansky (1981)	-9.08	-	based on Kashkay et al. (1975)	-
Kashkay et al. (1975)	-	-3299.7±4	'free-drift' precipitation experiments	-3299.6±4
	-15.8 (at 100°C)	-3184 (at 100°C)		-
Stoffregen (1993)	-	-3416.3±1.7 (200°C, 100 bar)	at 200°C, 100 bar	-
Vlek et al. (1974)	-14.56	-3310.4	used a 'chelation method'	-3331.4
Zotov et al. (1973)	-	-3305.8±4	based on a jarosite precipitated from a natural water sample	-3305.7
	-	-3317.9	estimated from a natural (Na,K)-jarosite precipitated at 45°C	-3317.8
present study	-11.0±0.3	-3309.8±1.7	-	-

* $\Delta G_{f,298}^0$ jarosite recalculated using the free energies for ions used in the present study (Table 4-2).

and recalculated $\Delta G_{f,298}^0$ as -3300 ± 25 kJ mol⁻¹ from the dissolution experiment and -3302 ± 84 kJ mol⁻¹ from the precipitation experiment. Vlek et al. (1974) dissolved a natural jarosite in a solution containing the chelating agent EDTA to increase total Fe(III) concentrations and calculated a $\Delta G_{f,298}^0$ of -3310.4 kJ mol⁻¹ and a log K_{sp} of -14.56 . Kashkay et al. (1975) conducted three precipitation experiments in which jarosite was allowed to precipitate from supersaturated solutions for 15 months at $25 \pm 5^\circ\text{C}$ and calculated $\Delta G_{f,298}^0$ as -3299.7 ± 4 kJ mol⁻¹. From another precipitation experiment conducted at 100°C , these researchers determined a log $K_{sp,373}$ of -15.83 and calculated $\Delta G_{f,373}^0$ as -3184 kJ mol⁻¹. Zotov et al. (1973) present two estimates of the free energy of formation of jarosite. Based on the synthesis of $(K_{0.9}Na_{0.1})Fe_3(SO_4)_2(OH)_6$ in a natural thermal water at 45°C they estimate $\Delta G_{f,298}^0$ as -3317.9 kJ mol⁻¹, and based on a precipitate from a natural water sample, they estimate $\Delta G_{f,298}^0$ as -3305.8 ± 4 kJ mol⁻¹. Stoffregen (1993) measured the solubility of jarosite under hydrothermal conditions and calculated a $\Delta G_{f,473,100\text{ bar}}^0$ of -3416.3 ± 1.7 kJ mol⁻¹. Chapman et al. (1983), Bladh (1982), Van Breemen (1973) and Hladky and Slansky (1981) have calculated solubility or free energy of formation based on reinterpretation of the above experimental studies.

One important source of the variation in the values for the free energy of formation of jarosite is the use of different values for the free energies for the ions used by different researchers. To compare the reported values better, we have recalculated the free energies for the formation of jarosite using the free energies for the ions used in this study and listed in Table 4-2. The results of these calculations are included in Table 4-1. However, even after eliminating the variation due to different free energies of the ions, a large variation in the reported free energies of formation of jarosite remains.

The values for the free energy of formation and the solubility product of jarosite that are currently considered the most reliable (e.g. Alpers et al., 1989, Nordstrom and Munoz, 1994) are the $\Delta G_{f,289}^0 = -3299.7 \pm 4$ kJ mol⁻¹ reported by Kashkay et al. (1975) and the log $K_{sp} = -9.21$ calculated from this free energy by Chapman et al. (1983). These values are considered the most reliable because they are based on actual solubility measurements and a consistent thermodynamic database. However, Alpers et al. (1989) noted that the free energies of formation of K-H₃O-Na jarosite solid solutions are more

Table 4-2. Thermodynamic data used in calculations.

Formula	State	$\Delta G_{f,298}^{\circ}$ (kJ mol ⁻¹)	ΔH_r° (kJ mol ⁻¹)	log K_r	Source
Fe ³⁺	aq	-17.87±1.0	-	-	2
FeSO ₄ ⁺	aq	-	16.36	3.92	1
FeHSO ₄ ²⁺	aq	-	-	2.48	4
Fe(SO ₄) ₂ ⁻	aq	-	19.3	5.42	1
FeOH ²⁺	aq	-	43.5	-2.19	1
Fe(OH) ₂ ⁺	aq	-	71.6	-5.67	5
Fe ₂ (OH) ₂ ⁴⁺	aq	-	56.5	-2.95	1
K ⁺	aq	-282.5±0.1	-	-	3
KSO ₄ ⁺	aq	-	9.41	0.85	1
SO ₄ ²⁻	aq	-744.0±0.4	-	-	3
HSO ₄ ⁻	aq	-	-22.4	1.98	3
OH ⁻	aq	-	55.836	-13.998	1
H ₂ O	l	-237.14±0.04	-	-	3

Sources:

- (1) Allison et al. (1990)
- (2) Naumov et al. (1971)
- (3) Cox et al. (1989)
- (4) Ball et al. (1987)
- (5) Nordstrom and Munoz (1994)

consistent with the free energy for pure jarosite reported by Vlek et al. (1974) and Zotov et al. (1973), indicating a lower free energy of formation and lower solubility than the Kashkay et al. (1975) value. It is not surprising, therefore, that Alpers et al. (1989) felt that additional experimental work was needed to determine accurately the solubility and free energy of formation of jarosite.

4.3 Experimental Methods

4.3.1 Synthesis of Jarosite

Synthetic jarosite often has a K deficiency because of hydronium substitution in the alkali ion position (Kubisz, 1970; Dutrizac and Kaiman, 1976). The factors that control hydronium substitution include the K^+ activity and the pH. To minimize hydronium substitution and to obtain a synthetic product with a composition close to the ideal formula, K^+ was added in excess to the synthesis solution as KOH, thus, simultaneously increasing the activity of K^+ and lowering the H_3O^+ activity. Jarosite was prepared by dissolving 5.6 g of reagent grade KOH and 17.2 g of reagent grade $Fe_2(SO_4)_3 \cdot 5H_2O$ in 100 mL H_2O at 95°C, 1 atm. The solution was placed in a covered beaker on a hot plate and continuously stirred. After four hours, the precipitate was allowed to settle and the residual solution decanted. The precipitate was then washed thoroughly with ultrapure water (18 megaohm cm) and dried at 110°C for 24 hours.

4.3.2 Characterization of Synthetic Jarosite

The synthetic solid was characterized using powder x-ray diffraction (XRD), scanning electron microscopy with energy dispersive spectroscopy (SEM/EDX), Fourier Transform Infrared Spectroscopy (FTIR), and thermogravimetric analysis (TGA). A small amount of precipitate was digested in HCl and analyzed for K and Fe using atomic absorption spectroscopy (AAS) and SO_4 using high performance ion chromatography (HPIC).

4.3.3 Dissolution Experiments

Two sets of dissolution experiments were implemented. The first was conducted at 25°C and the initial pH varied between 1.5 and 3.0. In the second set of experiments, the temperature was varied between 4 and 35°C with an initial pH of 2.0 for all experiments. For the dissolution experiments, 5 to 30 mg of the synthetic jarosite were added to ultrapure water with the pH adjusted to the desired value using $HClO_4$. To avoid formation of ferric oxyhydroxides at the higher pH values, 6.3×10^{-4} and 3.2×10^{-3} M of $CaSO_4 \cdot 2H_2O$ were added to the experiments with initial pH 2.6 and 3.0,

Table 4-3. Initial experimental conditions.

	amount of solution (mL)	amount of solid (mg)	initial pH	Temperature (°C)	[CaSO ₄ ·2H ₂ O] (mol L ⁻¹)	Duration of Experiment (days)
KJAR-1.5	20	30	1.50	25	0	166
KJAR-2.0	500	100	2.00	25	0	149
KJAR-2.3	20	5	2.30	25	0	166
KJAR-2.6	20	5	2.62	25	6.30×10^{-4}	166
KJAR-3.0	20	5	3.02	25	3.16×10^{-3}	166
KJAR-4C	20	5	2.00	4	0	176
KJAR-15C	20	5	2.00	15	0	176
KJAR-35C	20	5	2.00	35	0	176

All experiments were conducted in triplicate.

respectively. The solutions were placed in 20 mL glass vials and stirred with a stirrbar at a moderate rate (about 100 rpm) to provide good mixing. The temperature was maintained to within 0.1°C of the desired value using circulating water baths. The experiment with initial pH 2.0 and at 25°C (KJAR-2.0) was conducted prior to the other experiments to establish the approximate time required to achieve equilibrium. To allow more frequent sampling and analysis for K_{tot} , Fe_{tot} , SO_4^{2-} and pH for every sample, this experiment was conducted with 100 mg of synthetic jarosite in 500 mL of ultrapure water in a polyethylene bottle. The starting conditions for all dissolution experiments are listed in Table 4-3. All experiments were conducted in triplicate. The experiments were sampled over time to determine when equilibrium was achieved. Ten samples were collected from the experiments in which the pH was varied and 9 samples were collected from the experiments in which the temperature was varied. For each sample, 1 mL of the jarosite suspension was withdrawn. The samples were filtered using a 0.1 µm filter to remove suspended solids and then analyzed for potassium using AAS. After the K

concentration had not changed significantly (± 5 percent) for at least three consecutive samples a 4 mL sample was taken and analyzed for pH, Fe_{tot} and K_{tot} using AAS and SO_4^{2-} using HPIC. Since the dissolution experiments were conducted in oxidizing HClO_4 solutions and no reductants capable of reducing ferric iron were present, it was assumed that all iron was present as ferric iron.

4.4 Experimental Results

4.4.1 Solid Characterization

The yellow precipitate produced in the synthesis was identified as end-member jarosite by comparing powder x-ray diffraction patterns with those for jarosite reported in JCPDS card 22-827 (JCPDS, 1991) (Table 4-4, Figure 4-1). All the peaks produced by the precipitate could be identified as jarosite peaks. The absence of unidentified peaks indicates that no other crystalline phases are present in the precipitate at detectable levels. The unit cell dimensions were calculated as $a_0 = 7.291 \pm 0.005 \text{ \AA}$ and $c_0 = 17.136 \pm 0.015 \text{ \AA}$. These values are consistent with the those reported for pure end-member jarosite with no hydronium substitution (Alpers et al., 1989). Hydronium-jarosite has a_0 in the range of 7.34 to 7.36 \AA and jarosites with appreciable hydronium in solid solution have an elongated a-axis compared to pure endmember jarosite (Alpers et al., 1989). Examination with SEM/EDX showed that the precipitate consists of multicrystalline particles with uniform concentrations of K, Fe and S, ranging in size from 10-150 μm . No other crystalline or amorphous phases were observed.

Wet chemical analysis yielded a composition of the precipitate very close that of 'ideal' jarosite with a K:Fe: SO_4 ratio of 0.98:2.79:2 compared to the ideal 1:3:2 ratio. The measured stoichiometry indicates that the synthetic jarosite has almost no hydronium substitution and may have an Fe deficiency of approximately 7 percent. This deficiency is slightly larger than the analytical error of approximately 5 percent.

Thermogravimetric analysis was conducted by heating the synthetic jarosite from 30 to 900°C at a rate of 20°C/min (Figure 4-2). Curve A shows the weight loss versus temperature and curve B its derivative. The total weight loss over the interval is 38.5 percent. The curves show that the weight loss occurs in three principal temperature

Table 4-4. Powder x-ray diffraction peaks from synthetic jarosite used in dissolution experiments.

Synthetic jarosite used in this study		JCPDS Card 22-827 (JCPDS, 1991)		h k l
d-spacing (Å)	relative Intensity	d-spacing (Å)	relative Intensity	
5.94	30	5.93	45	1 0 1
5.72	15	5.72	25	0 0 3
5.09	58	5.09	70	0 1 2
3.66	22	3.65	40	1 1 0
3.55	5	3.55	4	1 0 4
3.11	85	3.11	75	0 2 1
3.08	100	3.08	100	1 1 3
2.969	11	2.965	15	2 0 2
2.855	16	2.861	30	0 0 6
2.542	21	2.542	30	0 2 4
2.302	10	2.302	12	1 2 2
2.282	29	2.287	40	1 0 7
1.979	37	1.977	45	0 3 3
1.935	7	1.937	10	0 2 7
1.909	6	1.909	8	0 0 9
1.828	30	1.825	45	2 2 0
1.769	6	1.776	6	2 0 8
1.740	6	1.738	6	2 2 3
1.720	5	1.717	6	3 1 2
1.690	4	1.690	2	1 1 9
1.659	5	1.656	2	1 0 10
1.625	5	1.621	6	1 3 4
1.592	5	1.595	6	1 2 8
1.572	5	1.572	4	4 0 1
1.560	6	1.560	6	3 1 5
1.551	7	1.552	6	0 4 2
1.534	15	1.536	20	2 2 6

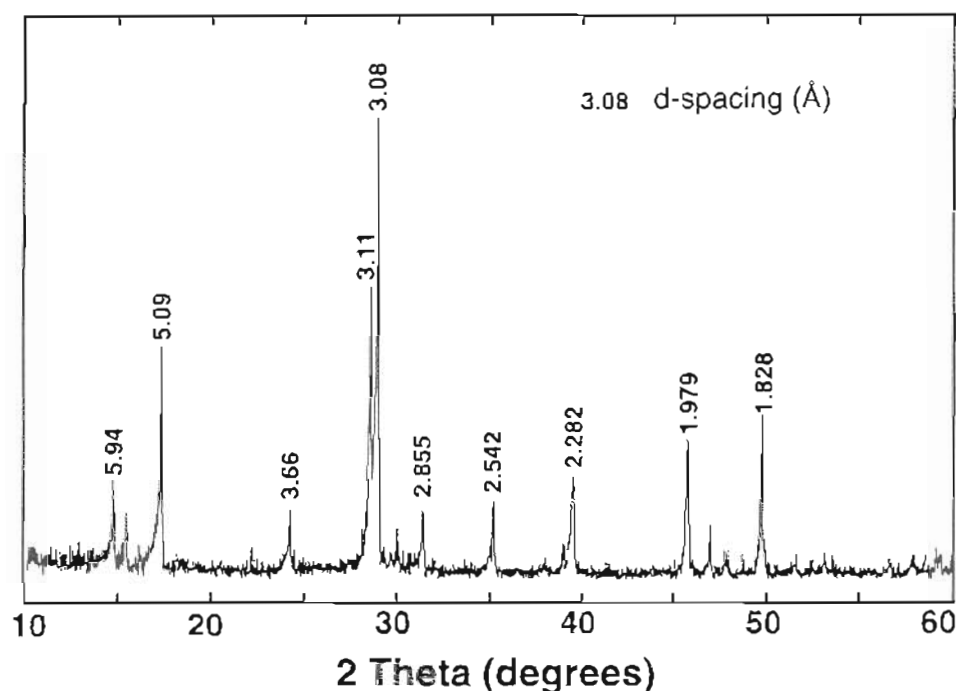


Figure 4-1. Powder X-ray diffraction spectrum of the synthetic jarosite. Some of the strongest peaks and the corresponding d-spacings are indicated.

intervals: (1) a 2.5 percent weight loss between 200 and 320°C, represented by a peak at about 260°C, (2) an 11 percent weight loss in the interval between 350 and 450°C, represented by a peak at about 430°C, and (3) a 25 percent weight loss between 560 and 800°C, represented by a group of four peaks at about 620, 720, 760 and 785°C.

The weight loss in the interval from 200 to 320°C is commonly attributed to the loss of hydronium (Brophy and Sheridan, 1965; Kubisz, 1970; Alpers et al., 1989). However, the weight loss of 2.5 percent observed in our experiments would correspond to about 0.66 moles of H_3O^+ per mol of jarosite, far exceeding the 0.02 moles of hydronium expected from the slight K deficiency determined in the chemical analysis. Similarly, the weight loss of around 2 to 3 percent in low-temperature, K-rich jarosites, commonly observed and attributed to hydronium (e.g. Brophy and Sheridan, 1965; Alpers et al., 1989), is inconsistent with the reported K^+ content of the jarosites. It appears that

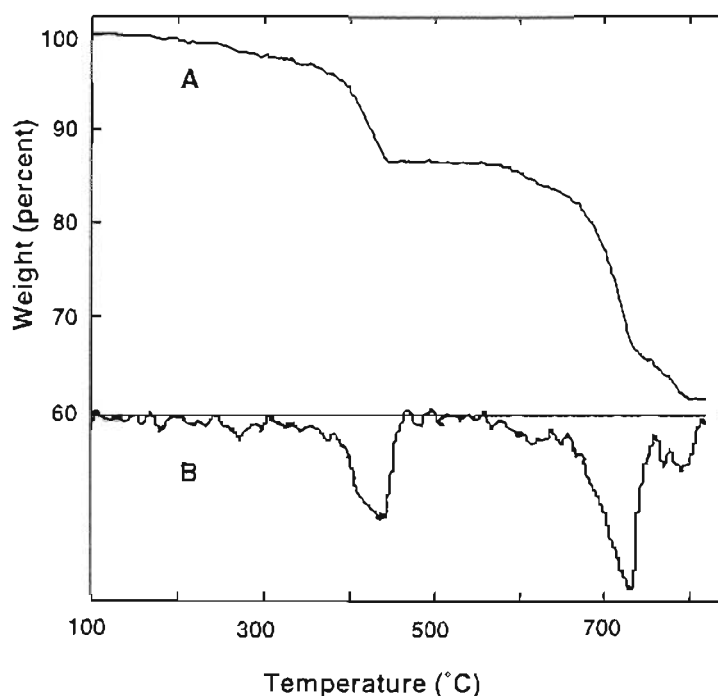


Figure 4-2. Thermogravimetric analysis of the synthetic jarosite. Curve A shows the weight loss versus temperature, curve B is its derivative.

most of the weight loss between 200 and 320°C must be from another source. An alternative explanation for this weight loss has been presented by Härtig et al. (1984). They noted that the charge deficiency caused by the Fe^{3+} deficit is likely balanced by a partial substitution of H_2O for OH^- , and argue that this water contributes a major portion of the weight loss between 200 and 320°C. Similar arguments are given by Kubisz (1972). The synthetic jarosite used in this study has an Fe deficit of 0.21 moles per mole of jarosite or a resultant charge deficiency of 0.63 positive charges per mole of jarosite. Thus, 0.63 moles of H_2O would have to be substituted for OH^- to balance the charge deficiency. This corresponds almost exactly to the 2.5 percent weight loss equivalent to a loss of 0.66 moles of water. The observed weight loss in the interval from 200 to 320°C can therefore almost completely be attributed to a loss of H_2O substituting for OH^- to balance the charge deficit due to the slight Fe deficiency and does not indicate a

significant hydronium substitution. A balanced, complete formula for the synthetic jarosite is $K_{0.98}(H_3O)_{0.02}Fe_{2.79}(SO_4)_2(OH)_{5.37}(H_2O)_{0.63}$.

The weight loss in the interval between 350 and 450°C corresponds to the decomposition of jarosite into $KFe(SO_4)_2$ and Fe_2O_3 and the loss of the remaining water in the crystal structure (Kulp and Adler, 1950). The 2.7 moles of water remaining in the crystal structure would correspond to 10 percent by weight which is close to the observed weight loss of 11.0 percent. The final weight loss between 560 and 800°C represents the second decomposition of the $KFe(SO_4)_2$ into K_2SO_4 and Fe_2O_3 and the release of 1.5 moles of SO_3 per mole of jarosite. The observed 25 percent weight loss is very close to the expected weight loss of 24 percent.

Comparison of the FTIR scan of the precipitate (Figure 4-3) and reported scans for jarosite (Kubisz, 1972; Wilkins et al., 1974; Powers et al., 1975) confirmed the identification as jarosite and the absence of other phases in the precipitate. The identification of hydronium in jarosites by FTIR is generally difficult and often not conclusive (Wilkins et al., 1974; Ripmeester et al., 1986). The only easily identifiable peak associated with hydronium in jarosite lies in the 1535-1575 cm^{-1} region as a weak peak on the shoulder of a stronger peak at 1635-1640 cm^{-1} , associated with H_2O (Kubisz, 1972; Wilkins et al., 1974). This hydronium peak is absent in the spectrum of our precipitate.

Based on these analyses, the synthetic jarosite has a composition of very close to the ideal stoichiometry with a small deficit of Fe^{3+} and some related substitution of H_2O for OH^- , but it does not have appreciable hydronium substitution in the alkali position.

4.4.2 Dissolution Experiments

In the dissolution experiments, the bulk of the reaction occurred within the first week of the experiment with rates declining with time. The evolution of the solution composition over time in the dissolution experiment at 25°C, initial pH 2 (KJAR-2.0) is shown in Figure 4-4 as an example for the dissolution process. Equilibrium was attained in the dissolution experiments after 80 to 125 days (Table 4-5). The equilibrium compositions of the solutions in the dissolution experiments are summarized in Table 4-5. The complete analytical results from the final sample taken from the triplicate

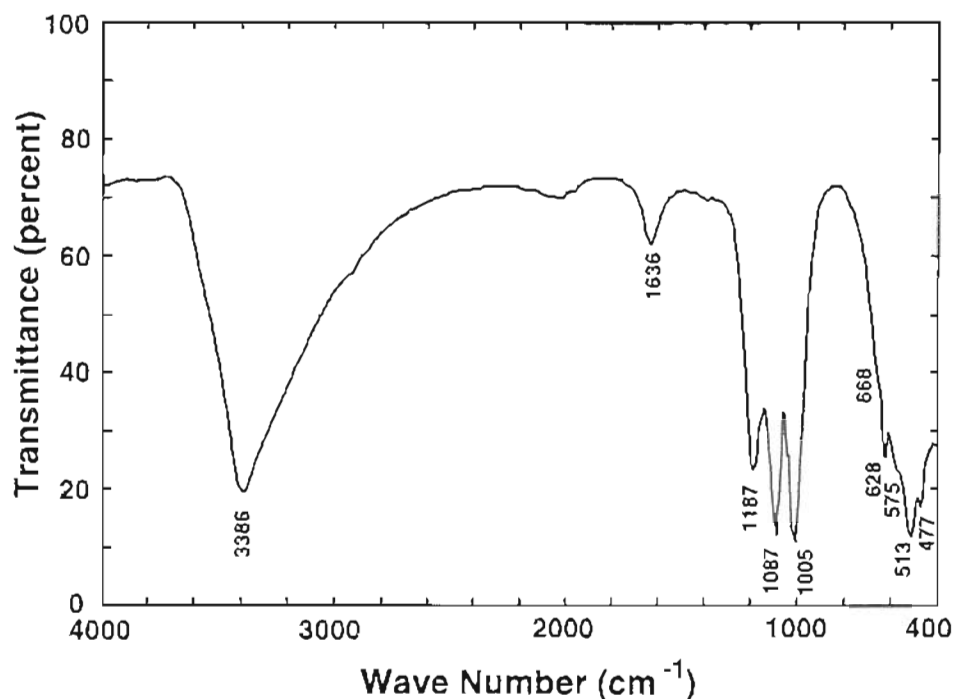


Figure 4-3. FTIR spectrum of the synthetic jarosite. The main vibrational bands in the spectrum are marked. They correspond to (Powers et al., 1975) the O-H stretch (3386 cm^{-1}), HOH deformation (1636 cm^{-1}), the ν_3 mode of SO_4^{2-} (1187 and 1087 cm^{-1}), OH deformation (1005 cm^{-1}), the ν_4 mode of SO_4^{2-} (668 and 628 cm^{-1}), and to the vibrations of the FeO_6 coordination octahedron (575 , 513 , and 477 cm^{-1}).

experiments are summarized in Table A-2 in Appendix A. Based on the measured equilibrium pH and K_{tot} , Fe_{tot} and SO_4^{2-} concentrations, equilibrium aqueous activities of K^+ , Fe^{3+} , and SO_4^{2-} were calculated using the geochemical speciation model MINTEQA2 (Allison et al., 1990). Activity corrections were made using the Davies Equation. The MINTEQA2 thermodynamic database was modified to include the $\text{FeHSO}_4^{2+}(\text{aq})$ ion pair. Other ion pairs included in the calculations and thermodynamic data used are listed in Table 4-2. These data are the currently most consistent dataset for the Fe-sulfate system (Alpers et al., 1989; D.K. Nordstrom, personal communication). Based on the calculated activities of H^+ , K^+ , Fe^{3+} , and SO_4^{2-} , the equilibrium ion activity products (IAP) were calculated using equation (2). The results of these calculations are

presented in Table 4-6. The average charge balance error in the MINTEQA2 calculations was 3 percent. The error associated with the log IAP values calculated from the standard deviation of the triplicate experiments range from 0.13 to 0.24 log units. The analytical error calculated from the precision of the analytical measurements (± 10 percent) and the precision of the pH buffer solutions (± 0.02 pH units) is 0.25 pH units (assuming that the covariance between these parameters equals zero). The error calculated from the triplicate experiments is smaller than the analytical error. The error associated with the log IAP values reported in Table 4-6 and used for subsequent calculations is the analytical error of ± 0.25 log units.

Table 4-5. Final concentrations in the dissolution experiments.

	pH	$[\text{SO}_4^{2-}]_{\text{tot}}$ (mmol L ⁻¹)*	$[\text{K}]_{\text{tot}}$ (mmol L ⁻¹)*	$[\text{Fe}]_{\text{tot}}$ (mmol L ⁻¹)*	Equilibrium established after (days)	Duration of Experiment (days)
KJAR-1.5	1.60 \pm 0.03	2.57 \pm 0.06	1.23 \pm 0.06	3.37 \pm 0.15	125	166
KJAR-2.0	2.10 \pm 0.02	0.332 \pm 0.04	0.178 \pm 0.004	0.434 \pm 0.005	80	149
KJAR-2.3	2.34 \pm 0.03	0.313 \pm 0.013	0.159 \pm 0.007	0.171 \pm 0.018	100	166
KJAR-2.6	2.60 \pm 0.03	0.632 \pm 0.06	0.111 \pm 0.004	0.051 \pm 0.004	120	166
KJAR-3.0	2.99 \pm 0.03	3.26 \pm 0.28	0.085 \pm 0.022	0.013 \pm 0.001	120	166
KJAR-4C	2.01 \pm 0.02	0.339 \pm 0.016	0.217 \pm 0.004	0.519 \pm 0.016	125	176
KJAR-15C	2.03 \pm 0.02	0.347 \pm 0.015	0.225 \pm 0.004	0.530 \pm 0.012	100	176
KJAR-35C	2.01 \pm 0.03	0.528 \pm 0.032	0.318 \pm 0.019	0.464 \pm 0.005	100	176

* The reported concentrations represent the mean \pm the standard deviation from triplicate experiments.

As previously discussed, the synthetic jarosite has a composition slightly different from the ideal composition on which equation (2) is based. However, using equation (2) with the ideal stoichiometry is consistent with previous work on the solubility of jarosite and appears justified since the non-ideality is only slight. If one was to use the actual composition as determined by the chemical analysis, calculated ion activity products

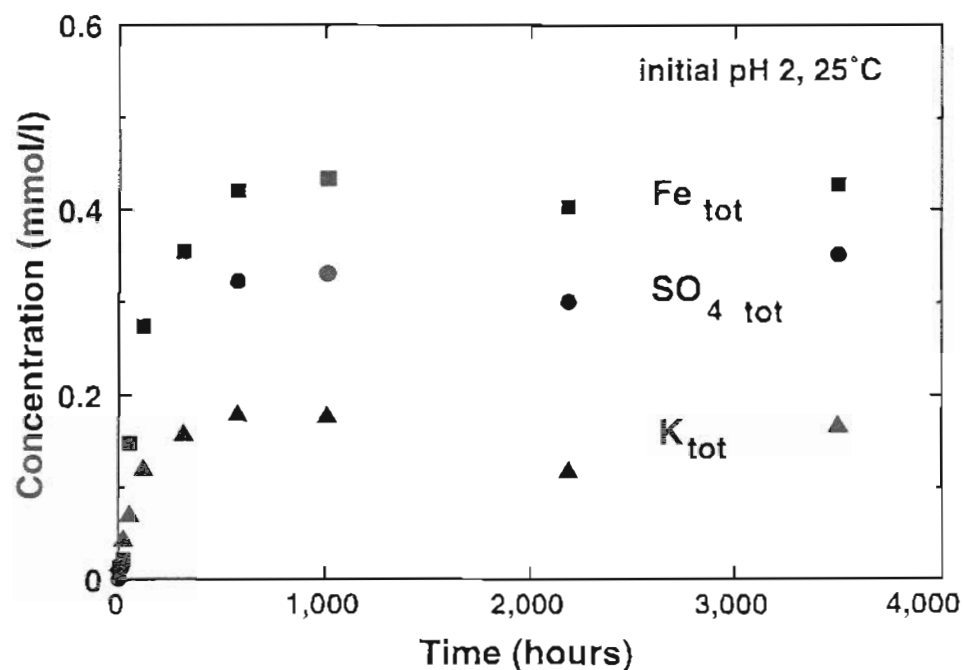


Figure 4-4. Concentrations of K_{tot} (▲), Fe_{tot} (■), and $SO_4^{2-}_{tot}$ (●) in the dissolution experiment with initial pH 2.0, equilibrium pH 2.10. Data points represent the average of triplicate experiments.

would be approximately 0.5 log units lower than the ones calculated using the ideal stoichiometry. This difference is due primarily to substitution of H_2O for OH^- groups.

To evaluate the effect of different activity correction models, ion activity products were also calculated using the extended Debye-Hückel equation. At the low ionic strengths of the experiments, the difference between these two methods is small. For the experiment with the highest ionic strength (0.04 M), the IAP calculated with the extended Debye-Hückel equation is about 0.2 log units greater than the one calculated using the Davies equation. For all other experiments, the difference between the IAP calculated with the two methods is less than 0.05 log units. The activity correction models used in this study are described in detail in Appendix B.

4.5 Discussion

The log IAP calculated using equilibrium activities from the experiments with different initial pH values and at 25°C varies from -10.81 to -11.36 (Table 4-6). A plot of log IAP versus pH (Figure 4-5) suggests that there is no trend in the data and a t-test indicates that the slope is not significantly different from zero at the 95 percent significance level ($t = -0.014$, 3 degrees of freedom). The average equilibrium log IAP represents the log K_{sp} at 25°C and it is calculated as -11.0 ± 0.3 . The error in the log K_{sp} value represents the total standard deviation over all experiments. An F-test indicates that the variance among the log IAP values at different pH values is not significantly different from the variance within the triplicate experiments at the 95 percent confidence level ($F=2.6$, $n_1=5$, $n_2=15$, $df_1=4$, $df_2=10$). At equilibrium, the Gibbs free energy of reaction at 25°C is given by

$$\begin{aligned} \Delta G_{\text{reaction}}^0 = & \Delta G_{f,298}^0(K^+) + 3\Delta G_{f,298}^0(Fe^{3+}) + 2\Delta G_{f,298}^0(SO_4^{2-}) \\ & + 6\Delta G_{f,298}^0(H_2O) - \Delta G_{f,298,\text{jarosite}}^0 \end{aligned} \quad (3)$$

with the free energy of reaction related to the K_{sp} by

$$\Delta G_{\text{reaction}}^0 = -RT \ln K_{sp} \quad (4)$$

Solving for the free energy of formation of jarosite

$$\begin{aligned} \Delta G_{f,298,\text{jarosite}}^0 = & \Delta G_{f,298}^0(K^+) + 3\Delta G_{f,298}^0(Fe^{3+}) + 2\Delta G_{f,298}^0(SO_4^{2-}) \\ & + 6\Delta G_{f,298}^0(H_2O) + RT \ln K_{sp} \end{aligned} \quad (5)$$

and using the free energies given in Table 4-2, we calculate $\Delta G_{f,298,\text{jarosite}}^0 = -3309.8 \pm 1.7 \text{ kJ mol}^{-1}$ where the variation represents the error introduced by the uncertainty in the K_{sp} value only. The error in the free energies of the individual ions (Table 4-2) adds an additional uncertainty of $\pm 4.5 \text{ kJ mol}^{-1}$. The error introduced by the uncertainty in the free energies of the individual ions is large compared to the error of the solubility

determination. The error in the free energies of some of the individual ions may be larger than reported in Table 4-2, resulting in an even larger uncertainty in the estimate of $\Delta G_{f,298,\text{jarosite}}^0$. For example, for $\Delta G_{f,298}^0(\text{Fe}^{3+})$ values as high as -4.6 kJ mol^{-1} have been reported (Wagman et al., 1969). Propagating an uncertainty of 13.3 kJ mol^{-1} for $\Delta G_{f,298}^0(\text{Fe}^{3+})$ through equation (5) results in an overall uncertainty of $\pm 43 \text{ kJ mol}^{-1}$ for $\Delta G_{f,298,\text{jarosite}}^0$.

Table 4-6. Calculated equilibrium activities.

	pH	log {SO ₄ ²⁻ }	log {K ⁺ }	log {Fe ³⁺ }	Ionic Strength (M)	calculated log IAP
KJAR-1.5	1.60	-3.54	-3.00	-3.44	4.69×10^{-2}	-10.81 ± 0.25
KJAR-2.0	2.10	-3.99	-3.80	-4.06	1.18×10^{-2}	-11.36 ± 0.25
KJAR-2.3	2.34	-3.84	-3.84	-4.51	6.15×10^{-3}	-11.03 ± 0.25
KJAR-2.6	2.60	-3.45	-3.99	-5.25	5.08×10^{-3}	-11.06 ± 0.25
KJAR-3.0	2.99	-2.79	-4.12	-6.37	1.16×10^{-2}	-10.89 ± 0.25
KJAR-4C	2.01	-3.94	-3.71	-3.85	1.34×10^{-2}	-11.06 ± 0.25
KJAR-15C	2.03	-3.98	-3.70	-3.89	1.34×10^{-2}	-11.14 ± 0.25
KJAR-35C	2.01	-3.87	-3.55	-4.14	1.31×10^{-2}	-11.68 ± 0.25

The $\log K_{sp} = -11.0 \pm 0.3$ and the free energy of formation, $\Delta G_{f,298}^0 = -3309.8 \pm 1.7 \text{ kJ mol}^{-1}$ are well within the range of values reported in the literature (Table 4-1). They are, however, significantly lower than the commonly accepted values of $\log K_{sp} = -9.21$ and $\Delta G_{f,298}^0 = -3299.7 \pm 4 \text{ kJ mol}^{-1}$ (Kashkay et al., 1975, Chapman et al., 1983). In a study of the solubility of (K-Na-H₃O)-jarosite solid solutions precipitated from natural water samples, Alpers et al. (1989) calculated the free energy of formation of these solid solutions and noted that their results were not consistent with the free energy of formation for jarosite reported by Kashkay et al. (1975). Based on their results, they suggested that

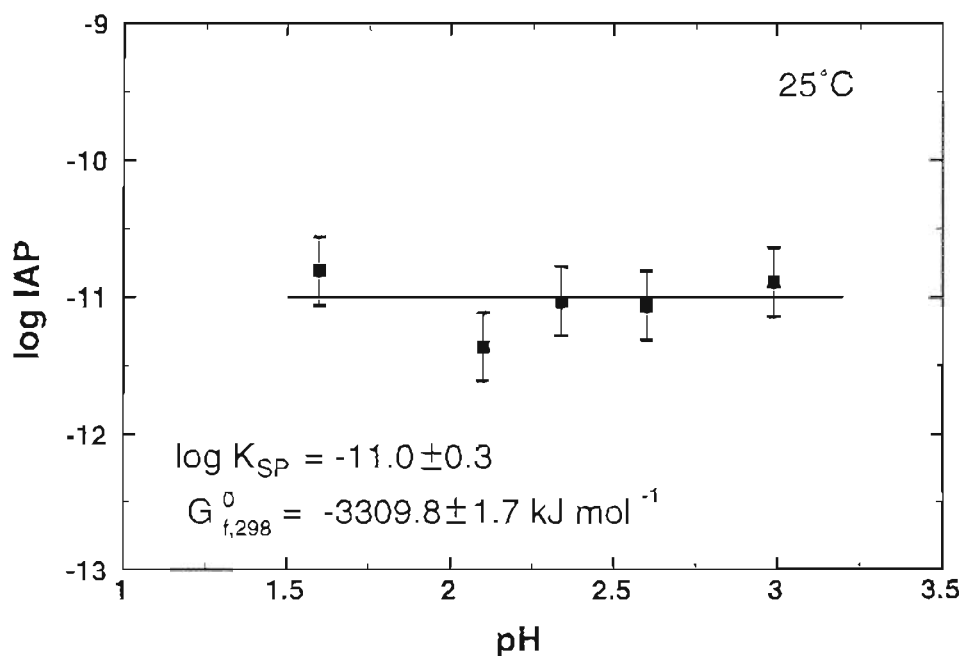


Figure 4-5. Calculated log ion activity product from five dissolution experiments at 25°C. The solid line represents the average log IAP from the five experiments (-11.0 ± 0.3).

the $\Delta G_{f,298}^0$ for jarosite may be closer to the value of $-3310.7 \text{ kJ mol}^{-1}$ reported by Vlek et al. (1974) or the $-3305.8 \pm 4 \text{ kJ mol}^{-1}$ reported by Zotov et al. (1973). Such values of $\Delta G_{f,298}^0$ imply that the K_{SP} may be 1 to 2 log units lower than the commonly quoted -9.21 . Our results are consistent with the results of Alpers et al. (1989). We have estimated the jarosite free energy of formation using the free energies for K-Na- H_3O jarosite solid solutions from Alpers et al. (1989) and from Zotov et al. (1973). Assuming an ideal solid solution in the pseudo-binary between $((\text{H}_3\text{O})_{0.75}\text{Na}_{0.25})$ -jarosite and jarosite, one can fit an ideal solid solution model to the free energies and estimate $\Delta G_{f,298,\text{jarosite}}^0$ from

$$\begin{aligned}
\Delta G^0_{f,298,(K,Na,H,O)-jarosite\ solid\ solution} &= (\Delta G^0_{f,298,(H,O,Na)-jarosite} \\
&+ X_K \times (\Delta G^0_{f,298,K-jarosite} - \Delta G^0_{f,298,(H,O,Na)-jarosite})) \\
&+ (X_K \times RT \times \ln(X_K) + (1-X_K) \times RT \times \ln(1-X_K))
\end{aligned} \tag{6}$$

where X_K is the mole fraction of potassium in the alkali position (Figure 4-6). The $\Delta G^0_{f,298,jarosite}$ was estimated as -3308.4 ± 2.2 kJ mol⁻¹ which is in excellent agreement with the value we obtained in our dissolution experiments.

Key questions that need to be addressed are the reasons for the apparent discrepancy between the results of this study and the results of Kashkay et al. (1975) and which results best represent the thermodynamic properties of jarosite. Possible sources of the discrepancy include the thermodynamic data and the speciation model used in the two studies. However, the free energies of formation of the ions used in the two studies are consistent and recalculating the log K_{sp} from the equilibrium solution compositions given by Kashkay et al. (1975) with the speciation model used in this study yields a value of log $K_{sp} = -8.4 \pm 0.7$, which is even greater than the value calculated by Chapman et al. (1983). Another possible reason for the apparent inconsistency is the substitution of hydronium in the crystal structure. Hydronium jarosite, which has a reported log K_{sp} of -5.39 and a $\Delta G^0_{f,298}$ of -3232.1 kJ mol⁻¹ (Kashkay et al., 1975; Chapman et al., 1983), is significantly more soluble than jarosite. Hydronium substitution in the jarosite crystal structure would therefore lead to a greater overall solubility and a greater $\Delta G^0_{f,298}$. A 15-30 percent hydronium substitution for K, a range commonly reported for both synthetic and natural jarosite (e.g. Brophy and Sheridan, 1965; Kubisz, 1970), would result in a solubility product about one to two log units greater than that of pure jarosite.

Kashkay et al. (1975) report that the compositions of their precipitates were close to ideal jarosite and that they did not detect any significant hydronium. However, if a hydronium-enriched jarosite was precipitated as a thin surface layer, it may not have been detected in the analysis of the bulk precipitate. Solutions would equilibrate with this

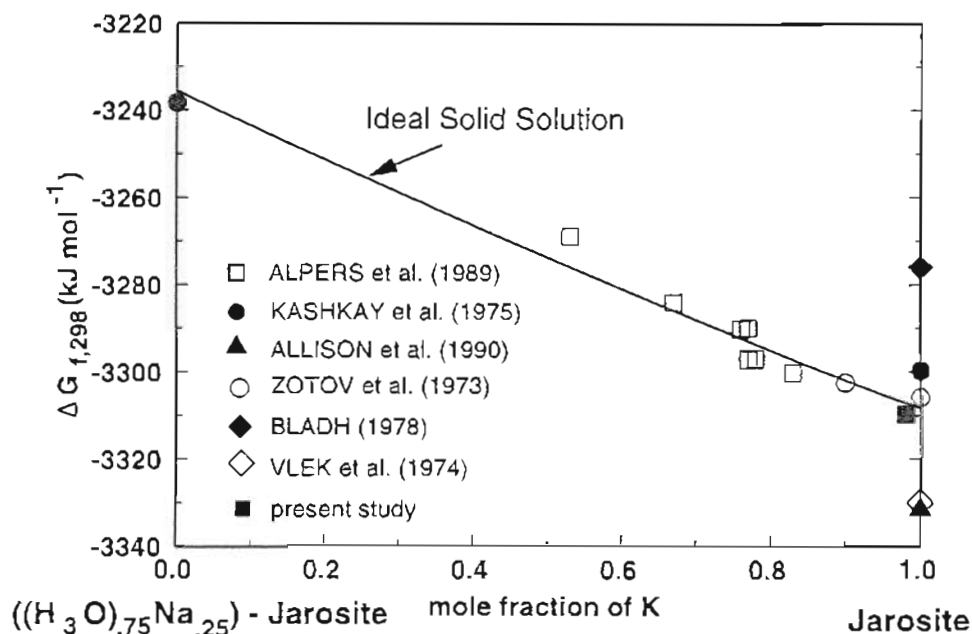


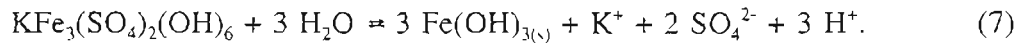
Figure 4-6. Free energy of formation for (K-Na-H₃O)-jarosite solid solutions from Alpers et al. (1989) (□) and Zotov et al. (1973) (○). The solid line represents the fit of an ideal solid solution mixing curve between jarosite and ((H₃O)_{0.75}Na_{0.25})-jarosite. Reported free energies of formation of jarosite from Kashkay et al. (1975) (●) and Zotov et al. (1973) (○), and calculated free energies of formation from Allison et al. (1990) (▲), Vlek et al. (1974) (◇), Bladh (1978) (◆), and from this study (■) are also included for comparison. For consistency, all free energies have been recalculated using the free energies of ions given in Table 4-2.

hydronium-enriched surface layer, rather than with the bulk solid and would yield greater apparent solubility products for jarosite.

The experiments conducted by Kashkay et al. (1975) were "free-drift" precipitation experiments in which jarosite was precipitated from supersaturated solutions. The solution composition was not held constant during the experiments and concentrations of K⁺, Fe(III) and SO₄²⁻, as well as pH, were allowed to drift freely as the precipitation proceeded. In all three experiments, the solutions at equilibrium were depleted in K relative to Fe and SO₄²⁻ and enriched in H₃O⁺ compared to the initial solutions.

Specifically, the K:SO₄ ratio at equilibrium decreased by more than an order of magnitude and the pH decreased by 0.2 to 0.4 units compared to the beginning of the experiments. It appears likely that the solids precipitated on the surface when the solutions were close to equilibrium would be hydronium enriched resulting in a more soluble surface layer on the bulk jarosite precipitate. The formation of a hydronium-enriched surface coating is unlikely when dissolving the less soluble end member of a solid solution as in the experiments reported in this study. We therefore believe that our values better represent the solubility of pure jarosite.

The solubility product for jarosite that was obtained in this study is lower than the commonly cited value of -9.21 (Kashkay et al., 1975; Chapman et al., 1983), which suggests that the stability field of jarosite is larger than previously expected. The stability of jarosite is generally limited to a relatively narrow range of acidic conditions. As pH increases, jarosite is transformed to ferric oxyhydroxide, represented in the following discussion as Fe(OH)_{3(s)}. The reaction between these two phases is



At equilibrium, this transformation can be expressed as

$$\begin{aligned} \log K_{SP, \text{jarosite}} - 3 \log K_{SP, \text{Fe}(\text{OH})_{3(s)}} = \\ \log \{K^+\} + 2 \log \{SO_4^{2-}\} + 3 \log \{H^+\} - 3 \log \{H_2O\} \end{aligned} \quad (8)$$

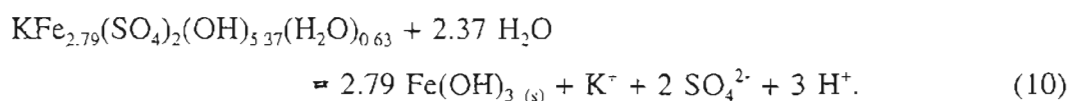
Therefore, the transition pH, pH_T, is

$$\begin{aligned} \text{pH}_T = -\frac{1}{3} \log K_{SP, \text{jarosite}} + \log K_{SP, \text{Fe}(\text{OH})_{3(s)}} + \frac{1}{3} \log \{K^+\} \\ + \frac{2}{3} \log \{SO_4^{2-}\} - \log \{H_2O\} \end{aligned} \quad (9)$$

From equation (9), it becomes apparent that pH_T is a function of the solubility products of jarosite and Fe(OH)_{3(s)}, and the activities of K⁺ and SO₄²⁻. The newly determined log

K_{sp} for jarosite of -11.0 results in a transition pH which is 0.6 pH units higher than calculated using the value of -9.21 from Kashkay et al. (1975) and Chapman et al. (1983). For a water (Nordstrom and Munoz, 1994) with $\{K^+\} = 10^{-4}$ and $\{SO_4^{2-}\} = 10^{-2}$ and taking $\log K_{sp}$ of $Fe(OH)_{3(s)}$ as 4.89 (Allison et al., 1990), we calculate $pH_T = 5.89$ versus a $pH_T = 5.29$ calculated from Kashkay et al. (1975) and Chapman et al. (1983). The solubility product for $Fe(OH)_{3(s)}$ in the MINTEQA2 data base (Allison et al. 1990) represents a freshly precipitated, poorly crystalline ferric oxyhydroxide (Langmuir and Whittemore, 1971). The solubility product of aged, more crystalline ferric oxyhydroxide is up to 6 orders of magnitude lower (Langmuir and Whittemore, 1971) and its stability field would be correspondingly larger. The transition pH between jarosite and aged, more crystalline ferric oxyhydroxide would therefore be correspondingly lower.

As previously discussed, incorporation of the non-ideal stoichiometry of jarosite with a measured Fe-deficit of 0.21 moles of Fe per mole of jarosite in the solubility expression leads to a calculated $\log K_{sp} = -11.5$, about 0.5 log units lower than the one calculated using the ideal stoichiometry. Using the specific stoichiometry of our jarosite, the transformation to $Fe(OH)_{3(s)}$ is written as



At equilibrium, the transformation is expressed as

$$\log K_{sp, jarosite} - 2.79 \log K_{sp, Fe(OH)_{3(s)}} \\ = \log \{K^+\} + 2 \log \{SO_4^{2-}\} + 3 \log \{H^+\} - 2.37 \log \{H_2O\} \quad (11)$$

and the transition pH is

$$\begin{aligned}
 \text{pH}_T = & -\frac{1}{3}\log K_{\text{SP,jarosite}} + (2.79/3)\log K_{\text{SP,Fe(OH)}_{3(s)}} + \frac{1}{3}\log\{K^+\} \\
 & + \frac{2}{3}\log\{SO_4^{2-}\} - (2.37/3)\log\{H_2O\}
 \end{aligned}
 \quad (12)$$

Substituting our $\log K_{\text{SP,jarosite}} = -11.5$ calculated for the non-ideal stoichiometry into equation (12) and using $\log K_{\text{SP}}$ of $\text{Fe(OH)}_{3(s)} = 4.89$ (Allison et al., 1990) yields a pH_T which is 0.17 pH units lower than the value obtained using the ideal composition. The transition pH determined using the $\log K_{\text{SP,jarosite}}$ calculated taking the non-ideal stoichiometry into account is 0.43 pH units higher than the value calculated using the $\log K_{\text{SP,jarosite}}$ from Kashkay et al. (1975) and Chapman et al. (1983). For our example water ($\{K^+\} = 10^{-4}$, $\{SO_4^{2-}\} = 10^{-4}$) we calculate $\text{pH}_T = 5.72$ using the ideal stoichiometry and our $\log K_{\text{SP,jarosite}}$ compared to a $\text{pH}_T = 5.89$ calculated using the ideal stoichiometry and a $\text{pH}_T = 5.29$ calculated with the $\log K_{\text{SP,jarosite}}$ from Kashkay et al. (1975) and Chapman et al. (1983).

The calculated log IAP decreases with increasing temperature, varying from -11.06 at 4°C to -11.68 at 35°C (Table 4-6, Figure 4-7), indicating a negative enthalpy of reaction, ΔH_r^0 , for the dissolution of jarosite. The dependence of log IAP on the inverse of the temperature is not linear, indicating that the enthalpy of reaction, ΔH_r^0 , varies over the temperature range from 4-35°C. Therefore, a variable enthalpy and constant heat capacity model (Nordstrom and Munoz, 1985) was used to model the temperature dependence

$$\log K_{\text{SP}} = \frac{\Delta S_r^0 - \Delta C_{p,r}}{R} - \frac{\Delta H_r^0}{RT} + \frac{(\Delta C_{p,r} \log T)}{R} \quad (13)$$

where ΔS_r^0 is the entropy of reaction, $\Delta C_{p,r}$ is the heat capacity of reaction, R is the gas constant ($8.314 \times 10^{-3} \text{ kJ mol}^{-1} \text{ K}^{-1}$), and T is the temperature in K. Fitting the temperature-dependent data to equation (13) (Figure 4-7) yields $\Delta H_{r,298}^0 = -45 \pm 5 \text{ kJ mol}^{-1}$, $\Delta S_{r,298}^0 = -350 \pm 35 \text{ J mol}^{-1} \text{ K}^{-1}$, and $\Delta C_{p,r} = -2.1 \pm 0.2 \text{ kJ mol}^{-1} \text{ K}^{-1}$. This model gives an excellent fit of the data ($r^2=0.999$) and although only four data points were used to

determine the three parameters ($\Delta H_{r,298}^0$, $\Delta S_{r,298}^0$, $\Delta C_{p,r}$), a t-test indicates that all parameters are statistically significant at the 95 percent confidence level. Further support for our results is provided by Kashkay et al. (1975) who report a $\log K_{SP,373}$ of -15.83 for a jarosite precipitated at 100°C. Extrapolating equation (13) with the parameters determined from the experiments at temperatures between 4 - 35°C to 100°C we obtain a $\log K_{SP,373}$ of -15.6 that is in excellent agreement with the value measured by Kashkay et al. (1975) (Figure 4-7). Unfortunately, we do not know the exact composition of the jarosite precipitated at 100°C by Kashkay et al. (1975) and if it contained a significant amount of hydronium. However, their result is consistent with our experiments and it appears that the parameters we determined adequately describe the temperature dependence of the K_{SP} of jarosite over at least the range from 4-100°C.

The dissolution experiment with initial pH 2 at 25°C (Figure 4-4) was used to evaluate the rate of the jarosite dissolution reaction. This experiment was sampled most frequently and the only one with sufficient data for a reaction rate analysis. The potassium concentrations were plotted as $\log(C_0 - C)$ versus time, where C_0 is the concentration at equilibrium and C is the concentration at time t (Figure 4-8). The linearity of the plot indicates that the dissolution kinetics can be described by a first-order model of the form

$$\frac{dC}{dt} = -k(C_0 - C) \quad (14)$$

where k is the apparent rate coefficient. Integration of equation (14) yields a linear equation for $\log(C_0 - C)$ versus time. The slope of the line is the apparent rate coefficient, k , and the intercept, k_0 , is the log of C_0 . The data were also plotted as $(C_0 - C)^{-1}$ versus time and C/t versus C to test for second-order behavior but deviations from second-order behavior become obvious in both types of plots. It appears that the dissolution reaction at pH 2 and 25°C can be best described by a first-order model with an apparent rate coefficient, k , of approximately $7.9 \pm 0.5 \times 10^{-7} \text{ s}^{-1}$.

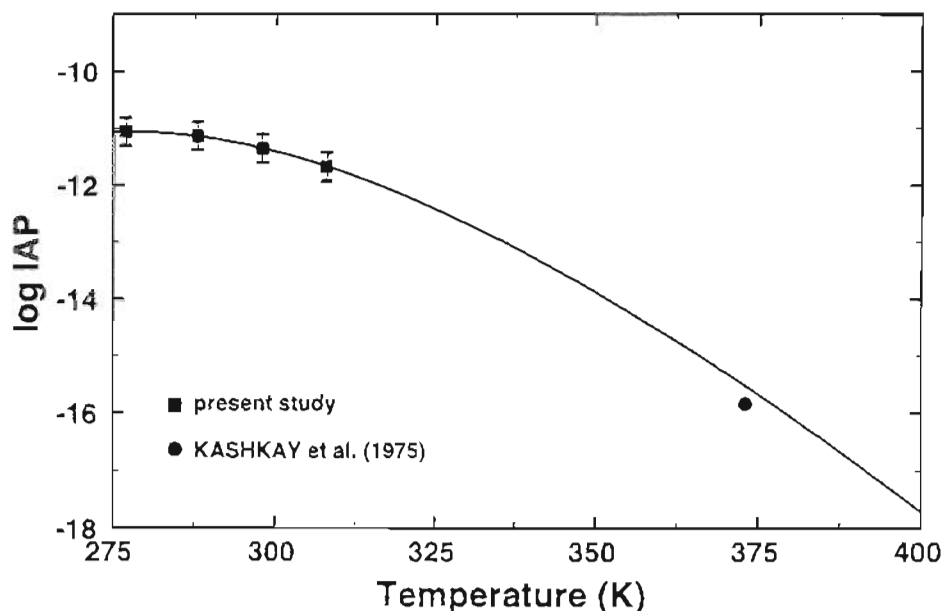


Figure 4-7. Calculated log ion activity product versus temperature from four dissolution experiments at 4, 15, 25 and 35°C, initial pH 2 (■). The solid line is the best fit of the variable enthalpy and constant heat capacity model to the experimental data extrapolated to 125°C. The solubility product measured by Kashkay et al. (1975) at 100°C (•) is also included, but it was not used to determine the model fit.

4.6 Summary

The solubility, free energy of formation, enthalpy of reaction, entropy of reaction, heat capacity, and dissolution kinetics of a synthetic jarosite were determined in a set of dissolution experiments conducted in the temperature range of 4 - 35°C and pH 1.5 to 3. The rate of the dissolution reaction can be described by a first-order model. Equilibrium is attained in the dissolution experiments after 80 to 125 days. The solubility and free energy of formation that we determined are in excellent agreement with data from Alpers et al. (1989) who studied (K-Na-H₃O)-jarosite solid solutions. The K_{sp} reported in the present study is almost two log units lower than the currently accepted value from Kashkay et al. (1975) and Chapman et al. (1983). The higher K_{sp} obtained by these

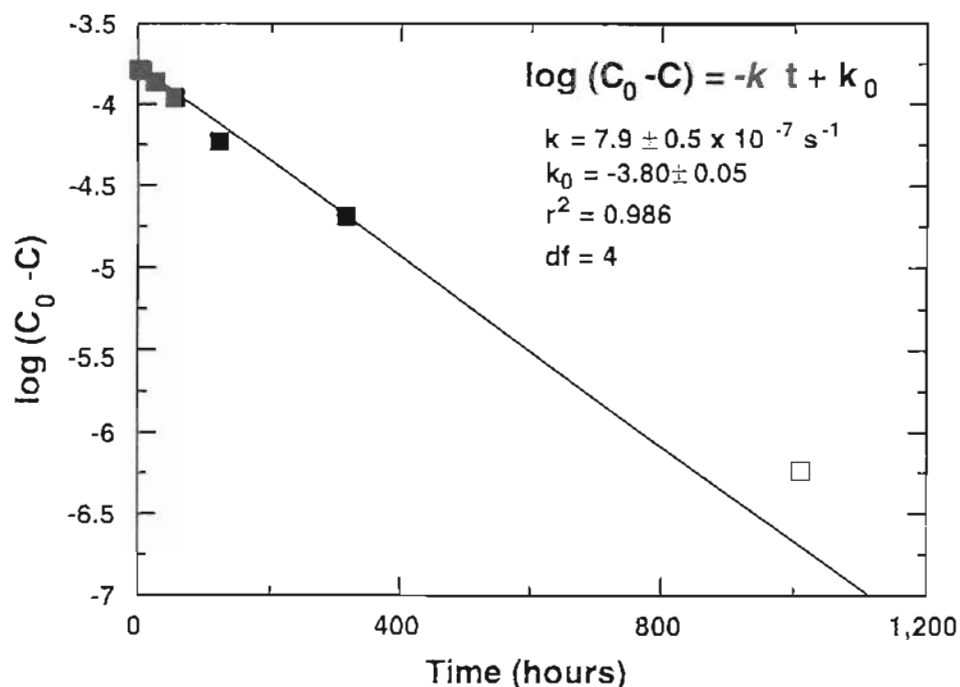


Figure 4-8. Plot of the log of the equilibrium concentration of potassium (C_0) minus the concentration of potassium at time t (C) for dissolution experiment KJAR-2.0, to test for first order behavior. Concentrations are in mol/l. The solid line is the regression. The last datapoint was not used for the regression since the difference between the measured and equilibrium concentrations is less than the analytical error.

researchers may represent the solubility product of a thin surface layer of hydronium-enriched jarosite that could have formed in their free-drift precipitation experiments. The significantly lower solubility product obtained in this study indicates that jarosite is more stable and may occur at pH values higher than previously thought.

The temperature dependence of the solubility product was determined for the temperature range from 4-35°C. Based on a solubility measurement at 100°C by Kashkay et al. (1975) it appears that the parameters we determined for the temperature range of our experiments can also be used to model the solubility up to 100°C.

4.7 References

- Allison J.D., Brown D.S., and Novo-Gradac K.J. (1990) *MINTEQA2/PRODEFA2, a geochemical assessment model for environmental systems: version 3.0*. U.S. Environmental Protection Agency, Athens, GA.
- Alpers C.N., Nordstrom D.K., and Ball J.W. (1989) Solubility of jarosite solid solutions precipitated from acid mine waters, Iron Mountain, California, U.S.A.. *Sci. Géol., Bull.* **42**, 281-298.
- Alpers C.N., Rye R.O., Nordstrom D.K., White L.D., and King B.S. (1992) Chemical, crystallographic and stable isotopic properties of alunite and jarosite from acid-hypersaline Australian lakes. *Chem. Geol.* **96**, 203-226.
- Ball J.W., Nordstrom D.K., and Zachmann D.W. (1987) WATEQ4F. A personal computer FORTRAN translation of the geochemical model WATEQ2 with revised data base. *Open-File Rept.* 87-150. U.S. Geological Survey.
- Bladh K.W. (1982) The formation of goethite, jarosite, and alunite during the weathering of sulfide bearing felsic rocks. *Econ. Geol.* **77**, 176-184.
- Brophy G.P., and Sheridan M.F. (1965) Sulfate studies. IV. The jarosite-natrojarosite-hydronium jarosite solid solution series. *Am. Miner.* **50**, 112-126.
- Brown J.B. (1970) A chemical study of some synthetic potassium-hydronium jarosites. *Can. Mineral.* **10**, 696-703.
- Carson C.D, and Dixon J.B. (1983) Mineralogy and acidity of an inland acid sulfate soil of Texas. *Soil Sci. Soc. Am. J.* **47**, 828-833.
- Chapman B.M., Jones D.R., and Jung R.F. (1983) Processes controlling metal ion attenuation in acid mine drainage streams. *Geochim. Cosmochim. Acta* **47**, 1957-1973.
- Cox J.D., Wagman D.D., and Medvedev V.A. (1989) *CODATA Key Values for Thermodynamics*. Hemisphere Publishing Corporation.
- Dutrizac J.E. (1983) Factors affecting alkali jarosite precipitation. *Metall. Trans. B* **14B**, 531-539.
- Dutrizac J.E. and Kaiman S. (1976) Synthesis and properties of jarosite-type compounds. *Can. Mineral.* **14**, 151-158.
- Härtig C., Brand P., and Bohmhammel K. (1984) Fe-Al-Isomorphie und Strukturwasser in Kristallen vom Jarosit-Alunit-Typ. *Z. anorg. allg. Chem.* **508**, 159-164.

Hladky G. and Slansky E. (1981) Stability of alunite minerals in aqueous solution at normal temperature and pressure. *Bull. Minéral.* **104**, 468-477.

JCPDS (Joint Committee on Powder Diffraction Standards) (1991) Mineral Powder Diffraction File. International Center for Diffraction Data. Swarthmore, Pennsylvania.

Kashkay C.M., Borovskaya Y.B., and Badazade M.A. (1975) Determination of $\Delta G^{\circ}_{f, 298}$ of synthetic jarosite and its sulfate analogues. *Geochem. Int.* **12**, 115-121.

Keith W.J., Calk L., and Ashley R.P. (1979) Crystals of coexisting alunite and jarosite, Goldfield, Nevada. *Shorter contributions to Mineralogy and Petrology* C1-C5. U.S. Geological Survey.

Kubisz J. (1964) A study of minerals in the alunite-jarosite group. *Polska Akad. Nauk, Prace Geol.* **22**, 1-93.

Kubisz J. (1970) Studies on synthetic alkali-hydronium jarosite. I. Synthesis of jarosite and natrojarosite. *Mineral. Pol.* **1**, 47-57.

Kubisz J. (1972) Studies on synthetic alkali-hydronium jarosite. III. Infrared adsorption study. *Mineral. Pol.* **3**, 23-37.

Kulp J.L. and Adler H.H. (1950) Thermal study of jarosite. *Am. J. Sci.* **248**, 475-487.

Langmuir D. and Whittemore D.O. (1971) Variations in the stability of precipitated ferric oxyhydroxides. In *Nonequilibrium systems in natural water chemistry* (ed. J.D. Hem), Advances in Chemistry Series, No. 106, 209-234. American Chemical Society, Washington, D.C.

Long D.T., Fegan N.E., McKee J.D., Lyons W.B., Hines M.E. and Macumber P.G. (1992) Formation of alunite, jarosite and hydrous iron oxides in a hypersaline system: Lake Tyrell, Victoria, Australia. *Chem. Geol.* **96**, 183-202.

Naumov G.B., Ryzhenko I.L. and Khodakovskiy I.L. (1971) *Handbook of Thermodynamic Data* (translated from Russian by G.J. Soleimami, edited by I. Barnes and V. Speltz). Washington D.C. NTIS publication PB-226 722.

Nordstrom D.K. (1977) Hydrogeochemical and microbiological factors affecting the heavy metal chemistry of an acid mine drainage system. PhD dissertation, Stanford University, California.

Nordstrom D.K. and Munoz J.L. (1994) *Geochemical Thermodynamics (2nd Edition)*. Blackwell Scientific Publications, Boston, Mass.

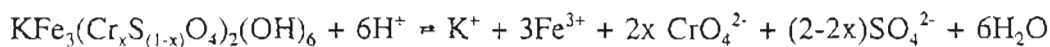
- Parker R.L. (1962) Isomorphous substitutions in natural and synthetic alunite. *Am. Miner.* **47**, 127-136.
- Powers D.A., Rossman G.R., Schugar H.J., and Gray H.B. (1975) Magnetic behavior and infrared spectra of jarosite, basic iron sulfate, and their chromate analogs. *J. Solid State Chem.* **13**, 1-13.
- Ripmeester J.A., Ratcliffe C.I., Dutrizac J.E., and Jambor J.L. (1986) Hydronium ion in the alunite-jarosite group. *Can. Mineral.* **24**, 435-447.
- Robie R.A and Waldbaum D.R. (1968) *Thermodynamic properties of minerals and related substances at 298.15 K (25°C) and one atmosphere (1.013 bars) pressure and at higher temperatures*. U.S. Geological Survey Bulletin 1259.
- Stoffregen R.E. (1993) Stability relations of jarosite and natrojarosite at 150-250°C. *Geochim. Cosmochim. Acta* **57**, 2417-2429.
- Stoffregen R.E. and Rye R.O. (1992) Jarosite-water ^{18}O and D fractionations. *Amer. Chem. Soc. Div. Geochem.* **204**, 86 (abstr.).
- Sullivan P.J. and Sobek A.A. (1982) Laboratory weathering studies of coal refuse. *Miner. Environ.* **4**, 9-17.
- Tkachenko R.I. and Zotov A.V. (1974) Ultra-acid therms of volcanic origin as mineralizing solutions. In *Hydrothermal Mineral-forming Solutions in the Areas of Active Volcanism* (ed. S.I. Naboko), 126-131. Oxoniam Press.
- Van Breemen N. (1973) Soil forming processes in acid sulfate soils. In *Acid Sulfate Soils, Proc. Int. Symp. on Acid Sulfate Soils* (ed. H. Dost), Vol I. Publ.18 ILRI, 66-130. Wageningen, The Netherlands.
- Vlek P.L.G., Blom T.J.M., Beek J., and Lindsay W.L. (1974) Determination of the solubility product of various iron hydroxides and jarosite by the chelation method. *Soil Sci. Soc. Amer. Proc.* **38**, 429-432.
- Wagman D.D., Evans W.H., Parker V.B., Halow I., Bailey S.M., and Schumm R.H. (1969) Selected values of chemical thermodynamic properties. *National Bureau of Standards Tech. Note* 270-4. U.S. Department of Commerce.
- Wilkins R.W.T., Mateen A., and West G.W. (1974) The spectroscopic study of oxonium in minerals. *Am. Miner.* **59**, 811-819.
- Zotov A.V., Miranova G.D., and Rusinov V.L. (1973) Determination of $\Delta G^\circ_{f, 298}$ of jarosite synthesized from a natural solution. *Geochem. Int.* **5**, 577-582.

CHAPTER 5

Solid Solution/Aqueous Solution

Reactions between Jarosite and its Chromate Analog

Jarosite ($\text{KFe}_3(\text{SO}_4)_2(\text{OH})_6$), its chromate analog ($\text{KFe}_3(\text{CrO}_4)_2(\text{OH})_6$), and seven precipitates with intermediate compositions ($\text{KFe}_3(\text{Cr}_x\text{S}_{(1-x)}\text{O}_4)_2(\text{OH})_6$) were synthesized. The unit cell volume of the precipitates varies linearly as a function of composition, suggesting a continuous solid solution. This solid solution dissolves stoichiometrically according to



and reaches stoichiometric saturation after approximately 40 to 60 days. Log K_{ss} values calculated from samples taken after 138 days are consistently lower than a linear interpolation between the log K_{sp} values of the endmembers, indicating that the solid solution deviates slightly from ideal behavior and that the excess free energy of mixing, G^E , is negative. G^E calculated from the log K_{ss} values can be closely modeled by the one-parameter Guggenheim expansion

$$G^E = \chi(\text{KFe}_3(\text{CrO}_4)_2(\text{OH})_6) \chi(\text{KFe}_3(\text{SO}_4)_2(\text{OH})_6) RT a_0$$

where a_0 is -2.9 ± 0.4 and $\chi(\text{KFe}_3(\text{CrO}_4)_2(\text{OH})_6)$ and $\chi(\text{KFe}_3(\text{SO}_4)_2(\text{OH})_6)$ are the mole fractions of $\text{KFe}_3(\text{CrO}_4)_2(\text{OH})_6$ and $\text{KFe}_3(\text{SO}_4)_2(\text{OH})_6$ in the solids.

5.1 Introduction

Chromium is a toxic and carcinogenic metal that is widely used in many industrial processes. It has been released into the environment at many sites and is a common soil and groundwater contaminant (Calder, 1988; Palmer and Wittbrodt, 1991). Because of the potential health hazards associated with chromium, there is interest in understanding the processes that control the mobility of chromium released into the environment in order to assess the risks associated with such releases and design clean-up measures for chromium contaminated sites. One of the key processes affecting chromium mobility in the subsurface is the precipitation of chromium containing solid phases. These solids can form as chromate-laden solutions interact with native soils, changing their chemical environment and leading to the dissolution of native soil minerals and the subsequent precipitation of new phases. These chromium containing solids can form as pure phases or as solid solutions with common soil minerals. Examples for such solids include $\text{Fe}_x\text{Cr}_{(1-x)}(\text{OH})_3$ solid solutions that are thought to control the concentrations of Cr(III) in soils under alkaline to slightly acidic conditions (Rai et al., 1987; Sass and Rai, 1987; Amonette and Rai, 1990), and $\text{Ba}(\text{Cr}_x\text{S}_{(1-x)})\text{O}_4$ solid solutions which are thought to control Cr(VI) concentrations in some soils (Rai et al., 1988).

Recently, Baron et al. (1996) identified $\text{KFe}_3(\text{CrO}_4)_2(\text{OH})_6$ in Cr(VI)-contaminated soil. The low solubility of $\text{KFe}_3(\text{CrO}_4)_2(\text{OH})_6$ suggests that this solid can form in large parts of a Cr(VI)-contaminated aquifer, affecting Cr(VI)-mobility and interfering with clean-up efforts (Baron and Palmer, 1996b). $\text{KFe}_3(\text{CrO}_4)_2(\text{OH})_6$ is the structural analog of jarosite ($\text{KFe}_3(\text{SO}_4)_2(\text{OH})_6$), a sulfate mineral that commonly occurs in acid sulfate soils (Van Breemen, 1973) and acid mine drainage environments (Chapman et al., 1983, Alpers et al., 1989). The fact that these two phases have the same crystal structure, as well as the equivalent charge, similar structure and thermochemical radii of sulfate and chromate (2.30 Å for sulfate and 2.40 Å for chromate; Waddington, 1959) suggest that solid solutions between $\text{KFe}_3(\text{CrO}_4)_2(\text{OH})_6$ and jarosite also exist. Sulfate is a common groundwater constituent and is also present in chrome-plating solutions, one of the primary sources of chromium contamination, making it possible that such solid solutions could form at many chromium contaminated sites. The aqueous Cr(VI) concentrations

in solutions equilibrated with such solutions could be dramatically different from concentrations in solutions equilibrated with pure $\text{KFe}_3(\text{CrO}_4)_2(\text{OH})_6$.

The purpose of this paper is to investigate solid solutions between jarosite and its chromate analog and to evaluate the potential impact of such solid solutions on chromium mobility. The specific objectives of are (1) to determine if a complete solid solution series exists between jarosite and its chromate analog, (2) to measure the solubility of solid solution phases with a range of Cr/S ratios under the acidic conditions in which these solids are expected to form, and (3) to determine an appropriate model to describe the solid solution/aqueous solution reactions of these phases.

5.2 Experimental Section

5.2.1 Synthesis of $\text{KFe}_3(\text{Cr}_x\text{S}_{(1-x)}\text{O}_4)_2(\text{OH})_6$ Solid Solutions

$\text{KFe}_3(\text{Cr}_x\text{S}_{(1-x)}\text{O}_4)_2(\text{OH})_6$ solid solutions were synthesized by controlled mixing of a solution of $\text{Fe}(\text{NO}_3)_3 \cdot 9\text{H}_2\text{O}$ and a solution of K_2CrO_4 and K_2SO_4 at 95°C . For the ferric nitrate solution, 10.10 to 30.29 g were added to 45 mL of water, and for the potassium chromate/sulfate solutions, 1.94 to 9.22 g of K_2CrO_4 and 0.44 to 6.96 g of K_2SO_4 were added to 45 mL of water. Reagent grade chemicals and ultrapure water (18 megaohm cm) were used for the synthesis and all experiments. The amount of K_2CrO_4 and K_2SO_4 was varied in individual syntheses to obtain synthetic solids with different Cr/S ratios. The compositions of the starting solutions are summarized in Table 5-1. The two solutions were slowly (50 mL h^{-1}) added to a covered beaker containing an initial 10 mL of ultrapure water. The resulting solution was kept at 95°C and stirred at a moderate rate (100 rpm) using a stirrbar. After 3 hours, the precipitates were allowed to settle and the residual solution decanted. The precipitates were then washed thoroughly and dried at 110°C for 24 hours.

5.2.2 Characterization of $\text{KFe}_3(\text{Cr}_x\text{S}_{(1-x)}\text{O}_4)_2(\text{OH})_6$ Solid Solutions

A small amount of the precipitates was digested in HCl and analyzed for K and Fe using atomic absorption spectroscopy (AAS), Cr(VI) using the diphenylcarbazide (DPC) method (APHA, 1985), and SO_4 using high performance ion chromatography

Table 5-1. Summary of synthesis of $\text{KFe}_3(\text{Cr}_x\text{S}_{(1-x)}\text{O}_4)_2(\text{OH})_6$ solid solutions.

	Solution 1		Solution 2			Solid Composition	Munsell Color
	H ₂ O (mL)	Fe(NO ₃)·9H ₂ O (g)	H ₂ O (mL)	K ₂ CrO ₄ (g)	K ₂ SO ₄ (g)		
JAR-05	45	30.29	45	9.22	0.44	K _{0.92} Fe _{2.80} (Cr _{0.90} S _{0.10} O ₄) ₂ (OH) ₆	2.5YR 4/8
JAR-10	45	30.29	45	8.73	0.87	K _{0.94} Fe _{2.80} (Cr _{0.80} S _{0.20} O ₄) ₂ (OH) ₆	5YR 5/8
JAR-25	45	30.29	45	7.28	2.18	K _{0.96} Fe _{3.12} (Cr _{0.53} S _{0.47} O ₄) ₂ (OH) ₆	5YR 5/8
JAR-30	45	30.29	45	6.80	2.61	K _{1.00} Fe _{3.14} (Cr _{0.42} S _{0.58} O ₄) ₂ (OH) ₆	7.5YR 5/8
JAR-40	45	20.19	45	5.82	3.48	K _{0.92} Fe _{2.84} (Cr _{0.27} S _{0.73} O ₄) ₂ (OH) ₆	7.5YR 5/8
JAR-50	45	10.10	45	4.85	4.35	K _{1.00} Fe _{2.86} (Cr _{0.17} S _{0.83} O ₄) ₂ (OH) ₆	7.5YR 6/8
JAR-80	45	20.19	45	1.94	6.96	K _{0.98} Fe _{2.98} (Cr _{0.09} S _{0.91} O ₄) ₂ (OH) ₆	2.5Y 6/8

(HPIC). All synthetic solids were characterized using powder x-ray diffraction (XRD). Selected synthetic solids were also examined by scanning electron microscopy with energy dispersive spectroscopy (SEM/EDX).

5.2.3 Dissolution Experiments

Dissolutions experiments with the synthetic $\text{KFe}_3(\text{Cr}_x\text{S}_{(1-x)}\text{O}_4)_2(\text{OH})_6$ solid solutions was conducted at $23 \pm 1^\circ\text{C}$ and with an initial pH of 2. For the dissolution experiments, 200 mg of synthetic solid was added to 200 mL of ultrapure water with the pH adjusted to 2 using HClO_4 . The solutions were placed in polyethylene bottles and placed on a shaker running at approximately 50 rpm. The experiments were sampled over time to monitor the evolution of the solution during the dissolution process and to determine when a steady state was achieved. A total of 9 samples was taken. For each sample, 4 mL of the $\text{KFe}_3(\text{Cr}_x\text{S}_{(1-x)}\text{O}_4)_2(\text{OH})_6$ suspension was withdrawn. The samples were filtered using a $0.1\mu\text{m}$ polysulfonate filter to remove suspended solids and then analyzed for pH, K and Fe using AAS, Cr using the DPC method, and SO_4 using HPIC. Since the experiments were conducted in oxidizing HClO_4 solutions and no reductants capable of reducing ferric iron were present, it was assumed that all Fe was present as ferric iron.

The uncertainty associated with the analytical measurements is $\pm 10\%$. The precision of the pH buffer solutions used calibrations for the pH measurements is ± 0.02 pH units.

5.3 Results

5.3.1 Solid Characterization

The synthesis yielded between 3.5 to 5 g of precipitates. In general, the solutions with higher concentrations of ferric nitrate yielded a larger amount of solid. The precipitates vary in color between the yellow of jarosite and red of $\text{KFe}_3(\text{CrO}_4)_2(\text{OH})_6$ (Table 5-1). Wet chemical analysis of the precipitates indicates the stoichiometry of the synthetic solids is close to that of jarosite type compounds (Table 5-1). The molar ratios of Cr:S in the solid vary from 1.80:0.20 to 0.18:1.82. In general, the solids are enriched in S compared to the synthesis solutions. For example, solid JAR-50 synthesized from a solution with equimolar concentrations of Cr and S, has a Cr:S molar ratio of 0.18:1.68. Most of the synthetic solids have a slight K and Fe deficit compared to the 'ideal' formula. Such deficits are commonly observed in natural and synthetic jarosites (e.g. Brophy and Sheridan, 1965; Kubisz, 1970; Härtig et al., 1984; Baron and Palmer, 1996). The K deficit is generally attributed to substitution of K by H_3O^+ (hydronium). The charge imbalance caused by the Fe deficit is generally thought to be balanced by substitution of some H_2O for the OH-groups in the crystal structure.

The synthetic solids were identified as jarosite-type compounds by comparing powder X-ray diffraction patterns with those reported for jarosite and $\text{KFe}_3(\text{CrO}_4)_2(\text{OH})_6$ in JCPDS cards 22-827 and 20-894 (JCPDS, 1994). The XRD peaks produced by the synthetic compounds are listed in Table 5-2. All the peaks produced by the precipitates are consistent with jarosite type compounds. The absence of unidentified peaks indicates that no other crystalline phases are present in the precipitates at detectable levels.

The unit cell of $\text{KFe}_3(\text{CrO}_4)_2(\text{OH})_6$ is larger than that of jarosite and the corresponding XRD peaks are shifted towards slightly smaller angles, representing the generally slightly larger d-spacings of $\text{KFe}_3(\text{CrO}_4)_2(\text{OH})_6$. As the Cr content of the

Table 5-2. Powder X-ray diffraction analysis of $\text{KFe}_3(\text{Cr}_x\text{S}_{(1-x)}\text{O}_4)_2(\text{OH})_6$ solid solutions.

h	k	l	d-spacing (Å)						
			Jar-05	Jar-10	Jar-25	Jar-30	Jar-40	Jar-50	Jar-80
1	0	1	6.01	6.01	5.97	5.96	5.94	5.98	5.93
0	0	3	5.82	5.82	5.77	5.75	5.73	5.70	5.71
0	1	2	5.16	5.16	5.12	5.14	5.10	5.10	5.09
1	1	0	3.71	3.71	3.68	3.68	3.66	3.66	3.65
1	0	4	3.60	3.59	3.59	3.56	3.56	3.55	3.54
0	2	1	3.15	3.15	3.14	3.13	3.12	3.12	3.12
1	1	3	3.13	3.12	3.10	3.10	3.09	3.08	3.08
2	0	2	3.02	3.01	3.00	2.99	2.98	2.98	2.97
0	0	6	2.91	2.90	2.88	2.88	2.87	2.86	2.85
0	2	4	2.585	2.581	2.565	2.562	2.555	2.548	2.544
2	1	1	2.371	2.371	2.371	2.371	2.371	2.371	2.371
1	2	2	2.322	2.321	2.318	2.315	2.309	2.305	2.305
0	3	3	2.007	1.979	1.994	1.993	1.988	1.978	1.981
0	2	7	1.966	1.965	1.954	1.953	1.946	1.943	1.941
0	0	9	1.940	1.938	1.931	1.922	1.916	1.900	1.902
2	2	0	1.855	1.850	1.840	1.838	1.833	1.829	1.830
2	0	8	1.804	1.803	1.792	1.788	1.784	1.777	1.776
2	2	3	1.772	1.768	1.764	1.753	1.749	1.747	1.744
3	1	2	1.746	1.746	1.732	1.731	1.728	1.723	1.721
1	1	9	1.720	1.717	1.706	1.703	1.706	1.690	1.694
1	3	4	1.646	1.641	1.636	1.636	1.630	1.626	1.627
1	2	8	1.624	1.620	1.612	1.606	1.603	1.598	1.591
4	0	1	1.598	1.597	1.588	1.584	1.581	1.580	1.580
3	1	5	1.581	1.577	1.575	1.573	1.570	1.569	1.564
0	4	2	1.577	1.571	1.569	1.568	1.564	1.564	1.557
2	2	6	1.563	1.560	1.554	1.550	1.545	1.542	1.542
Unit Cell Dimensions									
a-axis (Å)			7.412 ±0.008	7.391 ±0.011	7.370 ±0.006	7.357 ±0.004	7.340 ±0.004	7.333 ±0.005	7.322 ±0.005
c-axis (Å)			17.48 ±0.03	17.46 ±0.04	17.36 ±0.02	17.30 ±0.01	17.28 ±0.02	17.15 ±0.02	17.143 ±0.02
Volume (Å ³)			831.6±1.9	826.0±2.6	816.3±1.4	810.9±0.8	806.2±1.0	798.6±1.1	795.9±1.1

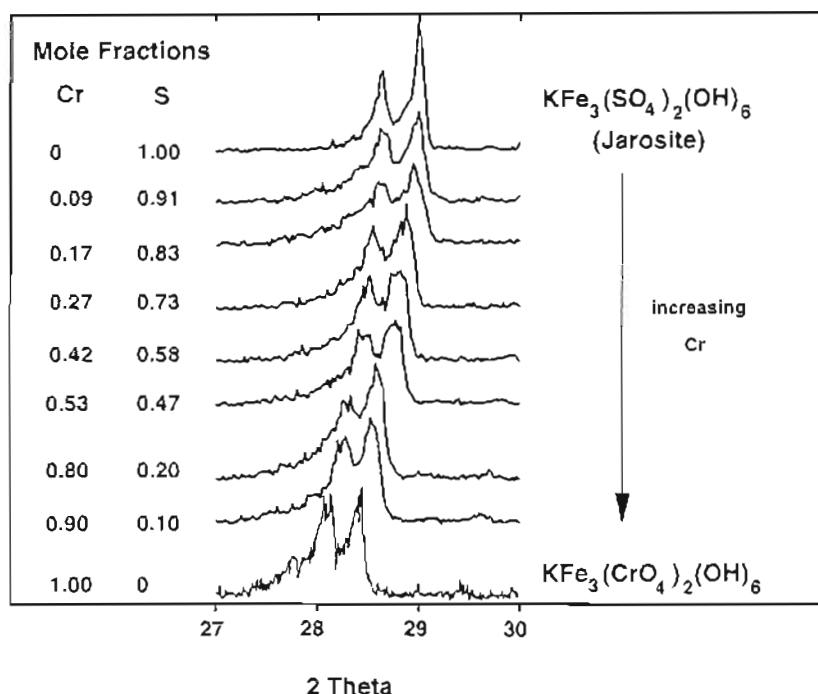


Figure 5-1. Main powder x-ray diffraction peaks of $\text{KFe}_3(\text{Cr}_x\text{S}_{(1-x)}\text{O}_4)_2(\text{OH})_6$ solid solutions. Peaks from jarosite (Baron and Palmer, 1996a) and $\text{KFe}_3(\text{CrO}_4)_2(\text{OH})_6$ (Baron and Palmer, 1996b) are also shown for comparison.

synthetic solids increases, the peaks generally shift towards lower angles and correspondingly larger d-spacings (Table 5-2). Figure 5-1 shows the region between 27 and 30° 2θ with the two strongest peaks as an example for this shift. Such a continuous shift indicates a solid solution series rather than a mixture of two phases. In a mixture, distinct sets of peaks from each phase would be present. The intensity of these peaks would vary as a function of the fraction of each separate phase in the mixture. The unit cell volume of the $\text{KFe}_3(\text{Cr}_x\text{S}_{(1-x)}\text{O}_4)_2(\text{OH})_6$ solid solutions obeys Retger's Rule and varies between the sulfate and chromate endmembers linearly as a function of composition (Figure 5-2, Table 5-2), also indicating a continuous solid solution series. A linear relation between composition and unit cell size has also been interpreted as an indicator of an ideal solid solution (Königsberger et al., 1991).

Examination of selected solids (Jar-50 and Jar-25) with SEM/EDX showed that

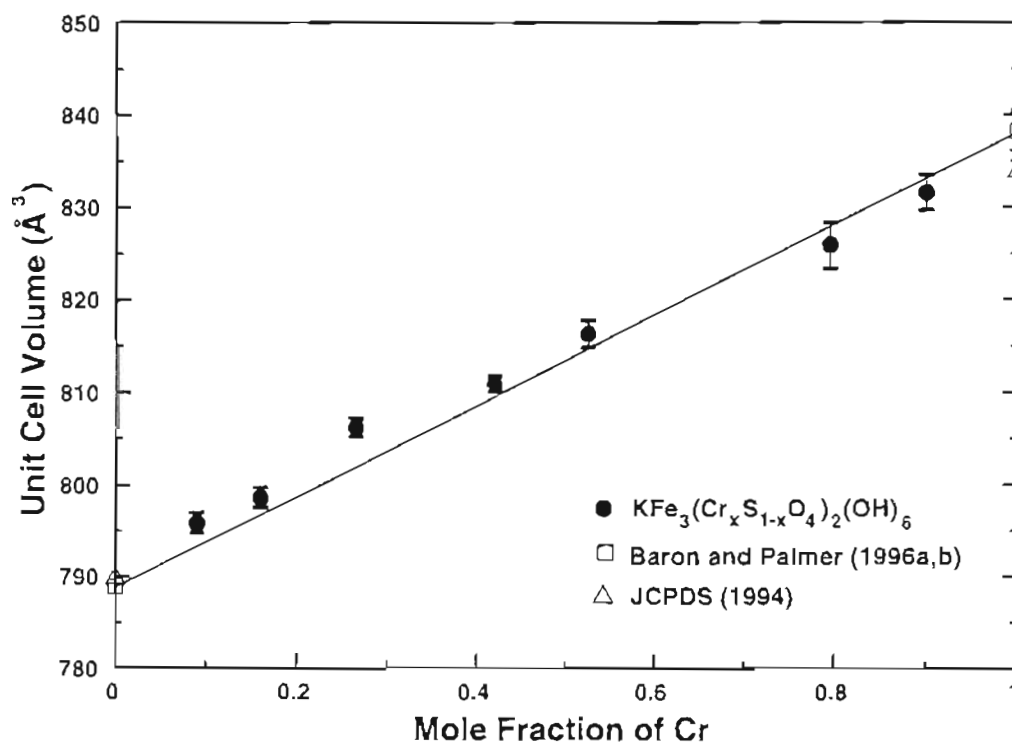


Figure 5-2. Unit cell dimension of $\text{KFe}_3(\text{Cr}_x\text{S}_{1-x}\text{O}_4)_2(\text{OH})_6$ solid solutions as a function of composition. Unit cell dimensions of jarosite (Baron and Palmer, 1996a; JCPDS, 1994) and $\text{KFe}_3(\text{CrO}_4)_2(\text{OH})_6$ (Baron and Palmer, 1996b; JCPDS, 1994) are also shown for comparison. The line represents a linear interpolation between the unit cell dimensions of jarosite and $\text{KFe}_3(\text{CrO}_4)_2(\text{OH})_6$.

the precipitates consist of multicrystalline particles with uniform concentrations of K, Fe, Cr, and S, ranging in size from 5 to 50 μm . No other crystalline or amorphous phases were observed.

5.3.2 Dissolution Experiments

In the dissolution experiments, the bulk of the reaction occurred within the first week of the experiment with rates declining with time. The evolution of the solution composition for the dissolution of solid Jar-25, with a Cr/S ratio of close to 1/1 is shown as an example of the dissolution process (Figure 5-3). The dissolution process for all solids is generally stoichiometric, with the mole fractions total of Cr(VI) and total SO_4^{2-}

Table 5-3. Final concentrations in the dissolution experiments.

	Sample Time (days)	pH	[K] _{tot} mol L ⁻¹	[Fe ³⁺] _{tot} mol L ⁻¹	[Cr(VI)] _{tot} mol L ⁻¹	[SO ₄ ²⁻] _{tot} mol L ⁻¹
Jar-05	138	2.07	2.37*10 ⁻⁴	6.24*10 ⁻⁴	4.56*10 ⁻⁴	3.98*10 ⁻⁵
Jar-10	138	2.06	2.28*10 ⁻⁴	6.52*10 ⁻⁴	3.89*10 ⁻⁴	1.00*10 ⁻⁴
Jar-25	138	2.05	2.36*10 ⁻⁴	6.66*10 ⁻⁴	2.49*10 ⁻⁴	1.96*10 ⁻⁴
Jar-30	138	2.05	2.28*10 ⁻⁴	6.24*10 ⁻⁴	2.20*10 ⁻⁴	2.23*10 ⁻⁴
Jar-40	138	2.05	2.26*10 ⁻⁴	5.96*10 ⁻⁴	1.69*10 ⁻⁴	3.50*10 ⁻⁴
Jar-50	138	2.05	2.60*10 ⁻⁴	6.37*10 ⁻⁴	7.50*10 ⁻⁵	3.60*10 ⁻⁴
Jar-80	138	2.05	2.15*10 ⁻⁴	5.82*10 ⁻⁴	4.00*10 ⁻⁵	3.82*10 ⁻⁴

in the solutions close to the mole fraction of Cr and S in the solids. The only exception is solid JAR-30 with a solid Cr/S ratio of 0.42/0.58. The average of the aqueous Cr/S ratios is 0.47/0.53. However, even in this case, the discrepancy is within the analytical error of $\pm 10\%$ associated with the chromium and sulfate measurements. Within the time frame of the experiments, there is no noticeable enrichment of either Cr or S in the solutions as the dissolution process proceeds.

A steady state was attained in the dissolution experiments after about 40-60 days. The compositions of the solutions after 138 days are summarized in Table 5-3. For all samples, aqueous activities of K⁺, Fe³⁺, CrO₄²⁻, and SO₄²⁻ were calculated using the geochemical speciation model MINTEQA2 (Allison et al., 1990). Activity corrections were made using the Davies equation as incorporated into MINTEQA2. The MINTEQA2 thermodynamic database was modified to include the FeHSO₄²⁺ and FeCrO₄⁺ ion pairs. Other ion pairs included in the calculations and thermodynamic data used are listed in Table 5-4. The aqueous activities calculated from the sample taken after 138 days, after a steady state was achieved, are listed in Table 5-5.

Table 5-4. Thermodynamic data used in calculations.

Formula	State	$\Delta G^0_{f,298}$ kJ mol ⁻¹	log K _f	Source
Fe ³⁺	aq	-17.87±1.0	-	1
FeSO ₄ ⁺	aq	-	3.92	2
FeHSO ₄ ²⁺	aq	-	2.48	3
Fe(SO ₄) ₂ ⁻	aq	-	5.42	2
FeCrO ₄ ⁺	aq	-	7.8	4
FeOH ²⁺	aq	-	-2.19	2
Fe(OH) ₂ ⁻	aq	-	-5.67	5
Fe ₂ (OH) ₂ ⁴⁺	aq	-	-2.95	2
K ⁺	aq	-282.5±0.1	-	6
KSO ₄ ⁻	aq	-	0.85	2
KCrO ₄ ⁻	aq	-	0.799	2
CrO ₄ ²⁻	aq	-720.86	-	1
HCrO ₄ ⁻	aq	-	6.5089	2
Cr ₂ O ₇ ²⁻	aq	-	14.5571	2
H ₂ CrO ₄ ⁰	aq	-	5.6513	2
SO ₄ ²⁻	aq	-744.0±0.4	-	6
HSO ₄ ⁻	aq	-	1.98	6
OH ⁻	aq	-	-13.998	2
H ₂ O	l	-237.14±0.04	-	6

Sources:

- (1) Naumov et al. (1971)
- (2) Allison et al. (1990)
- (3) Ball et al. (1987)
- (4) Baron and Palmer (1996b)
- (5) Nordstrom and Munoz (1994)
- (6) Cox et al. (1989)

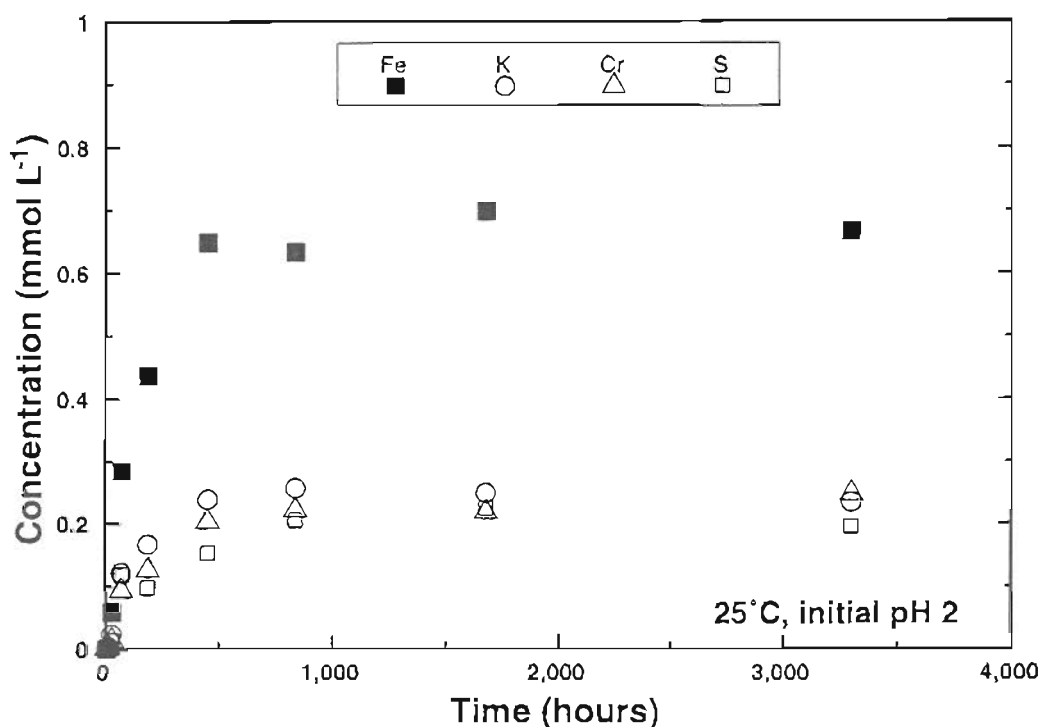


Figure 5-3. Dissolution of synthetic solid Jar-25 as an example for the dissolution of $\text{KFe}_3(\text{Cr}_x\text{S}_{(1-x)}\text{O}_4)_2(\text{OH})_6$ solid solutions.

5.4 Discussion

Seven $\text{KFe}_3(\text{Cr}_x\text{S}_{(1-x)}\text{O}_4)_2(\text{OH})_6$ solid solutions with a wide range of Cr/S ratios were synthesized and characterized. All synthetic solids are enriched in S compared to the Cr/S ratios of the synthesis solutions. In the acidic synthesis solutions, Cr(VI) is present primarily as HCrO_4^- and the activity of CrO_4^{2-} , which is incorporated into the solid is low compared the activity of total Cr(VI). Sulfur, however, is present primarily as SO_4^{2-} . It is therefore not surprising that the solids are enriched in S compared to the synthesis solutions.

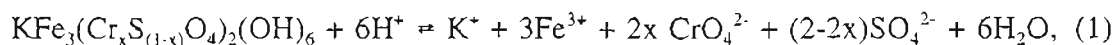
The dissolution process of the solid solutions is generally stoichiometric, with the mole fractions total of Cr(VI) and total SO_4^{2-} in the solutions close to the mole fractions of Cr and S in the solids. After about 40 to 60 days, the solutions reach a steady state with the aqueous Cr/S ratios close to the Cr/S ratios of the solids (stoichiometric

Table 5-5. Calculated final ion activities for the dissolution experiments.

	pH	log {K ⁺ }	log {Fe ³⁺ }	log {SO ₄ ²⁻ }	log {CrO ₄ ²⁻ }	Ionic Strength (M)	calculated log IAP _{ss}
Jar-05	2.07	-3.67	-3.89	-4.96	-7.97	1.01×10 ⁻²	-18.26
Jar-10	2.06	-3.69	-3.87	-4.57	-8.05	1.04×10 ⁻²	-17.61
Jar-25	2.05	-3.67	-3.85	-4.29	-8.25	1.05×10 ⁻²	-15.66
Jar-30	2.05	-3.69	-3.88	-4.22	-8.3	1.05×10 ⁻²	-14.90
Jar-40	2.05	-3.69	-3.92	-4.01	-8.49	1.04×10 ⁻²	-13.54
Jar-50	2.05	-3.63	-3.89	-4.01	-8.75	1.05×10 ⁻²	-12.54
Jar-80	2.05	-3.71	-3.92	-3.98	-9.03	1.04×10 ⁻²	-12.04

saturation state). Such stoichiometric dissolution and the attainment of a stoichiometric saturation state is often observed during the dissolution of solid solutions, especially if these are fairly insoluble (Thorstenson and Plummer, 1977). The stoichiometric saturation state in the dissolution of a solid solution was first defined by Thorstenson and Plummer (1977) for "situations where the composition of the solid phase remains invariant, owing to kinetic restrictions, even though the solid is part of a continuous compositional series." Under such circumstances solids behave as a one component solid phase with unit activity. Glynn (1990) further points out that the stoichiometric saturation concept may apply to situations where the equilibration time is sufficiently short, the solid to aqueous solution ratio is sufficiently high, and the solid is relatively insoluble.

For the stoichiometric dissolution of $\text{KFe}_3(\text{Cr}_x\text{S}_{(1-x)}\text{O}_4)_2(\text{OH})_6$ solid solutions according to



a stoichiometric ion activity product, IAP_{ss} can be written as

$$IAP_{ss} = \{K^+\} \{Fe^{3+}\}^3 \{CrO_4^{2-}\}^{2x} \{SO_4^{2-}\}^{(2-2x)} \{H_2O\}^6 \{H^+\}^{-6} \quad (2)$$

where brackets denote activity. The $\log IAP_{ss}$ is then given by

$$\log IAP_{ss} = \log \{K^+\} + 3 \log \{Fe^{3+}\} + 2x \log \{CrO_4^{2-}\} + (2-2x) \log \{SO_4^{2-}\} + 6 \log H_2O + 6 \text{ pH} \quad (3)$$

When a steady state is reached, IAP_{ss} equals the stoichiometric saturation constant, K_{ss} . $\log IAP_{ss}$ values for the all samples were calculated and are shown as a function of the aqueous mole fraction of chromium in Figure 5-4. $\log IAP_{ss}$ values from the sample taken after 138 days, after a steady state was reached, are listed in Table 5-5 and are shown as a function of the solid mole fraction of Cr in Figure 5-5. The analytical error associated with the $\log IAP_{ss}$ values calculated from the precision of the analytical measurements ($\pm 10\%$) and the precision of the pH buffer solutions (± 0.02 pH units) is 0.25 log units (assuming that the covariance between these parameters equals zero). The error associated with the aqueous concentrations of Cr and S is the analytical error of 10%. The steady state $\log IAP_{ss}$ values, representing $\log K_{ss}$ values, are close to, but consistently lower than a linear interpolation between the solubility products of jarosite and $KFe_3(CrO_4)_2(OH)_6$ (Figure 5-5), suggesting a negative excess free energy of mixing.

Assuming that a stoichiometric saturation state was attained in the dissolution experiments, the excess free energy of mixing, G^E , for a solid solution, $B_{(1-x)}C_xA$, can be calculated from

$$G^E = RT [\ln K_{ss} - x (\ln K_{CA} + \ln x) - (1-x) (\ln K_{BA} + \ln (1-x))], \quad (4)$$

where K_{CA} and K_{BA} are the solubility products of CA and BA, respectively (Glynn and Reardon, 1990). Guggenheim's (1937, 1952) expansion series for G^E is a commonly used model to represent the excess free energy of a binary solid solution as a function of composition

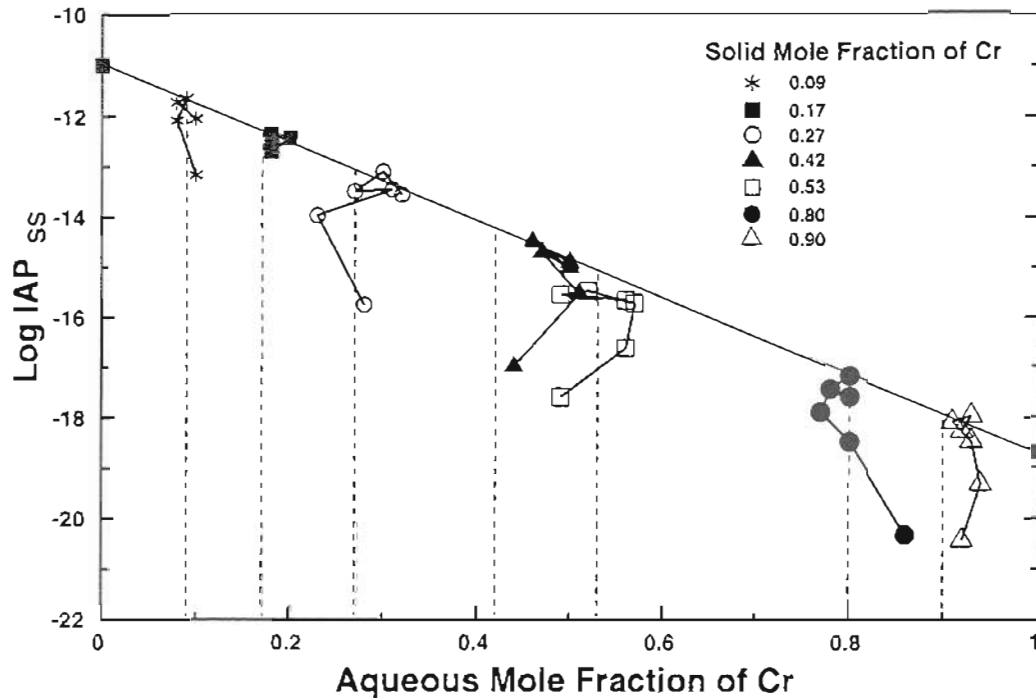


Figure 5-4. Evolution of $\log IAP_{SS}$ values as a function of aqueous mole fraction of Cr during the dissolution of $KFe_3(Cr_xS_{(1-x)}O_4)_2(OH)_6$ solid solutions. The dashed lines represent hypothetical stoichiometric dissolution pathways for the solid solutions. The solid line represents a linear interpolation between the $\log K_{sp}$ values of jarosite (Baron and Palmer, 1996a) and $KFe_3(CrO_4)_2(OH)_6$ (Baron and Palmer, 1996b).

$$G^E = x(1-x)RT[a_0 + a_1(x - (1-x)) + a_2(x - (1-x))^2 \dots], \quad (5)$$

where a_0 , a_1 , etc. are dimensionless coefficients. Combining equations (4) and (5) and writing them out for $KFe_3(Cr_xS_{(1-x)}O_4)_2(OH)_6$ while using only the first coefficient, a_0 , ('regular solution' model) yields

$$\ln K_{SS} = x(1-x)a_0 + (1-x)\ln[K_{KFe_3(SO_4)_2(OH)_6}(1-x)] + x\ln[K_{KFe_3(CrO_4)_2(OH)_6}x]. \quad (6)$$

Fitting our K_{SS} values as a function of solid composition to equation (6) yields a best fit

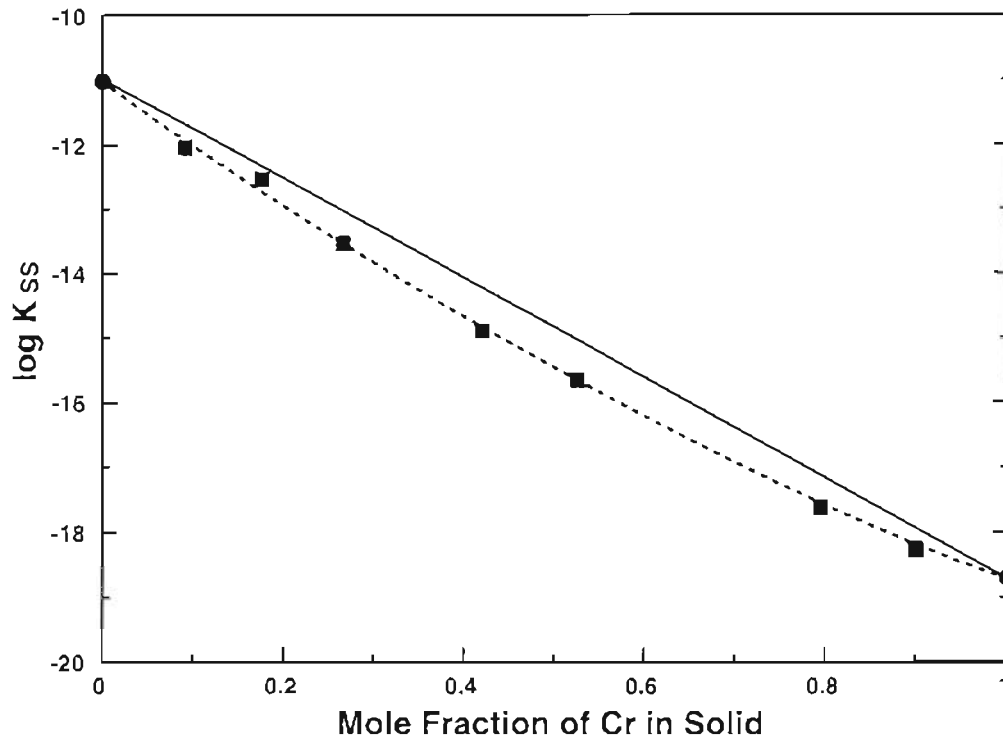


Figure 5-5. Log K_{ss} values as a function of the solid phase mole fraction of Cr. Data is from the samples taken after 138 days. The solid line represents a linear interpolation between the log K_{sp} values for jarosite (Baron and Palmer, 1996a) and $KFe_3(CrO_4)_2(OH)_6$ (Baron and Palmer, 1996b). The dashed line represents the best fit of a regular solution model (Equation 6) to the K_{ss} values.

with $a_0 = -2.9 \pm 0.4$ ($n=7$, $df=6$, $r^2=0.999$). The negative value for a_0 suggests that the excess free energy of mixing is negative and that mixing is energetically favored. Solid phase activity coefficients for $KFe_3(CrO_4)_2(OH)_6$ ($\gamma(KFe_3(CrO_4)_2(OH)_6)$) and $KFe_3(SO_4)_2(OH)_6$ ($\gamma(KFe_3(SO_4)_2(OH)_6)$) can then be calculated as a function of composition using the relationships

$$\ln \gamma(KFe_3(CrO_4)_2(OH)_6) = (1-x)^2 a_0 \quad (7)$$

$$\ln \gamma(KFe_3(SO_4)_2(OH)_6) = x^2 a_0 \quad (8)$$

(Redlich and Kister, 1948). The solid phase activity coefficients as a function of

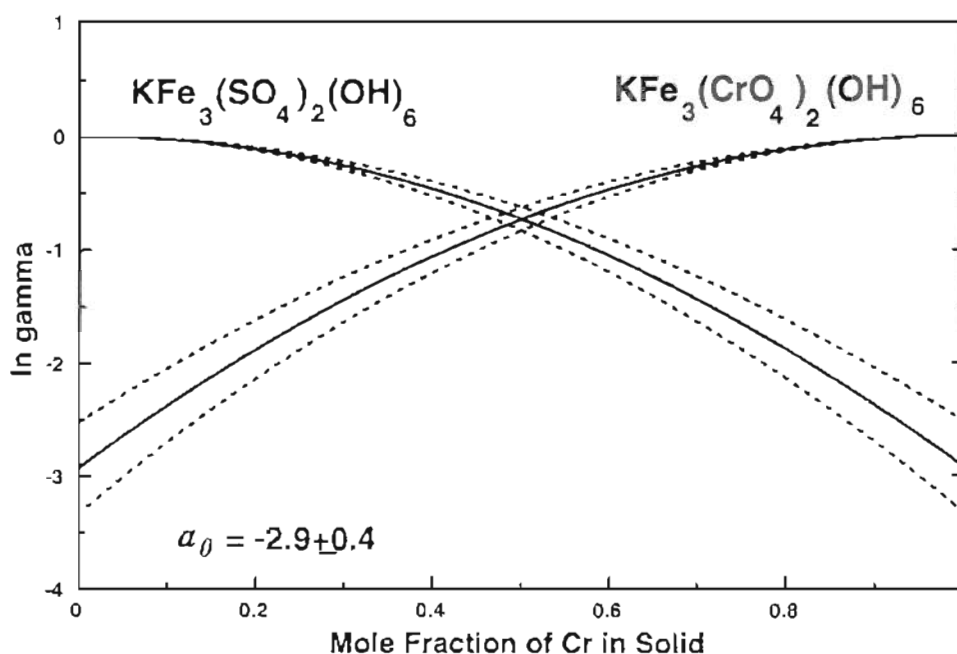


Figure 5-6. Solid phase activity coefficients of jarosite and $\text{KFe}_3(\text{CrO}_4)_2(\text{OH})_6$ in $\text{KFe}_3(\text{Cr}_x\text{S}_{(1-x)}\text{O}_4)_2(\text{OH})_6$ solid solutions calculated using equations 7 and 8 with $a_0 = -2.9 \pm 0.4$.

composition are shown in Figure 5-6.

5.5 Summary and Conclusions

Seven $\text{KFe}_3(\text{Cr}_x\text{S}_{(1-x)}\text{O}_4)_2(\text{OH})_6$ solid solutions with a wide range of Cr:S ratios were synthesized. Sulfate is preferentially incorporated into solids from the acidic synthesis solutions, because Cr(VI) is present predominantly as HCrO_4^- and the activity of CrO_4^{2-} is low. The unit cell volume of the solid solutions varies linearly as a function of composition, indicating a continuous solid solution series. The solid solutions dissolve stoichiometrically and reach a stoichiometric saturation state after 40-60 days. Calculated $\log K_{ss}$ values suggest that the solid solution is close to ideal with a small negative excess

free energy of mixing. The excess free energy of mixing can be modeled with a regular solution model with $a_0 = -2.9 \pm 0.4$.

The fact that sulfate is incorporated preferentially into $\text{KFe}_3(\text{Cr}_x\text{S}_{(1-x)}\text{O}_4)_2(\text{OH})_6$ from acidic synthesis solutions implies that the formation of such solids is possible even in environments with only moderate sulfate concentrations. $\text{KFe}_3(\text{Cr}_x\text{S}_{(1-x)}\text{O}_4)_2(\text{OH})_6$ maintains lower aqueous concentrations of Cr(VI) than pure $\text{KFe}_3(\text{CrO}_4)_2(\text{OH})_6$ and therefore could limit Cr mobility even more than pure $\text{KFe}_3(\text{CrO}_4)_2(\text{OH})_6$.

More work is required to elucidate the precipitation pathways in the $\text{KFe}_3(\text{CrO}_4)_2(\text{OH})_6$ - $\text{KFe}_3(\text{SO}_4)_2(\text{OH})_6$ - H_2O system. In addition, we need to determine the times scales for the solid solution-aqueous solution system to evolve from stoichiometric saturation to thermodynamic equilibrium.

5.6 References

- Allison J.D., Brown D.S., and Novo-Gradac K.J. (1990) *MINTEQA2/PRODEFA2, a geochemical assessment model for environmental systems: version 3.0*. U.S. Environmental Protection Agency, Athens, GA.
- Alpers C.N., Nordstrom D.K., and Ball J.W. (1989) Solubility of jarosite solid solutions precipitated from acid mine waters, Iron Mountain, California, U.S.A.. *Sci. Géol., Bull.* **42**, 281-298.
- Amonette J.E. and Rai D. (1990) Identification of noncrystalline $(\text{Fe,Cr})(\text{OH})_3$ by infrared spectroscopy. *Clays Clay Min.* **38**, 129-136.
- APHA (1985) *Standard methods for the examination of water and wastewater*. American Public Health Association, Washington, DC.
- Ball J.W., Nordstrom D.K., and Zachmann D.W. (1987) WATEQ4F. A personal computer FORTRAN translation of the geochemical model WATEQ2 with revised data base. *U.S. Geological Survey Open-File Rept.* 87-150.
- Baron D. and Palmer C.D. (1996a) Solubility of jarosite at 4 -35°C. *Geochim. Cosmochim. Acta* **60**, 185-195.
- Baron D. and Palmer C.D. (1996b) Solubility of $\text{KFe}_3(\text{CrO}_4)_2(\text{OH})_6$ at 4 - 35°C. (accepted for publication by *Geochim. Cosmochim. Acta*, March 1995).

- Baron D., Stanley J.T. and Palmer C.D. (1996) Identification of two iron-chromate precipitates in a Cr(VI)-contaminated soil. *Environ. Sci. Technol.* **30**, 964-968.
- Brophy G.P. and Sheridan M.F. (1965) Sulfate studies. IV. The jarosite-natrojarosite-hydronium jarosite solid solution series. *Amer. Mineral.* **50**, 112-126.
- Calder L.M. (1988) Chromium contamination of groundwater. In: *Chromium in the Natural and Human Environments* (eds. J.O. Nriagu and E. Nieboer), 215-579. John Wiley and Sons, New York.
- Chapman B.M., Jones D.R., and Jung R.F. (1983) Processes controlling metal ion attenuation in acid mine drainage streams. *Geochim. Cosmochim. Acta* **47**, 1957-1973.
- Cox J.D., Wagman D.D., and Mededev V.A. (1989) *CODATA Key Values for Thermodynamics*. Hemisphere Publishing Corporation.
- Glynn P. (1990) Modeling solid-solution reactions in low temperature systems. In: *Chemical Modeling of Aqueous Systems II*. (eds. D.C. Melchior and R.L. Bassett), 74-87. American Chemical Society Symposium Series, Vol. 416.
- Glynn P.D. and Reardon E.J. (1990) Solid-solution aqueous solution equilibria: thermodynamic theory and representation. *Am. J. Sci.* **290**, 164-201.
- Glynn P., Reardon E.J., Plummer L.N., and Busenberg E. (1990) Reaction paths and equilibrium end-points in solid-solution aqueous-solution systems. *Geochim. Cosmochim. Acta*. **54**, 267-282.
- Guggenheim E.A. (1937) Theoretical basis of Raoult's law. *Trans. Faraday Sec.* **33**, 151-159.
- Guggenheim E.A. (1952) *Mixtures* Oxford University Press, London.
- Härtig C., Brand P., and Bohmhammel K. (1984) Fe-Al-Isomorphie und Strukturwasser in Kristallen vom Jarosit-Alunit Typ. *Z. Anorg. Allg. Chem.* **508**, 159-164.
- JCPDS (Joint Committee on Powder Diffraction Standards) (1994) Powder diffraction file. Swathmore, Pennsylvania, International Center for Diffraction Data.
- Königsberger E., Hausner R., and Gamsjäger H. (1991) Solid-solute phase equilibria in aqueous solution V. The system Cd^{2+} - Ca^{2+} - CO_2 - H_2O . *Geochim. Cosmochim. Acta* **55**, 3505-3514.
- Kubisz J. (1970) Studies on synthetic alkali-hydronium jarosite. I. Synthesis of jarosite and natrojarosite. *Mineral. Pol.* **3**, 23-27.

Naumov G.B., Ryzhenko I.L. and Khodakovskiy I.L. (1971) *Handbook of Thermodynamic Data* (translated from Russian by G.J. Soleimani, edited by I. Barnes and V. Speltz), Washington D.C. NTIS publication PB-226 722.

Nordstrom D.K. and Munoz J.L. (1994) *Geochemical Thermodynamics (2nd Edition)*. Blackwell Scientific Publications, Boston, Mass.

Palmer C.D. and Wittbrodt P.R. Processes affecting the Remediation of chromium-contaminated sites. *Environ. Health. Perspect.* **92**, 25-40.

Rai D., Sass B.M., and Moore D.A. (1987) Chromium(III) hydrolysis constants and solubility of chromium(III) hydroxides. *Inorg. Chem.* **26**, 345-349.

Rai D., Zachara J.M., Eary L.E., Ainsworth C.C., Amonette J.E., Cowan C.E., Szelmeckza R.W., Resch C.T., Schmidt R.L., Smith S.C., and Girvin D.C. (1988) Chromium reactions in geologic materials. *Electric Power Research Institute Report EA-5741*, Palo Alto, CA.

Redlich O. and Kister A.T. Algebraic representation of thermodynamic properties and the classification of solutions. *Ind. Eng. Chem.* **40**, 345-348.

Sass D.M. and Rai D. (1987) Solubility of amorphous chromium(III)-iron(III) hydroxide solid solutions. *Inorg. Chem.* **26**, 228-2232.

Thorstenson D.C. and Plummer L.N. (1977) Equilibrium criteria for two component solids reacting with fixed composition in an aqueous-phase; example: the magnesian calcites. *Am. J. Sci.* **277**, 1203-1223.

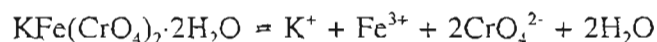
Van Breemen N. (1973) Soil forming processes in acid sulfate soils. In *Acid Sulfate Soils, Proc. Int. Symp. on Acid Sulfate Soils* (ed. H. DOST), Vol I. Publ.18 ILRI, 66-130. Wageningen, The Netherlands.

Waddington T.C. (1959) Lattice energies. In *Advances in inorganic chemistry and radiochemistry, Vol. I* (eds. H.J. Emeléus and A.G. Sharpe), 157-221. Academic Press, Inc., New York.

CHAPTER 6

Solubility of $\text{KFe}(\text{CrO}_4)_2 \cdot 2\text{H}_2\text{O}$ at 4 - 75°C

The solubility of $\text{KFe}(\text{CrO}_4)_2 \cdot 2\text{H}_2\text{O}$, a precipitate recently identified in a Cr(VI)-contaminated soil, was studied in dissolution and precipitation experiments. Ten dissolution experiments were conducted at 4-75°C and initial pH values between 0.8 and 1.2 using synthetic $\text{KFe}(\text{CrO}_4)_2 \cdot 2\text{H}_2\text{O}$. Four precipitation experiments were conducted at 25°C with final pH values between 0.16 and 1.39. The log K_{sp} for the reaction



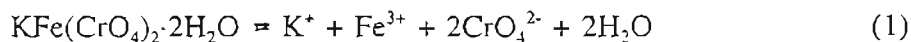
at 25°C is -19.34 ± 0.13 . From this measured solubility product, the free energy of formation, $\Delta G_{f,298}^0$, is $-2326.7 \pm 0.7 \text{ kJ mol}^{-1}$. Based on the temperature dependence of the solubility product, the enthalpy of reaction at 25°C, $\Delta H_{f,298}^0$, is $18.8 \pm 1.7 \text{ kJ mol}^{-1}$, the entropy of reaction, $\Delta S_{r,298}^0$ is $-310 \text{ J mol}^{-1} \text{ K}^{-1}$, and the heat capacity of the reaction, $\Delta C_{p,r}$, over the temperature range of the experiments is determined to be $-460 \pm 130 \text{ J mol}^{-1} \text{ K}^{-1}$. The measured solubility indicates that $\text{KFe}(\text{CrO}_4)_2 \cdot 2\text{H}_2\text{O}$ is stable under conditions of low pH and high Cr(VI) and K concentrations. It appears likely that this solid would form in the immediate vicinity of a release of acidic chromate-rich solutions, or along preferential flow paths of such solutions within a soil. This conclusion is consistent with the observed occurrence of $\text{KFe}(\text{CrO}_4)_2 \cdot 2\text{H}_2\text{O}$.

6.1 Introduction

Chromium is a toxic and carcinogenic metal that it widely used in many industrial processes. Due to spills, leakage, and improper storage, chromium has been released into the environment at many sites and is a common soil and groundwater contaminant (Calder, 1988; Palmer and Wittbrodt, 1991). Chromate-laden solutions released into soils can alter the chemical environment of native soils resulting in the dissolution of soil minerals and the precipitation of new phases that incorporate Cr(VI). The formation of these precipitates can affect Cr(VI) mobility, control its concentration in subsurface waters, and may limit its bioavailability. Identifying such precipitates and determining the conditions under which they form and remain stable can improve our estimates of the potential risks to human health and the environment at contaminated sites and can greatly contribute to the rational design of remediation systems. This study focusses on one such precipitate, $\text{KFe}(\text{CrO}_4)_2 \cdot 2\text{H}_2\text{O}$, which was recently identified in a chromium contaminated soil (Baron et al., 1996). We have studied the solubility of $\text{KFe}(\text{CrO}_4)_2 \cdot 2\text{H}_2\text{O}$ under the acidic and low temperature conditions typical for the environment where this solid has been observed to form.

Although $\text{KFe}(\text{CrO}_4)_2 \cdot 2\text{H}_2\text{O}$ has been synthesized and described (Bonnin et al., 1968; Bonnin, 1970; Graverneau and Hardy, 1972; Mellier and Graverneau, 1972; Mellier and Graverneau, 1973) until its recent discovery in a soil contaminated by acidic chrome plating solutions, it has not been found in the environment. In the chromium contaminated soil, $\text{KFe}(\text{CrO}_4)_2 \cdot 2\text{H}_2\text{O}$ was found together with another Fe-chromate precipitate, $\text{KFe}_3(\text{CrO}_4)_2(\text{OH})_6$ (Baron et al., 1996). $\text{KFe}(\text{CrO}_4)_2 \cdot 2\text{H}_2\text{O}$ was found primarily in cracks and fractures of the soil, while $\text{KFe}_3(\text{CrO}_4)_2(\text{OH})_6$ was interspersed in the bulk soil. The solubility product of $\text{KFe}_3(\text{CrO}_4)_2(\text{OH})_6$ which was recently determined (Baron and Palmer, 1996) indicates that this solid is stable over a wide range of acidic to neutral conditions. The reaction for the conversion of these two Fe-chromate phases suggests that, generally, $\text{KFe}(\text{CrO}_4)_2 \cdot 2\text{H}_2\text{O}$ is stable in more acidic, more Cr(VI)-enriched waters than those in which $\text{KFe}_3(\text{CrO}_4)_2(\text{OH})_6$ is stable (Baron and Palmer, 1996). However, there are no published thermodynamic data for $\text{KFe}(\text{CrO}_4)_2 \cdot 2\text{H}_2\text{O}$ that could be used to further constrain the conditions under which it is likely to form.

The purpose of this study is to measure the solubility of $\text{KFe}(\text{CrO}_4)_2 \cdot 2\text{H}_2\text{O}$ and to determine the solubility product (K_{sp}) for the reaction



at the acidic conditions and temperatures where this solid has been observed to form. This information is required to determine the range of conditions under which $\text{KFe}(\text{CrO}_4)_2 \cdot 2\text{H}_2\text{O}$ is stable and the extent to which it may affect the mobility of Cr(VI) in subsurface environments and interfere with the remediation of Cr(VI)-contaminated soil and groundwater.

6.2 Experimental Section

6.2.1 Synthesis of $\text{KFe}(\text{CrO}_4)_2 \cdot 2\text{H}_2\text{O}$ for the Dissolution Experiments

Synthetic $\text{KFe}(\text{CrO}_4)_2 \cdot 2\text{H}_2\text{O}$ used in the dissolution experiments was prepared using the method of Bonnin et al. (1968). Saturated solutions of $\text{Fe}(\text{NO}_3)_3$ and $\text{K}_2\text{Cr}_2\text{O}_7$ were prepared at 60°C. A 25 mL aliquot of the $\text{K}_2\text{Cr}_2\text{O}_7$ solution was then slowly (25 mL h⁻¹) added to 25 mL of the $\text{Fe}(\text{NO}_3)_3$ solution. The resulting solution was continuously stirred and kept at 60°C. A precipitate started forming about two hours after mixing of the two solutions started. Six hours after the start of the mixing process, the precipitate was allowed to settle and the residual solution was decanted. The precipitate was then washed thoroughly with ultrapure water (18 megaohm cm) and air dried.

6.2.2 Characterization of Synthetic $\text{KFe}(\text{CrO}_4)_2 \cdot 2\text{H}_2\text{O}$.

The synthetic solid was characterized using powder x-ray diffraction (XRD), scanning electron microscopy with energy dispersive spectroscopy (SEM/EDX), and Fourier Transform Infrared Spectroscopy (FTIR). A small amount of the precipitate was digested in HCl and analyzed for K and Fe using atomic absorption spectroscopy (AAS) and Cr(VI) using the diphenylcarbazide method.

Table 6-1. Initial experimental conditions.

	number of replicates	amount of solution (ml)	synthetic $\text{KFe}(\text{CrO}_4)_2 \cdot 2\text{H}_2\text{O}$ (mg)	$\text{Fe}(\text{NO}_3)_3 \cdot 9\text{H}_2\text{O}$ (g)	$\text{K}_2\text{Cr}_2\text{O}_7$ (g)	K_2CrO_4 (g)	initial pH	Temperature (°C)
Dissolution Experiments								
C2M-1.2	3	20	200	-	-	-	1.20	25
C2M-1.1	3	20	200	-	-	-	1.10	25
C2M-1.0	3	20	250	-	-	-	1.00	25
C2M-0.8	3	20	400	-	-	-	0.80	25
C2M-4C	3	5	60	-	-	-	1.00	4
C2M-15C	3	5	60	-	-	-	1.00	15
C2M-25C	3	5	60	-	-	-	1.00	25
C2M-35C	3	5	60	-	-	-	1.00	35
C2M-50C	3	5	80	-	-	-	1.00	50
C2M-75C	3	5	85	-	-	-	1.00	75
Precipitation Experiments								
PRECIP-A	1	50	-	15.15	4.60	8.50	-	25
PRECIP-B	2	20	-	1.21	0.37	0.68	-	25
PRECIP-C	3	20	-	0.61	0.18	0.34	-	25
PRECIP-D	3	20	-	0.38	0.12	0.21	-	25

6.2.3 Dissolution Experiments

Two sets of dissolution experiments were implemented. The first set was conducted at 25°C and the starting pH was varied between 0.8 and 1.2. In the second set of experiments, the temperature was varied between 4 and 75°C with an initial pH of 1.0 for all experiments. For the dissolution experiments synthetic $\text{KFe}(\text{CrO}_4)_2 \cdot 2\text{H}_2\text{O}$ was added to ultrapure water with the pH adjusted to the desired value using reagent grade HClO_4 . The solutions were placed in 20 ml glass vials and were stirred with a stirrbar at a moderate rate (about 100 rpm) to provide good mixing. The temperatures were maintained to within 0.1°C of the desired value using circulating water baths. The

starting conditions for all dissolution experiments are listed in Table 6-1. All experiments were conducted in triplicate. The experiments with different starting pH values were sampled in regular intervals to determine when equilibrium had been achieved. Nine samples were collected from the experiments in which the initial pH was varied. The experiments conducted at different temperatures were sampled once after five days. For each sample, 1 ml of the $\text{KFe}(\text{CrO}_4)_2 \cdot 2\text{H}_2\text{O}$ suspension was withdrawn. The samples were filtered using a 0.1 μm polysulfonate filter to remove suspended solids and analyzed for pH, Fe_{tot} and K_{tot} using AAS, and $\text{Cr}(\text{VI})_{\text{tot}}$ using the diphenylcarbazide method. Since the dissolution experiments were conducted in an oxidizing HClO_4 solution and reductants capable of reducing ferric iron were not present in the solution, it was assumed that all the iron was present as ferric iron. After completion of the experiments, the remaining solids were examined by powder x-ray diffraction for the presence of secondary solids.

6.2.4 Precipitation Experiments

Four precipitation experiments were conducted at 25°C. For the precipitation experiments, solutions of $\text{Fe}(\text{NO}_3)_3$, as well as $\text{K}_2\text{Cr}_2\text{O}_7$ and K_2CrO_4 were prepared. The ferric nitrate solutions and the potassium-chromate solutions were then mixed together. The resulting solutions were continuously stirred with a stirbar at a moderate rate (100 rpm) and maintained at $25 \pm 0.1^\circ\text{C}$ using a circulating water bath. The starting conditions for the precipitation experiments are summarized in Table 6-1. After 266 to 270 days, the resulting precipitates were filtered from the solutions using a 0.1 μm polysulfonate filter. The solutions were analyzed for pH, Fe_{tot} and K_{tot} using AAS, and $\text{Cr}(\text{VI})_{\text{tot}}$ using the diphenylcarbazide method. Since the dissolution experiments were conducted in an oxidizing perchloric acid solution and reductants capable of reducing ferric iron were not present in the solution, it was assumed that all the iron was present as ferric iron. The precipitates were examined by powder x-ray diffraction to confirm the formation of $\text{KFe}(\text{CrO}_4)_2 \cdot 2\text{H}_2\text{O}$ and to determine if other solids are present.

Table 6-2. Powder x-ray diffraction peaks from synthetic $\text{KFe}(\text{CrO}_4)_2 \cdot 2\text{H}_2\text{O}$ used in the dissolution experiments.

synthetic $\text{KFe}(\text{CrO}_4)_2 \cdot 2\text{H}_2\text{O}$ BONNIN (1970)			synthetic $\text{KFe}(\text{CrO}_4)_2 \cdot 2\text{H}_2\text{O}$ used in the dissolution experiments	
h,k,l	d-spacing (Å)	rel. Int.	d-spacing (Å)	rel. Int.
2 0 $\bar{1}$	5.17	s	5.17	78
2 0 $\bar{2}$	4.95	s	4.97	43
1 1 $\bar{2}$	3.63	s	3.64	68
2 0 $\bar{3}$	3.42	w	3.43	22
1 1 1	3.13	vs	3.14	100
3 1 $\bar{2}$	3.02	m	3.03	31
3 1 $\bar{3}$	2.83	m	2.84	39
0 2 0	2.75	m	2.76	65
3 1 $\bar{1}$ }	2.71	m	2.72	33
4 0 $\bar{3}$ }				
1 1 $\bar{3}$	2.584	w	2.58	22
2 0 1	2.541	vw	2.543	11
4 0 $\bar{4}$	2.475	vw		
2 2 $\bar{1}$	2.429	vw	2.434	12
1 1 2	2.277	m	2.278	18
4 0 $\bar{1}$	2.206	w	2.210	19
2 2 0	2.198	w	2.199	9
0 2 2	2.160	vw	2.162	13
2 2 $\bar{3}$	2.145	w	2.149	20
4 0 $\bar{5}$	2.075	vw		
1 1 $\bar{4}$	1.943	w	1.945	23
2 0 2	1.905	w	1.908	15
4 2 $\bar{2}$	1.885	vw	1.889	12
5 1 $\bar{3}$	1.862	m	1.868	30
5 1 $\bar{2}$	1.844	vw	1.853	8
2 2 $\bar{4}$	1.817	m	1.818	27
1 3 $\bar{1}$	1.807	m	1.811	16
0 2 3	1.774	w	1.776	14
0 0 4	1.740	w	1.741	12
1 3 $\bar{2}$	1.717	w	1.718	12
1 3 1	1.654	m	1.655	18
3 3 $\bar{2}$	1.638	vw	1.638	11
5 1 $\bar{1}$	1.625	w	1.627	9
3 3 $\bar{3}$	1.604	w	1.605	9
3 3 $\bar{1}$	1.583	vw		
2 2 2	1.5678	m	1.568	14

vs strongest peak
s strong peak
m medium peak

w weak peak
vw very weak peak

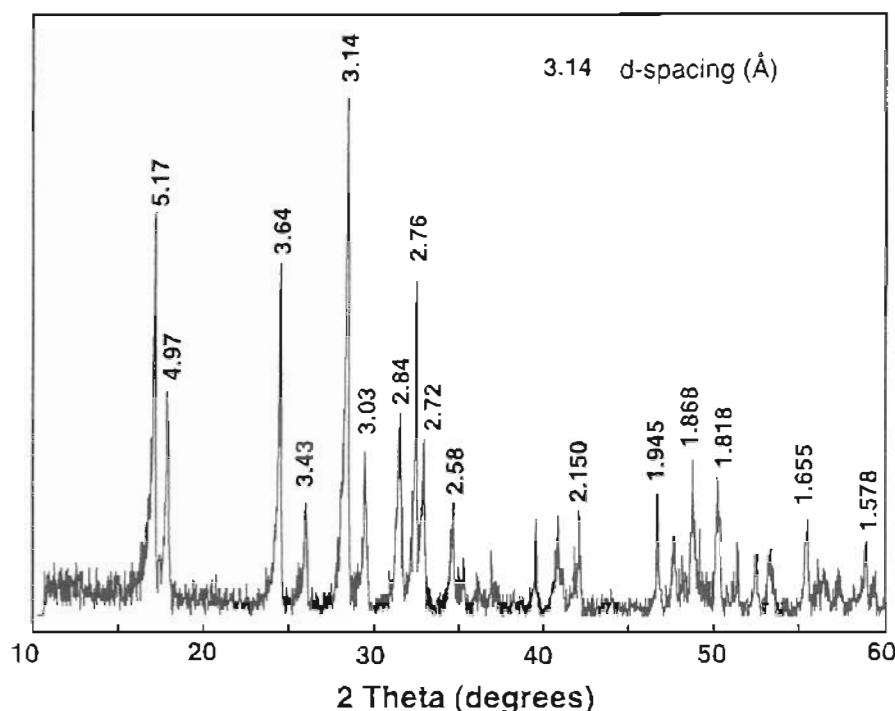


Figure 6-1. Powder x-ray diffraction pattern of synthetic $\text{KFe}(\text{CrO}_4)_2 \cdot 2\text{H}_2\text{O}$ used in the dissolution experiments. Some of the strongest peaks and the corresponding d-spacings are indicated.

6.3 Results

6.3.1 Characterization

The reddish yellow (Munsell Color 7.5YR 7/8) precipitate produced in the synthesis was identified $\text{KFe}(\text{CrO}_4)_2 \cdot 2\text{H}_2\text{O}$ by comparing powder x-ray diffraction patterns with those reported for synthetic $\text{KFe}(\text{CrO}_4)_2 \cdot 2\text{H}_2\text{O}$ (Bonnin, 1970) (Table 6-2, Figure 6-1). All the peaks produced by the precipitate could be identified as $\text{KFe}(\text{CrO}_4)_2 \cdot 2\text{H}_2\text{O}$ peaks. The absence of unidentified peaks indicates that no other crystalline phases are present in the precipitate at detectable levels. $\text{KFe}(\text{CrO}_4)_2 \cdot 2\text{H}_2\text{O}$ has a monoclinic structure and crystallizes in space group $C2/m$ (Bonnin, 1970). Using the measured d-spacings and the reported Miller indices, the unit cell parameters were calculated by multiple nonlinear regression as $a_0 = 10.865 \pm 0.003 \text{ \AA}$, $b_0 = 5.510 \pm 0.001 \text{ \AA}$, $c_0 = 10.384 \pm 0.003 \text{ \AA}$, and $\beta = 137.93 \pm 0.01^\circ$, which agrees well with the values of

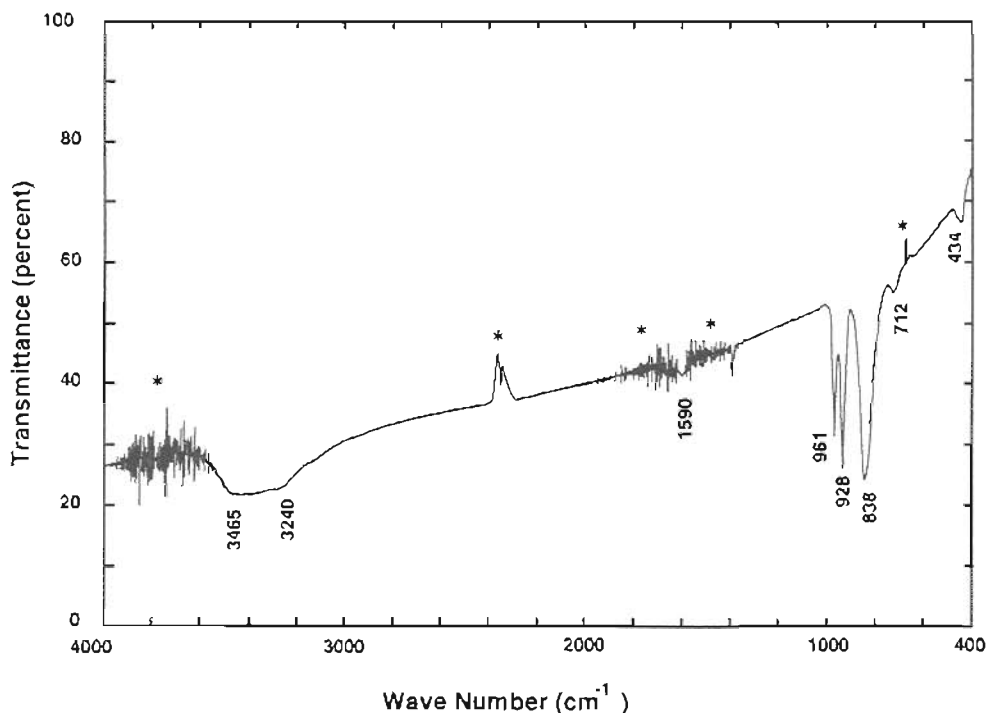


Figure 6-2. FTIR spectrum of the synthetic $\text{KFe}(\text{CrO}_4)_2 \cdot 2\text{H}_2\text{O}$ used in the dissolution experiments. The main vibrational bands in the spectrum are marked. They correspond to (Mellier and Graverneau, 1973) the O-H stretch (3465 and 3240 cm^{-1}), the OH deformation (1590 cm^{-1}), the ν_1 and ν_3 modes of Cr-O (961 , 928 , 838 , 712 cm^{-1}), and the ν_2 mode of $\delta\text{O-Cr-O}$ (434 cm^{-1}). Peaks that are artifacts due to background interference are marked with a *.

$a_0 = 10.857 \text{ \AA}$, $b_0 = 5.505 \text{ \AA}$, $c_0 = 10.374 \text{ \AA}$, and $\beta = 137.87^\circ$ reported by Bonnin (1970). Examination with SEM/EDX showed that the precipitate consists of uniform, K, Fe and Cr containing polycrystalline particles, ranging in size from 30 to $200 \mu\text{m}$. No secondary crystalline or amorphous phases were observed.

Wet chemical analysis confirmed the composition of the precipitate as corresponding to $\text{KFe}(\text{CrO}_4)_2 \cdot 2\text{H}_2\text{O}$ with a K:Fe:CrO₄ ratio of $0.96:1.04:2$ compared to the ideal $1:1:2$ ratio. The deviations from the ideal formula are within the analytical error of approximately 5 percent.

The FTIR spectrum of the precipitate (Figure 6-2) was compared to a scan of synthetic $\text{KFe}(\text{CrO}_4)_2 \cdot 2\text{H}_2\text{O}$ reported by Mellier and Graverneau (1973). All the absorption

bands in the precipitate could be assigned to $\text{KFe}(\text{CrO}_4)_2 \cdot 2\text{H}_2\text{O}$, confirming the identification as $\text{KFe}(\text{CrO}_4)_2 \cdot 2\text{H}_2\text{O}$ and indicating the absence of other phases in the precipitate. However, an absorption band at 798 cm^{-1} that Mellier and Graveriau (1973) found in their material and associate with $\nu\text{Fe-O}$ vibrations is absent in our precipitate. The reason for this discrepancy is not known.

Based on these analyses, the precipitate was identified as a $\text{KFe}(\text{CrO}_4)_2 \cdot 2\text{H}_2\text{O}$. There is no indication of any other phases in the precipitate.

Table 6-3. Final concentrations in the precipitation and dissolution experiments.

	final pH	$[\text{Cr(VI)}]_{\text{tot}}$ (mmol L ⁻¹)	$[\text{K}]_{\text{tot}}$ (mmol L ⁻¹)	$[\text{Fe}]_{\text{tot}}$ (mmol L ⁻¹)	$[\text{NO}_3]_{\text{tot}}$ (mol L ⁻¹)	Experiment Duration (days)	$\text{KFe}_3(\text{CrO}_4)_2(\text{OH})_6$ detected by XRD
C2M-1.2	1.39±0.03	35.8±1.6	21.5±0.9	11.9±0.7	-	181	yes
C2M-1.1	1.26±0.04	42.0±0.4	22.1±0.2	14.3±1.6	-	181	no
C2M-1.0	1.19±0.05	49.8±0.1	26.9±0.3	18.3±1.5	-	181	no
C2M-0.8	1.01±0.02	70.3±1.2	38.5±0.3	27.6±2.3	-	181	no
C2M-4C	1.08±0.03	41.6±0.5	22.4±0.1	17.1±0.1	-	5	no
C2M-15C	1.09±0.02	45.59±1.0	24.1±0.2	17.5±1.0	-	5	no
C2M-25C	1.13±0.04	52.0±0.2	26.8±0.7	20.4±0.1	-	5	no
C2M-35C	1.08±0.05	61.2±0.2	30.3±0.2	24.1±0.7	-	5	no
C2M-50C	1.06±0.06	70.6±0.4	35.7±0.8	28.1±0.8	-	5	no
C2M-75C	1.02±0.09	88.8±0.8	45.9±0.4	27.6±0.4	-	5	no
PRECIP-A	0.16	149	1830	41	2250	270	no
PRECIP-B	1.30±0.06	12.1±2.0	135±5	40.0±3.0	450	266	yes
PRECIP-C	1.38±0.01	13.6±0.3	81.3±0.9	14.8±0.5	225	266	yes
PRECIP-D	1.39±0.02	20.9±1.4	55.7±1.6	3.7±0.2	141	266	yes

* The reported concentrations represent the mean ± the standard deviation from triplicate experiments

** Calculated from initial solutions.

6.3.2 Dissolution and Precipitation Experiments

In the dissolution experiments, the bulk of the reaction occurred within the first 30 minutes of the experiment with rates declining over time. For example, the evolution

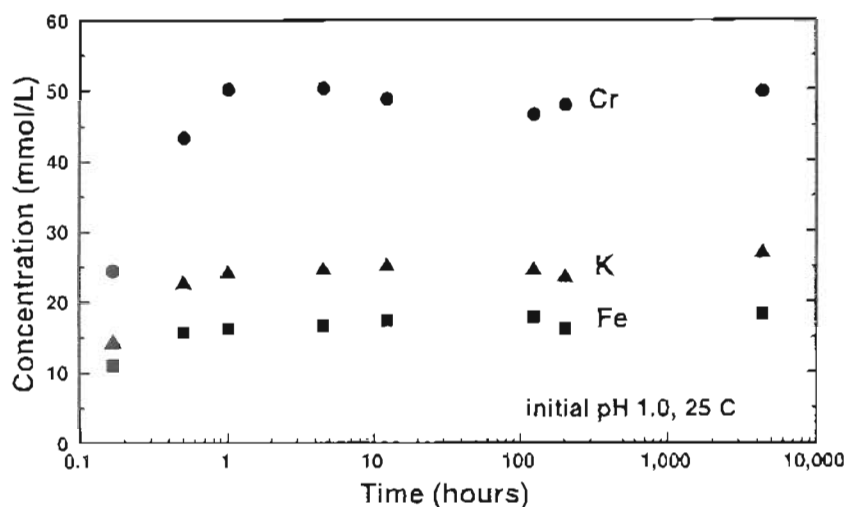


Figure 6-3. Concentration of $[K]_{tot}$ (▲), $[Fe]_{tot}$ (■), and $[CrO_4]_{tot}$ (•) in the dissolution experiment with initial pH 1 at 25°C. Data points represent the average of triplicate experiments.

of the solution composition over time in the dissolution experiment at 25°C, initial pH 1 (C2M-1.0) shows a rapid increase over the first 30 minutes reaching approximately 80 % of the steady state value while the remaining 20 % required an additional 30 minutes (Figure 6-3). The compositions of the solutions at the completion of the dissolution experiments (5-181 days) are summarized in Table 6-3. In all dissolution experiments, the molar ratio of K and Cr correspond very well to the 1:2 ratio in the $KFe(CrO_4)_2 \cdot 2H_2O$ formula. However, in several of the dissolution experiments Fe concentrations are lower than would be expected based on the $KFe(CrO_4)_2 \cdot 2H_2O$ formula (Table 6-3).

In all four precipitation experiments, a precipitate started forming immediately after the mixing of the ferric nitrate and potassium-chromate solutions. The bulk of the precipitate was produced within the first day of the experiments. After a day, the amount of precipitate in the experiments did not change visibly. The compositions of the solutions at the completion of the precipitation experiments (266-270 days) are summarized in Table 6-3.

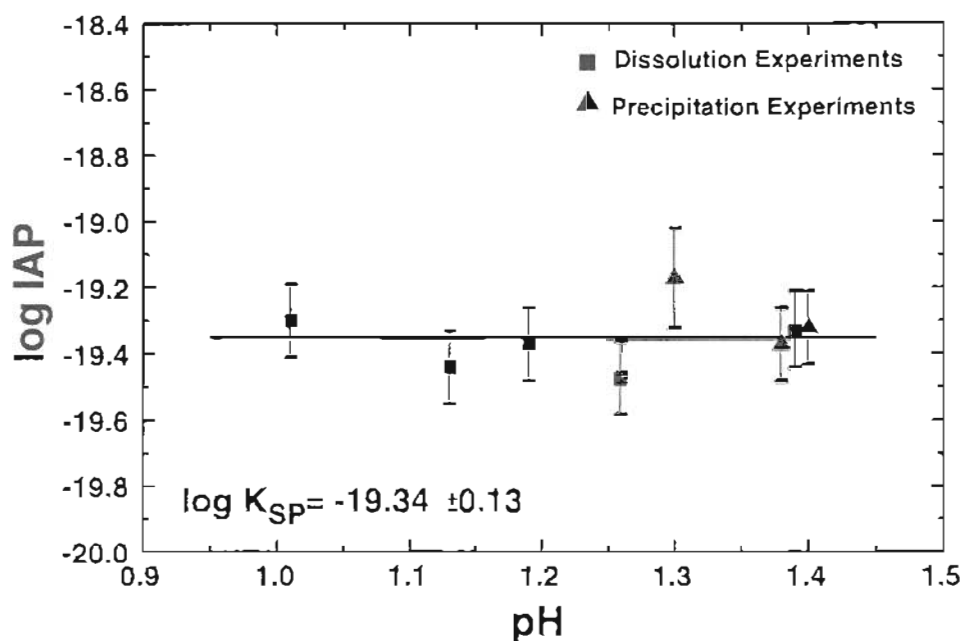


Figure 6-4. Log of the ion activity product from dissolution (■) and precipitation (□) experiments at different pH values and 25°C. Solid line represents the average of the eight log ion activity product values (-19.34 ± 0.13).

Based on the measured final pH, K_{tot} , Fe_{tot} and $\text{Cr(VI)}_{\text{tot}}$, final aqueous activities of K^+ , Fe^{3+} , and CrO_4^{2-} were calculated for all experiments except precipitation experiment PRECIP-A using the geochemical speciation model MINTEQA2 (Allison et al, 1990). Experiment PRECIP-A was excluded from the speciation calculation because of the high ionic strength (~2.6 M) in this experiment makes activity corrections unreliable. Activity corrections for the other experiments were made using the Davies Equation in the MINTEQA2 code. Thermodynamic data used in the calculations are listed in Table 6-4. The results of these calculations are listed in Table 6-5.

If the dissolution reaction of $\text{KFe}(\text{CrO}_4)_2 \cdot 2\text{H}_2\text{O}$ is written as in equation (1), then the log ion activity product (IAP) is given by

$$\log \text{IAP} = \log\{\text{K}^+\} + \log\{\text{Fe}^{3+}\} + 2 \log\{\text{CrO}_4^{2-}\} + 2 \log\{\text{H}_2\text{O}\} \quad (2)$$

Table 6-4. Thermodynamic data used for calculations.

Formula	State	$\Delta G_{f,298}^{\circ}$ (kJ mol ⁻¹)	ΔH_f° (kJ mol ⁻¹)	log K_f	Source
Fe ³⁺	aq	-17.87±1.0	-	-	Naumov et al. (1973)
FeCrO ₄ ⁺	aq	-	19.1	7.8	Baron and Palmer (1996)
FeOH ²⁺	aq	-	43.5	-2.19	Allison et al. (1990)
Fe(OH) ₂ ⁺	aq	-	71.6	-5.67	Nordstrom and Munoz (1994)
Fe ₂ (OH) ₂ ⁴⁺	aq	-	56.5	-2.95	Allison et al. (1990)
K ⁺	aq	-282.5±0.1	-	-	Cox et al. (1989)
KCrO ₄ ⁻	aq	-	-	0.799	Allison et al. (1990)
CrO ₄ ²⁻	aq	-720.86	-	-	Naumov et al. (1971)
HCrO ₄ ⁻	aq	-	3.8	6.5089	Allison et al. (1990)
Cr ₂ O ₇ ²⁻	aq	-	-	14.5571	Allison et al. (1990)
H ₂ CrO ₄ ⁰	aq	-	-	5.6513	Allison et al. (1990)
OH ⁻	aq	-	-	-13.998	Allison et al. (1990)
H ₂ O	l	-237.1±0.04	-	-	Cox et al. (1989)

where { } denotes activity. If the solutions are equilibrated with KFe(CrO₄)₂·2H₂O, the IAP is equal to the solubility product, K_{sp} . Based on the calculated activities of K⁺, Fe³⁺, and CrO₄²⁻, the final IAP was calculated using equation (2). The results of these calculations are presented in Table 6-5. The saturation indices for KFe₃(CrO₄)₂(OH)₆ and goethite are also included in Table 6-5. The average charge balance error in the MINTEQA2 simulations was 4 percent for the dissolution experiments and 14 percent in the precipitation experiments (Table 6-5). The errors associated with the log IAP values calculated from the standard deviation of the triplicate experiments range from 0.01 to 0.05 log units. The analytical error calculated from the precision of the analytical

Table 6-5. Results of MINTEQA2 speciation calculations.

	final pH	log {CrO ₄ ²⁻ }	log {K ⁺ }	log {Fe ³⁺ }	Ionic Strength (M)	Saturation Index KFe ₃ (CrO ₄) ₂ (OH) ₆	Saturation Index Goethite	Charge Balance Error (%)	log IAP
C2M-1.2	1.39	-7.15	-1.79	-3.24	0.139	0.7	0.4	5	-19.33±0.11
C2N-1.1	1.26	-7.24	-1.79	-3.17	0.175	0.0	0.1	2	-19.44±0.11
C2M-1.0	1.19	-7.28	-1.71	-3.10	0.225	-0.3	-0.1	4	-19.37±0.11
C2M-0.8	1.01	-7.38	-1.56	-2.98	0.362	-1.0	-0.5	8	-19.30±0.11
C2M-4C	1.08	-7.47	-1.78	-3.02	0.237	-2.9	-1.1	4	-19.74±0.11
C2M-15C	1.09	-7.42	-1.75	-3.06	0.237	-1.8	-0.7	2	-19.65±0.11
C2M-25C	1.13	-7.33	-1.71	-3.06	0.243	-0.6	-0.2	1	-19.43±0.11
C2M-35C	1.08	-7.32	-1.66	-3.05	0.267	-0.1	0.0	5	-19.35±0.11
C2M-50C	1.06	-7.29	-1.60	-3.09	0.283	0.9	0.4	8	-19.27±0.11
C2M-75C	1.02	-7.24	-1.50	-3.28	0.293	1.8	0.8	7	-19.26±0.11
PRECIP-B	1.30	-7.67	-1.02	-2.81	0.497	1.2	0.6	18	-19.17±0.15
PRECIP-C	1.38	-7.48	-1.23	-3.18	0.246	0.7	0.4	14	-19.37±0.11
PRECIP-D	1.39	-7.31	-1.38	-3.32	0.173	0.6	0.4	9	-19.32±0.11

measurements ($\pm 10\%$) is ± 0.11 log units (assuming that the covariance between the errors of the individual analytical measurements equals zero). The error from the triplicate experiments is smaller than the analytical error. The error reported with the log IAP values reported in Table 6-5 and used for subsequent calculations is the analytical error.

Powder X-ray diffraction analysis conducted on the solids after completion of the experiments indicate that in all experiments $\text{KFe}(\text{CrO}_4)_2 \cdot 2\text{H}_2\text{O}$ is present and that in some experiments, significant quantities of $\text{KFe}_3(\text{CrO}_4)_2(\text{OH})_6$ have also formed (Table 6-5).

6.4 Discussion

The final solutions in many of the experiments are supersaturated with $\text{KFe}_3(\text{CrO}_4)_2(\text{OH})_6$ and goethite (Table 6-5). Powder x-ray diffraction of the resulting

solids indicates that $\text{KFe}_3(\text{CrO}_4)_2(\text{OH})_6$ is present in some of the experiments (Table 6-3). Goethite, however, was not detected by XRD. It is possible that formation of $\text{KFe}_3(\text{CrO}_4)_2(\text{OH})_6$ and possibly some ferric oxyhydroxide was still continuing at the completion of the experiments and the solutions were not at complete equilibrium. However, the kinetics of $\text{KFe}_3(\text{CrO}_4)_2(\text{OH})_6$ precipitation are slow (Baron and Palmer, 1996) compared to the fast reaction observed for $\text{KFe}(\text{CrO}_4)_2 \cdot 2\text{H}_2\text{O}$, and it is expected that even if the solutions are not at overall equilibrium, they are equilibrated with $\text{KFe}(\text{CrO}_4)_2 \cdot 2\text{H}_2\text{O}$. The IAP values calculated using the final concentrations in the experiments therefore represent the equilibrium IAP for $\text{KFe}(\text{CrO}_4)_2 \cdot 2\text{H}_2\text{O}$. The log IAP values calculated using the final activities from the experiments precipitation and dissolution experiments at 25°C all fall in a very narrow range and vary from -19.44 to -19.28 (Table 6-5). A plot of log IAP versus pH (Figure 6-4) suggests that there is no trend in the data and a t-test indicates that the log IAP values calculated for the dissolution experiments (average = -19.37, standard deviation = 0.06) are not statistically different from those calculated from the precipitation experiments (average = -19.29, standard deviation = 0.10) at the 10 percent significance level ($t = -1.5$, $df = 6$). It appears that equilibrium with $\text{KFe}(\text{CrO}_4)_2 \cdot 2\text{H}_2\text{O}$ in the experiments is approached from dissolution and precipitation. The average of the final log IAP values represents the log K_{sp} at 25°C and it is calculated as -19.34 ± 0.13 . The error in the log K_{sp} value represents the total standard deviation over all experiments. An F-test indicates that the variance among the log IAP values at different pH values is not significantly different from the variance within the triplicate experiments at the 95 percent confidence level ($F = 2.1$, $n_1 = 8$, $n_2 = 24$, $df_1 = 7$, $df_2 = 16$).

Based on the solubility product for $\text{KFe}(\text{CrO}_4)_2 \cdot 2\text{H}_2\text{O}$, the free energy of formation of this solid can be calculated. At equilibrium, the Gibbs free energy of reaction at 25°C, $\Delta G_{r,298}^0$ is given by

$$\begin{aligned} \Delta G_{r,298}^0 = & \Delta G_{f,298}^0(\text{K}^+) + \Delta G_{f,298}^0(\text{Fe}^{3+}) + 2\Delta G_{f,298}^0(\text{CrO}_4^{2-}) \\ & + 2\Delta G_{f,298}^0(\text{H}_2\text{O}) - \Delta G_{f,298}^0(\text{KFe}(\text{CrO}_4)_2 \cdot 2\text{H}_2\text{O}) \end{aligned} \quad (3)$$

with the free energy of reaction related to the K_{sp} by

$$\Delta G_{f,298}^0 = -2.303 RT \log K_{sp} \quad (4)$$

Solving for the free energy of formation of $KFe(CrO_4)_2 \cdot 2H_2O$

$$\begin{aligned} \Delta G_{f,298}^0(KFe(CrO_4)_2 \cdot 2H_2O) &= \Delta G_{f,298}^0(K^+) + \Delta G_{f,298}^0(Fe^{3+}) \\ &+ 2\Delta G_{f,298}^0(CrO_4^{2-}) + 2\Delta G_{f,298}^0(H_2O) + 2.303 RT \log K_{sp} \end{aligned} \quad (5)$$

and using the free energies given in Table 6-3, we calculate $\Delta G_{f,298}^0(KFe(CrO_4)_2 \cdot 2H_2O) = -2326.7 \pm 0.7 \text{ kJ mol}^{-1}$ where the variation represents the error introduced by the uncertainty in the K_{sp} value only. Including the error in the free energies of the individual ions (Table 6-4) results in an additional uncertainty of $\pm 1.2 \text{ kJ mol}^{-1}$. Considering that the error in the free energies of some of the individual ions may be larger than reported in Table 6-4 would result in an even larger uncertainty in the estimate of $\Delta G_{f,298}^0(KFe_3(CrO_4)_2(OH)_6)$. For example, for $\Delta G_{f,298}^0(Fe^{3+})$ values as high as -4.6 kJ mol^{-1} have been reported (Wagman et al., 1969). Propagating an uncertainty of 13.3 kJ mol^{-1} for $\Delta G_{f,298}^0(Fe^{3+})$ through equation (5) results in an overall uncertainty of $\pm 14.2 \text{ kJ mol}^{-1}$ for $\Delta G_{f,298}^0(KFe(CrO_4)_2 \cdot 2H_2O)$.

The calculated log IAP values increase with increasing temperature, varying from -19.74 at 4° to -19.26 at 75°C (Table 6-5, Figure 6-5), indicating a positive enthalpy of reaction, ΔH_r^0 , for the dissolution of $KFe(CrO_4)_2 \cdot 2H_2O$. The dependence of log IAP on the inverse of the temperature is not linear, indicating that the ΔH_r^0 varies over the temperature range from 4 to 75°C. Therefore, a variable enthalpy and constant heat capacity model (Nordstrom and Munoz, 1994) was used to model the temperature dependence

$$\log K_{sp} = \frac{\Delta S_r^0 - \Delta C_{p,r}}{R} - \frac{\Delta H_r^0}{RT} + \frac{(\Delta C_{p,r} \log T)}{R} \quad (6)$$

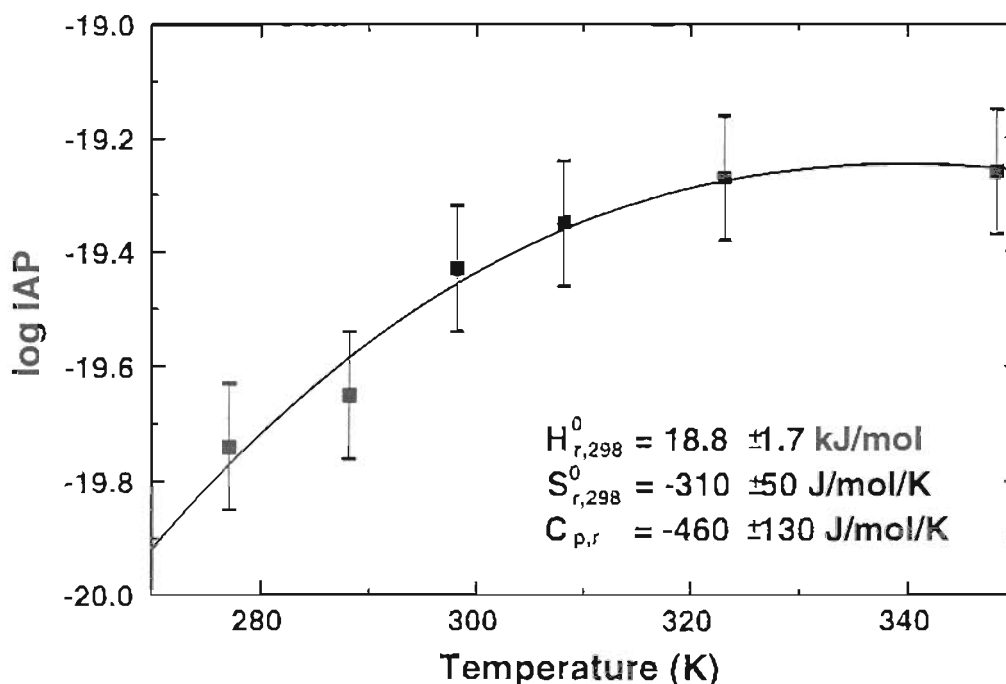


Figure 6-5. Calculated log ion activity product versus temperature from four dissolution experiments at 4, 15, 25, 35, 50, and 75°C, initial pH 1.0. The solid line is the best fit of the variable enthalpy and constant heat capacity model to the experimental data.

where ΔS_r^0 is the entropy of reaction, $\Delta C_{p,r}$ is the heat capacity of reaction, R is the gas constant ($8.314 \times 10^{-3} \text{ kJ mol}^{-1} \text{ K}^{-1}$), and T is the temperature in K. Fitting the temperature-dependent data to equation (6) (Figure 6-5) yields $\Delta H_{r,298}^0 = 18.8 \pm 1.7 \text{ kJ mol}^{-1}$, $\Delta S_{r,298}^0 = -310 \pm 35 \text{ J mol}^{-1} \text{ K}^{-1}$, and $\Delta C_{p,r} = -460 \pm 130 \text{ J mol}^{-1} \text{ K}^{-1}$. This model gives a good fit of the data ($r^2=0.97$) and although only six data points were used to determine the three parameters ($\Delta H_{r,298}^0$, $\Delta S_{r,298}^0$, $\Delta C_{p,r}$), a t-test indicates that all parameters are significantly different from zero at the 95 percent confidence level.

Based on the calculated log K_{sp} , the conditions under which $\text{KFe}(\text{CrO}_4)_2 \cdot 2\text{H}_2\text{O}$ can be evaluated. The transition between $\text{KFe}(\text{CrO}_4)_2 \cdot 2\text{H}_2\text{O}$ and $\text{KFe}_3(\text{CrO}_4)_2(\text{OH})_6$ is of particular interest because $\text{KFe}_3(\text{CrO}_4)_2(\text{OH})_6$ limits the stability field of $\text{KFe}_3(\text{CrO}_4)_2(\text{OH})_6$ at higher pH values. Assuming that all the available Fe(III) in the soil is tied up by these Fe-chromate phases, and expressing chromate as HCrO_4^- , the dominant species under the

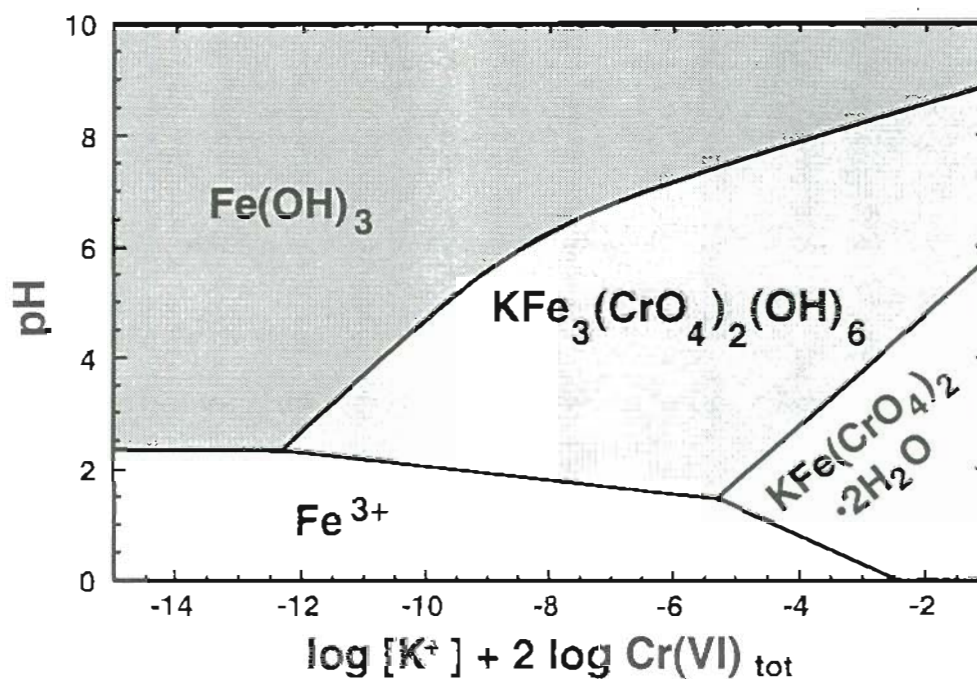
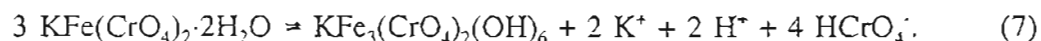


Figure 6-6. Diagram of the predominance regions of $\text{KFe}(\text{CrO}_4)_2 \cdot 2\text{H}_2\text{O}$, $\text{KFe}_3(\text{CrO}_4)_2(\text{OH})_6$, and $\text{Fe}(\text{OH})_3$ in the K-Fe(III)-Cr(VI)- H_2O system as a function of pH and $\log [\text{K}^+] + 2 \log [\text{Cr(VI)}]_{\text{tot}}$. The activity of dissolved Fe_{tot} is $10^{-4} \text{ mol L}^{-1}$.

acidic conditions of interest, the transition is given by



At equilibrium, this transformation can be expressed as

$$\begin{aligned} 3 \log K_{\text{sp}}(\text{KFe}(\text{CrO}_4)_2 \cdot 2\text{H}_2\text{O}) - \log K_{\text{sp}}(\text{KFe}_3(\text{CrO}_4)_2(\text{OH})_6) - 4 \log K(\text{HCrO}_4^-) \\ = 2 \log \{\text{K}^+\} + 4 \log \{\text{HCrO}_4^-\} + 2 \log \{\text{H}^+\} \end{aligned} \quad (8)$$

Therefore, the transition pH, pH_T , is

$$\begin{aligned} \text{pH}_T = & - (3/2) \log K_{\text{sp}}(\text{KFe}(\text{CrO}_4)_2 \cdot 2\text{H}_2\text{O}) + 1/2 \log K_{\text{sp}}(\text{KFe}_3(\text{CrO}_4)_2(\text{OH})_6) \\ & + 2 \log K(\text{HCrO}_4^+) + \log\{\text{K}^+\} + 2 \log\{\text{HCrO}_4^-\}. \end{aligned} \quad (9)$$

From equation (9), it becomes apparent that pH_T is a function of the solubility products of $\text{KFe}(\text{CrO}_4)_2 \cdot 2\text{H}_2\text{O}$ and $\text{KFe}_3(\text{CrO}_4)_2(\text{OH})_6$, and the activities of K^+ and HCrO_4^- . In general, higher combined activities of K^+ and Cr(VI) result in a higher pH_T and a larger stability field for $\text{KFe}(\text{CrO}_4)_2 \cdot 2\text{H}_2\text{O}$. The predominance regions for $\text{KFe}_3(\text{CrO}_4)_2(\text{OH})_6$ and hydrous ferric oxide, represented here as $\text{Fe}(\text{OH})_3$, as a function of pH and the activities of K^+ and $\text{Cr(VI)}_{\text{tot}}$ are shown in Figure 6-6. Solubility products and equilibrium constants for aqueous species were taken from (Nordstrom and Munoz, 1994) and (Baron and Palmer, 1996), additional constants are listed in Table 6-3. Based on the above discussion and Figure 6-6, $\text{KFe}(\text{CrO}_4)_2 \cdot 2\text{H}_2\text{O}$ is stable in oxidizing environments under conditions of low pH and high Cr(VI) and K concentrations. These conditions are typical for the immediate vicinity of a release of acidic chromate-rich solutions, or for preferential flow paths of such solutions within a soil. The observed occurrence of $\text{KFe}(\text{CrO}_4)_2 \cdot 2\text{H}_2\text{O}$ in cracks and fractures, the preferential flow paths within the Cr(VI) -contaminated soil, is consistent with the solubility of this phase and its stability fields.

6.5 References

- Allison J.D., Brown D.S., and Novo-Gradac K.J. (1990) *MINTEQA2/PRODEFA2, a geochemical assessment model for environmental systems: version 3.0*. U.S. Environmental Protection Agency, Athens, GA.
- Baron D. and Palmer C.D. Solubility of $\text{KFe}_3(\text{CrO}_4)_2(\text{OH})_6$ at 4 - 35°C. *Geochim. Cosmochim. Acta* (accepted for publication, March, 1996).
- Baron D., Stanley J.T., and Palmer C.D. (1996) Identification of two iron-chromate precipitates in a Cr(VI) -contaminated soil. *Environ. Sci. Technol.* **30**, 964-968.
- Bonnin, A.; Hardy, A.; Lecerf, A. (1968) Les chromates de fer et de métaux monovalents: $\text{MFe}(\text{CrO}_4)_2 \cdot 2\text{H}_2\text{O}$. *C. R. Acad. Sci. Paris, Sér. C* **266**, 1227-1229.
- Bonnin A. (1970) Préparations et étude de chromates de fer. Ph.D. Dissertation, Univ. Rennes, France.

Calder L.M. (1988) Chromium contamination in groundwater. In: *Chromium in the Natural and Human Environments* (eds. J.O. Nriagu and E. Nieboer), 215-230. John Wiley and Sons, New York.

Cox J.D., Wagman D.D., and Mededev V.A. (1989) *CODATA Key Values for Thermodynamics*. Hemisphere Publishing Corporation.

Gravereau P. and Hardy A. (1972) La série $M^I M^{III}(XO_4)_2 \cdot nH_2O$: structure cristalline de $KFe(CrO_4)_2 \cdot 2H_2O$, nouveau type dans la série des chromates des fer dihydratés. *Acta Crystallogr. Sec.B* **28**, 2333-2337.

Mellier A. and Gravereau P. (1972) Spectres de vibration infrarouge à bases températures de chromates doubles métalliques dihydratés de type $M_1Fe(CrO_4)_2 \cdot 2H_2O$ avec $M_1 = Na, K, Tl$. *C. R. Seances Acad. Sci. Paris, Sér. B* **274**, 1024-1027.

Mellier, A.; Gravereau, P. (1973) La série $M^I M^{III}(CXO_4)_2 \cdot nH_2O$: étude structurale des éléments $M^I Fe(CrO_4)_2 \cdot 2H_2O$ avec $M^I = Na, K, Fl, NH_4$ par voies radiocristallographique et vibrationnelle conjuguées. *Spectrochim. Acta* **29A**, 2043-2054.

Naumov G.B., Ryzhenko I.L. and Khodakovsky I.L. (1971) *Handbook of Thermodynamic Data* (translated from Russian by G.J. Soleimami, edited by I. Barnes and V. Speltz), Washington D.C. NTIS publication PB-226 722.

Nordstrom D.K. and Munoz J.L. (1994) *Geochemical Thermodynamics (2nd Edition)*. Blackwell Scientific Publications, Boston, Mass.

Palmer C.D. and Wittbrodt P.R. (1991) Processes affecting the Remediation of chromium-contaminated sites. *Environ. Health. Perspect.* **92**, 25-40.

Wagman D.D., Evans W.H., Parker V.B., Halow I., Bailey S.M., and Schumm R.H. (1969) Selected values of chemical thermodynamic properties. *National Bureau of Standards Tech. Note* 270-4. U.S. Department of Commerce.

CHAPTER 7

Summary and Conclusions

7.1 Summary of Results

The formation of chromate-containing precipitates is one of the key processes controlling the mobility of chromium in the environment. This dissertation documents the occurrence of two Fe-chromate precipitates, $\text{KFe}_3(\text{CrO}_4)_2(\text{OH})_6$ and $\text{KFe}(\text{CrO}_4)_2 \cdot 2\text{H}_2\text{O}$, in a chromium contaminated soil and examines their solubility as well as solid solution/aqueous solution reactions between the sulfate mineral jarosite ($\text{KFe}_3(\text{SO}_4)_2(\text{OH})_6$) and $\text{KFe}_3(\text{CrO}_4)_2(\text{OH})_6$. The key findings and contributions of the individual experimental chapters of this dissertation include the following:

Chapter 2 is the first documentation of the occurrence of $\text{KFe}_3(\text{CrO}_4)_2(\text{OH})_6$ and $\text{KFe}(\text{CrO}_4)_2 \cdot 2\text{H}_2\text{O}$ in chromium contaminated soils. Although both these phases had been synthesized and described by others, they have not previously been identified in the environment. The identification of these phases raises interesting questions about their potential impact on Cr(VI) mobility and the remediation of Cr(VI)-contaminated sites, and about the potential formation of solid solutions between jarosite and its chromate analog. This study also demonstrates the practicability and usefulness of a combination of electron microscopy and powder x-ray diffraction for the identification of heavy metal containing precipitates in contaminated soils.

Chapter 3 is the first study of the solubility of $\text{KFe}_3(\text{CrO}_4)_2(\text{OH})_6$. The measured $\log K_{sp}$ indicates that this phase can form under a wide range of conditions and be present in large parts of a chromium contaminated aquifer, limiting Cr(VI)-mobility and interfering with the remediation of Cr(VI)-contaminated sites. This study also suggests that FeCrO_4^+ is an important ion pair in acidic Fe(III)- and chromate-containing solutions.

The formation constant calculated for this ion pair is in good agreement with other spectroscopic studies of the Fe(III)-chromate system.

Reported values for the solubility and the free energy of formation of the sulfate mineral jarosite vary widely, making it difficult to assess the conditions under which this important mineral forms. Reliable values for the solubility and free energy of formation of jarosite are also necessary as a basis for investigations of $\text{KFe}_3(\text{Cr}_x\text{S}_{(1-x)}\text{O}_4)_2(\text{OH})_6$ solid solutions. Chapter 4 includes an extensive critical review of previous studies of the solubility of jarosite and a discussion of the reasons for the wide range of reported values. In addition, the results of experiments to determine the solubility of a carefully characterized synthetic jarosite with a composition close to ideal are presented. The solubility and free energy of formation for jarosite determined in this study are in excellent agreement with a recent study of K-Na-H₂O jarosite solid solutions.

Chapter 5 is the first report of the existence of $\text{KFe}_3(\text{Cr}_x\text{S}_{(1-x)}\text{O}_4)_2(\text{OH})_6$ solid solutions and the first study of their solid solution/aqueous solution reactions. Jarosite and $\text{KFe}_3(\text{CrO}_4)_2(\text{OH})_6$ are miscible over all proportions. The unit cell volume of the $\text{KFe}_3(\text{Cr}_x\text{S}_{(1-x)}\text{O}_4)_2(\text{OH})_6$ solid varies linearly between the endmembers as a function of composition, indicating a continuous solid solution series. $\text{KFe}_3(\text{Cr}_x\text{S}_{(1-x)}\text{O}_4)_2(\text{OH})_6$ solid solutions dissolve stoichiometrically and reach a stoichiometric saturation state after about 40-60 days. Stoichiometric saturation constants calculated from a sample taken after 138 days indicate that the solid solution is close to ideal with a small negative excess free energy of mixing. The experimental results suggest that $\text{KFe}_3(\text{Cr}_x\text{S}_{(1-x)}\text{O}_4)_2(\text{OH})_6$ solid solutions could form in chromium contaminated aquifers. Groundwater equilibrated with such solid solutions would maintain significantly lower Cr(VI) concentrations than groundwater equilibrated with pure $\text{KFe}_3(\text{CrO}_4)_2(\text{OH})_6$.

The first study of the solubility of $\text{KFe}(\text{CrO}_4)_2 \cdot 2\text{H}_2\text{O}$ is reported in Chapter 6. The measured high solubility suggests that this solid could form under conditions of very low pH and high chromate concentrations, typical for the immediate vicinity of a release of acidic chrome plating solutions. $\text{KFe}(\text{CrO}_4)_2 \cdot 2\text{H}_2\text{O}$ is unlikely to form in larger parts of a chromium contaminated aquifer and is not likely to interfere with the remediation of chromium contaminated sites. This chapter also presents an overall overview of the

stability fields of $\text{KFe}_3(\text{CrO}_4)_2(\text{OH})_6$ and $\text{KFe}(\text{CrO}_4)_2 \cdot 2\text{H}_2\text{O}$ in the K-Fe(III)-Cr(VI)- H_2O system.

7.2 Overall Conclusions

This dissertation contributes important new information to our understanding of the geochemistry of chromium. While it is conventionally thought that under most conditions the mobility of Cr(VI) in subsurface environments is controlled by adsorption and redox reactions, the present findings suggest that the formation of Cr(VI)-containing solid phases, such as the phases that are the focus of this study, can also be important factors.

The results of this study suggest that $\text{KFe}_3(\text{CrO}_4)_2(\text{OH})_6$ and $\text{KFe}_3(\text{Cr}_x\text{S}_{(1-x)}\text{O}_4)_2(\text{OH})_6$ solid solutions can form in large parts of chromium contaminated aquifers. These precipitates could bind significant quantities of Cr(VI), thereby decreasing the mobility of Cr(VI) the subsurface. The presence of these precipitates and their slow dissolution during pump-and-treat cleanup of contaminated aquifers could be an important factor prolonging such cleanups.

7.3 Suggestions for Future Work

While this work has contributed much to the understanding of the role of Fe-chromate precipitates in chromium contaminated soils, some issues remain unresolved and other interesting questions have been raised by this work. The purpose of this final section of the dissertation is to summarize these questions as suggestions for future work.

Due to time restraints and the slow nature of the solid solution-aqueous solution reactions of $\text{KFe}_3(\text{Cr}_x\text{S}_{(1-x)}\text{O}_4)_2(\text{OH})_6$, much work remains to be done to elucidate these reactions and to determine thermodynamic equilibrium conditions in the $\text{KFe}_3(\text{CrO}_4)_2(\text{OH})_6$ - $\text{KFe}_3(\text{SO}_4)_2(\text{OH})_6$ - H_2O system. It remains to be seen if and how the dissolution experiments evolve over the long term and it is suggested that the solutions are sampled regularly over a period of several years. If the evolution of the solutions suggest that secondary precipitates are forming, the solids and in particular the composition of their surfaces should be examined to determine the nature and composition

of these secondary phases. Very little is known about the precipitation of $\text{KFe}_3(\text{Cr}_x\text{S}_{(1-x)}\text{O}_4)_2(\text{OH})_6$ solid solutions. Precipitation experiments from supersaturated solutions with varying chromate to sulfate ratios are needed to evaluate the precipitation pathways in the $\text{KFe}_3(\text{CrO}_4)_2(\text{OH})_6$ - $\text{KFe}_3(\text{SO}_4)_2(\text{OH})_6$ - H_2O system. The composition of these potentially heterogeneous precipitates should be examined carefully.

The discovery of the two Fe-chromate precipitates that are the focus of this dissertation raises the question whether other, not yet discovered, chromate containing phases could also be forming in chromium contaminated soils. Potential candidates are other members of the jarosite-alunite family of compounds, e.g. $\text{NaFe}_3(\text{CrO}_4)_2(\text{OH})_6$, $\text{KAl}_3(\text{CrO}_4)_2(\text{OH})_6$, or even $\text{KCr}_3(\text{SO}_4)_2(\text{OH})_6$, and some of the other Fe-chromate phases synthesized and described by Bonnin (1970) such as $\text{KFe}(\text{CrO}_4)_2 \cdot \text{H}_2\text{O}$ (the chromate analog of the sulfate mineral krausite) $\text{KFe}(\text{CrO}_4)_2$, and FeOHCrO_4 . Little is known about the conditions under which these phases could form. The discovery of these two Fe-chromate precipitates underlines the need for careful examination of contaminated soils for the presence of chromate containing solid phases. The successful use of a combination of electron microscopy and x-ray diffraction in this study suggests that this technique is suitable to identify such phases in contaminated soils. Furthermore, the use of this identification technique is not limited to chromium contaminated soils but should be suitable to identify heavy metal containing precipitates in soils contaminated with other metals.

Finally, the overall groundwater chemistry of the United Chrome Products site should be reexamined in the light of the results of these new results. Regions of the contaminated aquifer that are supersaturated with respect to these Fe-chromate phases should be delineated both before and after the implementation of the currently operating pump-and-treat system. The presence of $\text{KFe}_3(\text{CrO}_4)_2(\text{OH})_6$ and of $\text{KFe}_3(\text{Cr}_x\text{S}_{(1-x)}\text{O}_4)_2(\text{OH})_6$ solid solutions and in parts of the contaminated aquifer and their slow dissolution could be one of the main reasons for the observed 'tailing' of Cr(VI) concentrations (McKinley et al., 1992) in the groundwater extracted by the currently operating pump-and-treat remediation system.

7.4 References

- Bonnin A. (1970) Préparations et étude de chromates de fer. Ph.D. Dissertation, Univ. Rennes, France.
- McKinley W.S., Pratt R.C., and McPhillips L.C. (1992) Cleaning up chromium. *Civ. Eng.* **62**, 69-71.

APPENDIX A

Supplemental Analytical Results

Table A-1. Complete analytical results from the final sample taken in the $\text{KFe}_3(\text{CrO}_4)_2(\text{OH})_6$ dissolution experiments (Chapter 3).

		pH final	$[\text{Cr(VI)}]_{\text{tot}}$ (mmol L ⁻¹)	$[\text{K}]_{\text{tot}}$ (mmol L ⁻¹)	$[\text{Fe}]_{\text{tot}}$ (mmol L ⁻¹)
KCRJAR-1.5	A	1.75	1.23	0.786	2.62
	B	1.65	1.58	0.865	2.87
	C	1.61	1.91	0.845	2.76
KCRJAR-2.0	A	2.12	0.403	0.179	0.536
	B	2.12	0.407	0.180	0.542
	C	2.14	0.405	0.180	0.542
KCRJAR-2.3	A	2.41	0.288	0.116	0.278
	B	2.39	0.258	0.108	0.256
	C	2.41	0.299	0.128	0.246
KCRJAR-2.6	A	2.65	0.567	0.048	0.119
	B	2.65	0.551	0.041	0.111
	C	2.65	0.532	0.035	0.104
KCRJAR-3.0	A	3.05	2.33	0.020	0.026
	B	3.05	2.37	0.021	0.020
	C	3.04	2.39	0.015	0.017
KCRJAR-4C	A	2.01	0.347	0.181	0.519
	B	2.04	0.409	0.199	0.573
	C	2.03	0.410	0.197	0.573
KCRJAR-15C	A	2.05	0.413	0.197	0.579
	B	2.06	0.422	0.201	0.590
	C	2.05	0.420	0.202	0.590
KCRJAR-35C*	A	2.13	0.37	0.34	0.84
	B	2.09	0.53	0.35	0.93
	C	2.29	0.21	0.28	0.72

* Experiments KCRJAR-35 A and C were not used in further analysis because of low Cr concentrations relative to K and Fe. The reason for the low Cr concentrations in these experiments is not known.

Table A-2. Complete analytical results from final sample in jarosite dissolution experiments (Chapter 4).

		pH final	[SO ₄ ²⁻] _{tot} (mmol L ⁻¹)	[K] _{tot} (mmol L ⁻¹)	[Fe] _{tot} (mmol L ⁻¹)
KJAR-1.5	A	1.61	2.60	1.19	3.30
	B	1.60	2.61	1.31	3.58
	C	1.59	2.48	1.17	3.22
KJAR-2.0	A	2.10	0.279	0.184	0.430
	B	2.11	0.362	0.175	0.440
	C	2.10	0.356	0.174	0.430
KJAR-2.3	A	2.33	0.303	0.149	0.158
	B	2.34	0.330	0.164	0.158
	C	2.34	0.305	0.164	0.196
KJAR-2.6	A	2.60	0.487	0.116	0.055
	B	2.61	0.614	0.106	0.046
	C	2.57	0.607	0.112	0.053
KJAR-3.0	A	2.95	2.93	0.100	0.013
	B	2.99	3.22	0.101	0.014
	C	3.01	3.62	0.054	0.013
KJAR-4C	A	2.01	0.318	0.219	0.535
	B	2.01	0.343	0.211	0.497
	C	2.02	0.357	0.220	0.524
KJAR-15C	A	2.03	0.355	0.229	0.546
	B	2.04	0.327	0.224	0.524
	C	2.03	0.361	0.220	0.519
KJAR-35C	A	2.03	0.484	0.291	0.470
	B	1.97	0.543	0.331	0.464
	C	2.02	0.558	0.331	0.459

Table A-3. Complete analytical results from final sample in $\text{KFe}(\text{CrO}_4)_2 \cdot 2\text{H}_2\text{O}$ solubility experiments (Chapter 6).

		final pH	$[\text{Cr(VI)}]_{\text{tot}}$ (mmol L ⁻¹)	$[\text{K}]_{\text{tot}}$ (mmol L ⁻¹)	$[\text{Fe}]_{\text{tot}}$ (mmol L ⁻¹)
C2M-1.2	A	1.36	37.9	24.0	11.0
	B	1.38	33.9	19.4	12.8
	C	1.43	35.5	21.5	11.9
C2M-1.1	A	1.23	41.6	22.3	15.9
	B	1.28	-	-	-
	C	1.25	42.4	22.0	12.7
C2M-1.0	A	-	49.9	26.5	22.86
	B	1.19	49.7	27.3	16.71
	C	1.18	49.8	26.9	19.79
C2M-0.8	A	1.02	69.4	38.8	27.6
	B	1.01	69.1	38.4	33.1
	C	1.01	71.5	38.1	29.9
C2M-4C	A	1.08	42.1	22.5	17.2
	B	1.12	41.9	22.3	17.0
	C	1.05	40.9	22.5	-
C2M-15C	A	1.08	46.9	24.4	18.5
	B	1.06	45.0	24.0	16.2
	C	1.12	44.5	24.0	17.7
C2M-25C	A	1.14	52.0	26.2	20.3
	B	1.23	52.2	27.7	20.5
	C	1.13	51.8	26.4	20.4
C2M-35C	A	1.09	61.1	30.0	24.2
	B	1.07	61.1	30.3	29.9
	C	1.07	61.5	30.5	23.1
C2M-50C	A	1.06	70.9	34.6	27.5
	B	1.01	70.0	35.9	27.7
	C	1.13	70.9	36.5	29.2
C2M-75C	A	0.92	87.7	46.4	27.9
	B	1.05	89.5	45.9	27.9
	C	1.03	89.2	45.5	27.0
PRECIP-A		0.16	149	1830	41
PRECIP-B	A	1.26	11.1	138	43.4
	B	1.34	10.4	132	36.6
	C	-	14.9	-	-
PRECIP-C	A	1.39	14.0	81.3	15.1
	B	1.38	13.4	80.2	15.1
	C	1.37	13.3	82.5	14.1
PRECIP-D	A	1.42	20.4	54.3	3.80
	B	1.41	18.9	59.2	4.68
	C	1.37	21.1	60.7	2.53

APPENDIX B

Activity Correction Models

The following activity correction models were used in this study as incorporated into MINTEQA2 (Allison et al., 1990):

Davies Equation:

The Davies equation depends only on the charge of the ion and the ionic strength of the medium:

$$\log \gamma_i = -Az_i^2 \left(\frac{\sqrt{I}}{1 + \sqrt{I}} - 0.24I \right)$$

where γ_i is the activity coefficient for species i , z_i is the charge of species i , and I is the ionic strength. A is the limiting Debye-Hückel parameter given by $A = 1.82 \times 10^6 (\epsilon T)^{-3/2}$ where ϵ is the temperature dependent dielectric constant of water and T is the temperature in K.

Debye-Hückel Equation:

The extended Debye-Hückel algorithm has one extra general parameter, B , and two ion specific parameters a_i and b_i , e.g.,

$$\log \gamma_i = -Az_i^2 \frac{\sqrt{I}}{1 + Ba_i\sqrt{I}} + b_i I$$

B is given by $B=50.3(\epsilon T)^{-1/2}$. If the Debye-Hückel parameters a_i and b_i are not known for a given ion, MINTEQA2 will revert to the Davies formulation to calculate its activity coefficient. The Debye-Hückel parameters included in the MINTEQA2 database for ions considered in this study are listed in Table A-4.

Table A-4. Debye-Hückel parameters included in the MINTEQA2 database for ions considered in this study.

	a_i	b_i
OH^-	3.5	-
Ca^{2+}	6.0	0.165
CrO_4^{2-}	4.0	-
Fe^{3+}	9.0	-
H^+	9.0	-
K^+	3.0	0.15
NO_3^-	3.0	-
SO_4^{2-}	4.0	-0.04
FeSO_4^+	5.0	-
$\text{Fe}(\text{OH})_2^+$	5.4	-
HSO_4^-	4.5	-

Reference:

Allison J.D., Brown D.S., and Novo-Gradac K.J. (1990) *MINTEQA2/PRODEFA2, a geochemical assessment model for environmental systems: version 3.0*. U.S. Environmental Protection Agency, Athens, GA.

VITA

The author was born in 1960 and grew up in the North of what was then West Germany. He completed his 'Abitur' (roughly equivalent to a high school diploma) at the Holstenschule Neumünster in 1979. The following years brought various jobs including almost two years as a nurse's aide in a hospital and lots of travelling. In 1984 he entered the Geology Program at the Freie Universität Berlin. After completing his 'Vordiplom' (roughly equivalent to a Bachelors degree) in 1986 he came to the U.S. in 1987 on what started out as a one-year exchange program at Portland State University. Little did he know that he was still going to be in Portland almost nine years later. At Portland State he got involved in a groundwater study for the Army Corps of Engineers and ended up completing an M.S. in Geology. Subsequently the author worked for Squier Associates in Lake Oswego, Oregon as a hydrogeologist and project manager on a wide variety of environmental investigation and remediation projects. He became more interested and involved in environmental issues and decided in 1991 to pursue a Ph.D. in Environmental Science and Engineering at OGI. Although he is off to a Postdoc at the California Institute of Technology, he hopes to eventually come back to the beautiful Pacific Northwest.

Publications

Baron D., Palmer C.D., and Stanley J.T. (1996) Identification of two Fe-chromate precipitates in a Cr(VI)-contaminated soil. *Env. Sci. Technol.* **30**, 964-968.

Baron D. and Palmer C.D. (1996) Solubility of jarosite at 4-35°C. *Geochim. Cosmochim. Acta* **60**, 185-195.

Baron D. and Palmer C.D. Solubility of $\text{KFe}_3(\text{CrO}_4)_2(\text{OH})_6$ at 4-35°C. *Geochim. Cosmochim. Acta* (accepted for publication, March 1996).

Baron D., Scofield D.H., Johnson D.H., Malin R.D., and Graham J.D. (1991) Three dimensional modeling of groundwater flow and temperatures at Bonneville Dam, Oregon. *Proceedings, 1991 Geotechnical Engineering Congress, Boulder, CO*, 1186-1197. American Society of Civil Engineers, New York.